Title
Thermodynamics of Miscible Polymer Electrolytes

Author
Shah, Neel Jaymin

Publication Date
2023

Peer reviewed|Thesis/dissertation

Thermodynamics of Miscible Polymer Electrolytes

By

Neel Jaymin Shah

A dissertation submitted in partial satisfaction of the

requirements for the degree of

Doctor of Philosophy

in

Chemical Engineering

in the

Graduate Division

of the

University of California, Berkeley

Committee in charge:

Professor Nitash P. Balsara, Chair
Professor Rui Wang
Professor Mary C. Scott

Summer 2023

Thermodynamics of Miscible Polymer Electrolytes

Abstract

Thermodynamics of Miscible Polymer Electrolytes

by

Neel Jaymin Shah

Doctor of Philosophy in Chemical Engineering

University of California, Berkeley

Professor Nitash P. Balsara, Chair

There is a growing need for improvements in renewable energy sources and in energy storage devices as the effects of global warming become more acute. Conventional lithium-ion batteries are composed of a lithium-graphite composite anode, a liquid electrolyte and a transition metal oxide cathode. Replacing the lithium-graphite anode with a lithium metal anode would greatly increase the energy density of these batteries, enabling higher range electric vehicles and significant improvements in consumer electronics. However, lithium metal anodes are incompatible with conventional liquid electrolytes, prone to dendrites and pose significant safety hazards. There has been significant research into replacing conventional liquid electrolytes with polymer electrolytes, which are significantly less flammable than liquid electrolytes, and have a higher modulus thereby suppressing dendrite growth. However, current polymer electrolytes cannot match the ion transport characteristics of conventional liquid electrolytes. To address this, researchers have attempted to combine various polymeric components with lithium salt to create an electrolyte that is both highly conductive and mechanically rigid. The thermodynamics of conventional polymer electrolytes are still poorly understood. In this Dissertation we study the effect of added salt on the thermodynamic properties of block copolymers and polymer blends comprised of poly(ethylene oxide) (PEO) and poly(methylmethacrylate) (PMMA). This Dissertation represents the first comprehensive study of the thermodynamics of a miscible polymer electrolyte system.

In Chapter 2, we synthesize a series of PEO-PMMA block copolymers and analyze the effect of added lithium bis(trifluoromethane) sulfonimide (LiTFSI) salt on the phase behavior utilizing small angle X-ray scattering (SAXS). We calculate thermodynamics interaction parameters for this system and find that the effective thermodynamic interaction parameter, χ_{eff}, varies nonmonotonically with respect to salt concentration. We shed light upon the complex phase separation of PEO-PMMA/LiTFSI block copolymer electrolytes, which deviates from conventional block copolymer electrolytes.

In Chapter 3, we prepare a series of PEO/PMMA/LiTFSI blend electrolytes and analyze the

phase behavior of these blends via small angle neutron scattering. We find that both blend composition and salt concentration have a significant effect on polymer blend electrolyte phase behavior. We extract thermodynamic interaction parameters from the collected scattering data and build a thermodynamic model to predict blend phase behavior. We find that our model is in good agreement with our experimental data.

In Chapter 4, we expand on our characterization of PEO/PMMA/LiTFSI blend electrolyte phase behavior by using light scattering to augment our previous phase characterization work. We create a comprehensive phase diagram of PEO/PMMA/LiTFSI polymer blends. This phase diagram presents some of the first experimental evidence of multiple immiscible windows in polymer blend electrolytes. We utilize our previously developed thermodynamic model to create a simulated phase diagram and find good agreement between theory and experiment.

This work provides new insights into polymer-salt interactions and the underlying thermodynamics of polymer electrolytes. The goal of this Dissertation is to further analyze the complex thermodynamics of polymer electrolytes to enable design of future polymer electrolytes for lithium metal batteries.

"That's all it is Miles... a leap of faith"

-Into the Spiderverse

Contents

List of Figures

List of Tables

List of Schemes

Acknowledgments

To begin, I would like to thank my mentor, Nitash Balsara. Our journey together was long and winding, and I think we have learned an enormous amount from each other. I want to thank you for your patience with me during my early years as I struggled to enter the daunting world of polymer thermodynamics. I will always cherish our long discussions on neutron scattering and thermodynamic interaction parameters and more. Your attention to detail and conviction that we should always strive to do fundamental, comprehensive science, over what simply seemed exciting at the time has been an enormous guiding influence on my career. Thank you for caring for me as both a researcher and a person. The grace you showed me during difficult times of my PhD means the world to me. Thank you for everything.

I would like to thank my dissertation committee, Rui Wang and Mary Scott for reading this dissertation and providing incredibly useful feedback during my qualifying exam. I would also like to thank Negar Behasti Pour, Markita Landry, Susan Muller, Alex Katz and Esayas Kelkile for the privilege of being your GSI for CBE 154. It was wonderful to teach this class twice and be a small positive influence on the next generation of chemical engineers.

The Balsara lab has been an integral part of my PhD experience. I have always loved the labs emphasis on good science, but also close friendships. I believe we have created a supportive community of scientists who truly care about each other. Although we overlapped for a very short time, Dr. Hee Jeung Oh was a source of incredible kindness and her incredible work ethic was an example I aspired to emulate. Dr. Louise Frenck set the standard for careful, detail oriented electrochemical studies, and taught me an enormous amount about how to be a better researcher. Dr. Youngwoo Choo took me under his wing, and patiently taught me the ins and outs of electrochemical characterization, at a time in my career when I greatly needed guidance and mentorship. Dr. Xiaopeng Yu was a brilliant chemist and coworker. Dr. Jaeyong Lee is enormously hard working and dedicated, and I will miss our conversations on polymer thermo and fun weekend activities. Dr. David Halat's love of fundamental ion transport has continuously inspired me throughout my career, and I feel incredibly lucky to count him as a close friend. I will always cherish our bike rides to Tilden and our random conversations at lunch time. Dr. Saheli Charkaborty was my rock throughout my five years in the lab. During my first year, she patiently taught me polymer synthesis, and never lost her temper with me, despite my many mistakes. She has been a source of constant support throughout my five years in this lab and I always cherish her wisdom and advice. I will reluctantly admit that she also finally convinced me that boba wasn't that bad.

The graduate students in the Balsara lab have been an integral part of my life for 5 years. I feel lucky to count them not just as my coworkers, but also as my friends. Whitney Loo was an incredible researcher and her love of fundamental polymer thermodynamics was an enormous influence on my career. Jackie accomplished so much in the realm of tomography and her love of softball always reminded me that there is a life outside of the lab. Deep was an incredible electrochemist, and his warmth and kindness always made me feel welcome in the lab.

Mike Galluzo was a pioneer, and I am in awe of his accomplishments developing the in-situ scattering project. Gumi's careful, precise work on PEO-POSS taught me an enormous amount about the importance of precision in research. Both Mike and Gumi were amazing teachers at beamline 7.3.3. and I will forever appreciate their patience and kindness.

Kevin Gao taught me an enormous amount about neutron scattering and I have always appreciated his thoughtful approach to research, never being afraid to go down a rabbit hole to learn more. Lorena Grundy tackled a staggering number of projects with her characteristic tenacity and brilliance. She always took the time to help younger students and was an indispensable mentor to me.

Zach and Alec, I will never be able to properly articulate what a pleasure it has been working with you guys. You are both amazing friends and I feel so lucky that we joined the lab together. Thank you for being my partners in crime. Zach, I have never met anyone as hard working and as kind as you. You always tackle problems with a smile and a can-do attitude, and I am in awe of what you have accomplished here. You are an amazing electrochemist and leader of building 33. Thank you for being my friend, and for cheerfully driving me all across California since I hate driving. Thank you for always being there to listen to me complain, even when you had problems of your own to deal with. Alec, you simply astound me. Although it took me a little bit to understand your sense of humor, I feel really lucky to be your friend. You tackled dozens of beamtimes throughout your time here without a single complaint and have single handedly pushed forward anode characterization research with your work. I will always cherish our conversations on weird coffee and cool breweries and restaurants to check out in Oakland.

Darby, my Tan Hall buddy, I will miss you enormously. Your work ethic is simply astounding, and you have become a singularly accomplished electrochemist. Although it is a thankless job, you have been an incredible safety coordinator and greatly improved the lab. I will greatly miss our little Friday gossip sessions when we both gave up on research for the day.

Morgan, you are a pioneer. It has been a great pleasure watching you bring a new field of research into the lab, accomplishing so much, when most of the lab has little background or experience in microscopy. We have all learned a great deal thanks to your excellent work. Your kindness lights up every room you are in, and I will miss working with you.

Vivaan, you are truly a jack of all trades. I am in awe of your ability to learn new research skills quickly and master them. You treat everyone well and I feel very lucky to have worked with you. I will also miss our silly conversations about Never Have I Ever and Emily in Paris. Karim, you are one of a kind. You have a unique perspective and insight into research, and you never shy away from asking tough questions. These traits make you an exceptional researcher. We may never see eye to eye on Dallas or Houston, but I appreciate you trying.

Emily, Michael, and Lily, the lab is in good hands. Emily you have tackled a technically complex project with skill and accomplished so much in your two years here. I admire your love of lab social events and love how much you care about building a better work environment for everyone. Michael, you are incredibly smart and resilient. I am so excited

to see you introduce new techniques and concepts, such as machine learning, to the lab and look forward to reading your future papers. Lily, it has been a real pleasure to have been your mentor, and I am excited to see you picking up the X-ray scattering baton. You have grown so much as a researcher, and I look forward to seeing what you accomplish here.

I have been incredibly lucky to have made so many wonderful friends during my time at Berkeley. Thank you to Eric, my stalwart roommate who has joined me on many a national park adventure (and misadventure). Matt, thank you for being my amazing biking buddy and cheerfully fixing up my road bike no matter how minor the problem is. Clay, Zach, Johnny and Branden made Hearst House feel like another home with their endless hospitality. Ana and Natalie, thank you for being amazing co-GSI's our first year here (105 for life!), and I love that we became great friends. Sam, thank you for accompanying me on many bike rides into the Berkeley hills. Nick, thank you for always being available to get a drink when I need to complain about something to a friend, and I look forward to bending your ear in San Francisco. Emily, your constant kindness has made rough patches here brighter, and I love our chaotic hangouts.

My friends from home and college have been an incredibly supportive community over my PhD. Shashwat, thank you for everything. We have been best friends since third grade, and you have always been a text or call away, whenever I have needed support, despite your demanding responsibilities at medical school. I am so proud of you, soon-to-be Dr. Kala. Baird, thank you for always being there for me, and sharing my love of Star Wars. Tom and Nate, thank you for opening your home to me when I need to escape grad school stress. Milo, thank you for always checking in on me, and supporting me. I cherish our Sunday morning phone calls. Jack, thank you for being my San Francisco partner in crime, and always being down for an adventure when I need to escape Berkeley. Justin, Priya, Greg and Cory, you have all been there for me since college and supported me through some incredibly tough moments in grad school.

Lastly, I want to thank my family. My aunt and uncle, Himanshu and Shital have been like a second set of parents to me. Mom and Dad, I love you both so much. You have worked tirelessly to make a better life for me, and I will never be able to thank you enough. Mom, you are the hardest worker I know and the most supportive mom I could ever ask for. Dad, you are my professional and personal inspiration. Vidita, thank you for being my little sister. You brighten my life, and are the best sibling I could have ever asked for.

Funding Acknowledgement

This work was jointly supported by the Joint Center for Energy Storage Research (JCESR), an Energy Innovation Hub funded by the U.S. Department of Energy, Office of Science, Office of Basic Energy Science, under Contract No. DE-AC02-06CH11357 and by National Science Foundation grant DMR 1904508. This work used resources at the Advanced Light Source, a U.S. DOE Office of Science User Facility under contract no. DE-AC02-05CH11231. Research at SLAC National Accelerator Laboratory, was supported by the U.S. Department of Energy, Office of Science, Office of Basic Energy Sciences under Contract No. DE-AC02-76SF00515. This work also used resources at the High Flux Isotope Reactor, a DOE Office of Science User Facility operated by the Oak Ridge Laboratory.

Chapter 1

Introduction

1.1 Motivation

The rapid rise in global carbon dioxide levels and the resultant climate change has driven the need for significant improvements in renewable energy resources as well as energy storage technologies. At the center of these efforts is the lithium-ion battery. The lithium-ion battery is present in numerous consumer devices from cellphones to laptops to wearable devices and more. As the world moves towards adopting electric vehicles to reduce automotive carbon dioxide emissions, the need to improve battery energy density, lifetime and stability becomes even more urgent.[1] Improvements in battery technology will improve consumer products, as well as enable a low carbon emission future.

One approach to improving battery energy density is moving from a lithium-graphite composite anode to a lithium metal anode. Lithium metal has a significantly higher specific capacity than graphite, making the lithium metal anode an excellent candidate to replace the conventional lithium-graphite anodes.[2,3] However, there are numerous issues that have hindered commercialization of lithium metal batteries. Lithium metal is highly incompatible with standard liquid electrolytes such as ethylene carbonate and propylene carbonate, and prone to dendrite formation, introducing significant safety risks.[4,5] To address this issue, significant efforts have been made to develop polymer electrolytes as a replacement for conventional liquid electrolytes.[3,6,7]

1.2 Polymer Electrolytes

The potential of polymer electrolytes was first established by Fenton and coworkers who discovered that poly(ethylene oxide) (PEO) could solvate lithium ions.[8] Polymer electrolytes are non-flammable, and have a higher modulus than conventional liquid electrolytes, providing significant safety advantages to current liquid electrolytes.[3,4,6] However, ion transport in polymer electrolytes is driven by segmental motion, and PEO and PEO-derived polymer electrolytes must be heated to temperatures as high as 90°C to have usable ionic conductiv-

ities. These electrolytes are still 2 orders of magnitude less conductive than standard liquid electrolytes.[3,9] Furthermore, low molecular weight PEO electrolytes have a low storage modulus, limiting their ability to suppress dendrite formation.[10] Researchers have attempted to address this issue by creating PEO-based composites, blends and block copolymers to increase the modulus of the resulting polymer electrolyte, without significantly suppressing ion transport.[9,10] The development of complex polymer electrolytes introduced the need to understand the underlying thermodynamics of these systems, which governs the miscibility of various components in the electrolyte.

Typical liquid electrolytes are a blend of ethylene carbonate (EC), and propylene carbonate (PC). EC has a higher dielectric constant than water, and is an excellent ion shuttle, but is a solid at room temperature, making it seemingly impractical for battery applications.[5] By adding PC, a liquid electrolyte with a lower dielectric constant than EC, researchers were able to create a mixed electrolyte that was both liquid at room temperature and highly conductive.[5,11] Polymer electrolyte researchers have attempted to replicate this approach by creating polymer blends where one polymer is ionically conductive, and one is mechanically rigid, or block copolymers where one block is ionically conductive and one is mechanically rigid in an attempt to make a polymer electrolyte that is both effective at ion transport and able to suppress dendrites.[6] While the thermodynamics of liquid mixtures is well understood, the thermodynamics of polymers and polymer electrolytes in particular is still a significant ongoing field of research.

The thermodynamics of polymer blends and block copolymers in the absence of salt has been well studied and characterized. Polymer blends can macrophase separate, similar to liquid mixtures such as oil and water, while block copolymers can microphase separate into complex nanostructures.[12,13] Flory and Huggins developed the thermodynamic framework for polymer blends, finding that the free energy of mixing was a function of chain length (N), blend composition (ϕ_1), temperature and Flory-Huggins interaction parameter, χ which describes the interaction energies of the two unlike monomers in the system.[14,15] χ is positive when repulsive forces dominate, and negative when attractive forces dominate. Systems with a negative χ are generally assumed to be miscible. The thermodynamics of salt free polymer blends have been extensively studied using the Flory-Huggins framework.[16–26] For block copolymers, Leibler, Fredrickson and Cochran developed the theoretical basis for block copolymer phase behavior and found that block copolymer phase behavior is also a function of chain length (N), block copolymer composition (ϕ_1), temperature and Flory-Huggins interaction parameter, χ.[27,28] There have been numerous experimental studies of salt free block copolymer phase behavior, and the thermodynamics of these systems match well with available theoretical predictions.[29,30]The χ parameter can be obtained experimentally for polymer blends and block copolymers using the Random Phase approximation (RPA).[27,31,32] χ parameters are calculated by fitting the RPA framework to scattering profiles of polymer blends and block copolymers.[18,26,33,34]

The addition of salt to polymer melt systems introduced a new avenue of thermodynamics. Early experimental work found that the addition of lithium bis(trifluoromethane) sulfonimide (LiTFSI) salt to a polystyrene-block-poly(ethylene) oxide block copolymer in-

duced microphase separation.[35,36] We define a new interaction parameter, χ_{eff} which captures the interactions between both polymer blocks and lithium salt. Microphase separation in block copolymers is driven by preferential segregation of ions into the high dielectric block. Wang and coworkers captured the theoretical basis of χ_{eff} by creating models based on Born Solvation energy.[37,38] This theoretical framework defines the effective Flory-Huggins parameter as

$$\chi_{\text{eff}} = \chi + mr \tag{1.1}$$

where χ is the Flory-Huggins parameter for salt free systems, r is the salt concentration, and m is a proportionality constant.[37] This form was first suggested by early experimental work by Mayes and coworkers.[39] Later work on both PEO/PS/LiTFSI blend electrolytes and PEO-PS/LiTFSI block copolymer electrolytes supported this framework.[36,40]

In addition to redefining the interaction parameter, significant research was conducted to predict the phase behavior of salt containing block copolymer and polymer blend systems. In a pioneering paper, Sing and coworkers developed ionic self consistent field theory, accounting for electrostatic cohesion, and used this framework to generate phase diagrams for a block copolymer system where one block contains charged monomers and the other is neutral.[41] For salt-free systems, Fredrickson and Cochran plotted phase behavior on a χN versus ϕ_1, where χN is the segregation strength and ϕ_1 is the volume fraction of component 1 (PEO in this work).[28] They predicted a symmetric phase diagram, with phase separation being most energetically favorable at $\phi_1 = 0.50$.[28] Sing and coworkers predicted an asymmetric phase diagram with a "chimney" of stable ordered phases at $\phi_1 = 0.10$.[41] Later theoretical work by Hou and coworkers on block copolymer electrolyte phase behavior predicted a similar chimney.[42] However, a comprehensive study of PEO-PS/LiTFSI phase behavior found that these systems largely follow the predictions of Fredrickson and Cochran, not Sing and coworkers.[43]

Similar discrepancies can be found in polymer blend electrolytes. Based on equation 1, the addition of salt to a polymer blend, where one polymer has a higher dielectric constant than the other, will lead to preferential segregation of salt and an increase in χ_{eff}.[44] In other words, increasing the salt concentration in the blend leads to macrophase separation. Phase diagrams of these polymer blend electrolytes, where phase behavior is characterized at a constant temperature, should feature a single large window of immiscibility. Experimental work by Xie et al for squalene (SQ)/PEO blends and Wu et al for PS/PEO blends show a clear increase in interaction parameter as a function of salt.[40,45] The SQ/PEO phase diagram also features a single large window of phase separation.[40] However, theoretical work by de la Cruz and coworkers accounted for ionic correlations within polymer blend electrolyte systems and predicted the presence of multiple windows of immiscibility in polymer blend electrolyte phase diagrams.[46,47]

The vast majority of polymer blend electrolyte thermodynamic studies, as well as block copolymer electrolyte studies have been confined to systems with a positive χ parameter in the neat state.[35,40,43,45,48,49] In these systems, net repulsive forces dominate, and the addition of salt further drives phase separation. This naturally leads to the question "what is the

thermodynamic effect of added salt on block copolymer and polymer blend systems with a negative χ parameter?" PEO/poly(methyl methacrylate) (PMMA) blends in the absence of salt have been thoroughly studied and found to be miscible.[50–54] Ito and coworkers conducted small angle neutron (SANS) studies of PEO/PMMA blends, and found that these blends have a negative χ parameter, and are miscible at a wide range of compositions and temperatures, making PEO/PMMA a perfect model system.[55] In this thesis, we examine the effect of added LiTFSI salt on the thermodynamic parameters and phase behavior of PEO-PMMA block copolymers and PEO/PMMA blends and compare these results to theory. This work represents the first comprehensive investigation of the thermodynamics of miscible polymer electrolyte systems.

1.3 Structure of Dissertation

The goal of this work is to examine the effect of added salt on the thermodynamics of a miscible polymer electrolyte system. Chapter 2 details the synthesis of PEO-PMMA block copolymers, and characterization of the phase behavior of PEO-PMMA block copolymer electrolytes via small angle X-ray scattering (SAXS). Thermodynamic parameters are extracted from the SAXS data. Chapter 3 is a study of the phase behavior of PEO/PMMA/LiTFSI polymer blend electrolytes, characterized via small angle neutron scattering (SANS). The SANS data is used to extract thermodynamic interaction parameters and create a model for polymer blend electrolyte phase behavior. Chapter 4 combines SANS and light scattering experiments to characterize PEO/PMMA/LiTFSI blend phase behavior and develop a comprehensive phase diagram. The phase behavior model developed in Chapter 3 is used to develop a theoretical phase diagram, which is compared against the experimental phase diagram. Chapter 5 summarizes the conclusions of these studies.

Chapter 2

Effect of Added Salt on Disordered Poly(ethylene oxide)-Block-Poly(methyl methacrylate) Copolymer Electrolytes[1]

2.1 Abstract

We studied the effect of salt addition on a diblock copolymer system with a negative Flory-Huggins interaction parameter, χ , indicative of attractive interactions between the two blocks. The system studied is poly(ethylene oxide)-block-poly(methyl methacrylate) (PEO-PMMA) with added lithium bis(trifluoromethanesulfonyl)imide (LiTFSI) salt. We studied two asymmetric block copolymers, PEO-PMMA(10-33) and PEO-PMMA(10-64), where the numbers refer to the molar masses of the blocks in kg mol^{-1}. The small angle X-ray scattering (SAXS) profiles for PEO-PMMA(10-33) were featureless at all salt concentrations. In contrast, PEO-PMMA(10-64) exhibited SAXS peaks when the salt concentration was between $0.22 \leq m$ (mol Li/kg polymer) ≤ 0.44. The appearance of SAXS peaks only in PEO-PMMA(10-64) is consistent with the predictions of ionic self-consistent field theory developed by de la Cruz and coworkers, which predicts that in systems with negative χ, ordered phases are only found when the volume fraction of the ionic block is about 10%.

2.2 Introduction

There is continuing interest in the thermodynamic driving forces that underlie the transition from disorder to order in block copolymers.[27,28,56–60] At sufficiently high temperatures, entropy dominates and block copolymers are disordered. In the simplest of systems, lowering temperature results in the formation of periodic ordered structures that depend mainly on the composition of the copolymers. The disorder-to-order phase transition is governed by

[1]Adapted from Shah, N. J., *et al.* Effect of Added Salt on Disordered Poly(Ethylene Oxide)- Block-Poly(Methyl Methacrylate) Copolymer Electrolytes. ***Macromolecules*** 2021, 54 (3), 1414–1424.

three parameters: the Flory Huggins interaction parameter, χ, overall chain length, N, and volume fraction of one of the blocks, The phase diagram of block copolymer melts is usually shown on a χN versus plot ϕ.[27–30,56,57,61] An example of such a plot is shown in Figure 2.1a where we plot the results of self-consistent field theory (SCFT) obtained by Cochran and Frederickson.[28] This well-established phase diagram is symmetric about $\phi = 0.50$; implying for a given chemistry, the chain length at which ordering is seen is lowest for symmetric block copolymers with $\phi = 0.50$. In other words, in systems with a small enough χ parameter such that the disordered phase can be accessed, the driving force for order formation at constant N, is largest at $\phi = 0.50$.

The effect of added salt on block copolymer thermodynamics has attracted considerable attention in recent years.[1,39,41,42,46,62–69] The extent to which the classical block copolymer phase diagram applies to salt-containing block copolymers remains an interesting open question. It has long been recognized that many observations on the phase behavior of block copolymers wherein the salt interacts strongly with one of the blocks can be rationalized by defining an effective χ parameter, χ_{eff}, that reflects interactions between the two blocks in the presence of salt. The concept of Born solvation introduced by Wang and co-workers provided a rational basis for the use of χ_{eff}.[38] Significant progress was made by determining χ_{eff} empirically and mapping the observed phase behavior on the classical block copolymer phase diagram for uncharged blocks.[34,43] In an important paper, de la Cruz and coworkers[41] introduced an approach that they called ionic self-consistent field theory to predict the phase behavior of charged block copolymers. This theory was originally developed for the case when one of the block copolymers contained charged monomers, but more recent work by Qin and coworkers shows that similar phase behavior is obtained when salt was added to a neutral diblock copolymer.[42] We show one of the phase diagrams taken from ref. 41 in Figure 2.1a (Figure 4c of ref. 41).[41] The striking difference in the phase behavior between pure block copolymers and those with added salt is the appearance of a narrow chimney in the vicinity of ϕ= 0.10, where ϕ is the volume fraction of the block with a high affinity for the salt ions such as poly(ethylene oxide). It should be noted that the ionic SCFT phase diagram is plotted assuming that the ions are solvated exclusively in the PEO block; the model in ref. 41 assumes that one of the charged species is covalently bonded to one block of the diblock copolymer.[41] In such systems if χ is small enough such that the disordered phase can be accessed, the driving force for order formation at constant N, is largest at ϕ = 0.10.

The main purpose of this work is to test the predictions of ionic SCFT. The system that we have studied is poly(ethylene oxide)-b-poly(methyl methacrylate) (PEO-PMMA) with added lithium bis(trifluoromethanesulfonyl)imide (LiTFSI) salt. Numerous studies have been conducted on PEO/PMMA homopolymer blends, since it is one of the few polymer blend systems that is completely miscible.[50–54] The value of χ between PEO and PMMA is -7.8E-04 based on a reference volume of 0.1 nm^3, and it is independent of temperature.[55,70] A negative χ parameter is generally taken as a signature of attractive interactions between the blocks. We synthesized two block copolymers, starting with a 10 kg mol^{-1} PEO macroinitiator and then polymerizing methyl methacrylate via atom transfer radical polymerization.[71] We

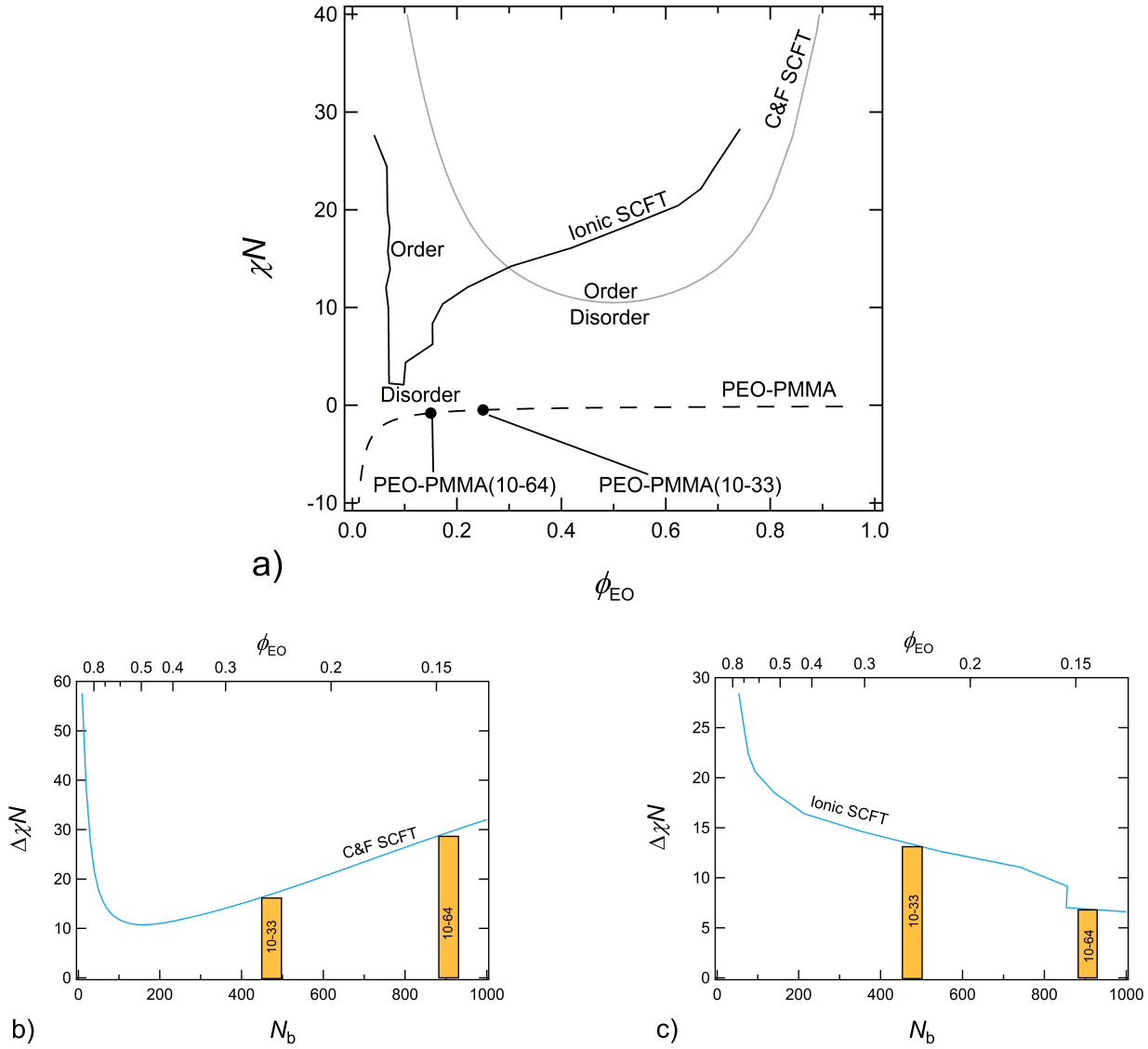

Figure 2.1: Phase diagrams for PEO-PMMA block copolymer. Segregation strength χN, is plotted as a function of volume fraction of ethylene oxide ϕ_{EO} and number of PMMA units, N_{b}. In (a) the Fredrickson and Cochran order to disorder transition is plotted as the gray trace, as a function of ϕ_{EO}. The black trace is the ionic SCFT phase diagram by de la Cruz and coworkers. In (b) the change in segregation strength, $\Delta\chi N$ is shown between the classical phase diagram and the segregation strength of a PEO-PMMA block copolymer series with a 10 kg mol^{-1} block. Yellow bars mark the location of the two synthesized asymmetric block copolymers. In (c) the change in segregation strength, $\Delta\chi N$ is shown between the ionic SCFT phase diagram and the segregation strength of the PEO-PMMA block copolymer series.

thus change ϕ in our system by keeping N_a, the number of repeat units in the PEO block, fixed at 154 and changing N_b, the number of repeat units in the PMMA block. The trajectory traversed by a series of block copolymers with $N_a = 154$ on the χN versus ϕ phase diagram is shown by a dashed curve in Figure 2.1a; a value of χ = -7.8E-04 was used to create the trajectory. This trajectory is located entirely within the disordered region of the classical block copolymer phase diagram. In other words, all block copolymers along this trajectory are predicted to be disordered regardless of temperature because χ for PEO/PMMA is independent of temperature. The two polymers of interest have PEO volume fractions of ϕ= 0.15 and ϕ= 0.25, and they are represented by dots on this trajectory. The vertical distance between this trajectory and the order-disorder transition boundary is a measure of the driving force for order formation. This driving force quantified by $\Delta\chi N$ is plotted as a function N_b in Figure 2.1b. The driving force for order formation for the ionic SCFT phase diagram in Figure 2.1a is plotted using the same axes in Figure 2.1c. The bars in Figures 2.1b and 2.1c represent the driving force for order formation in the two polymers of interest. We note in passing that mapping experimental results onto the ionic phase diagram requires considerable effort[72] that goes beyond the scope of the present paper. While we have used a particular phase diagram taken from ref. 41 to construct Figure 2.1, the same qualitative behavior would be seen if any of the other phase diagrams were used either from ref. 41 or ref. 42. If we hypothesize that the classical block copolymer phase diagram was applicable to PEO-PMMA/LiTFSI mixtures, then it would be easier to induce order in the copolymer with $\phi = 0.25$. In contrast, if we hypothesize that the ionic SCFT block copolymer phase diagram was applicable then it would be easier to induce order in a polymer with $\phi = 0.15$. Our main objective is to determine which hypothesis is correct.

Two series of block copolymer electrolytes were prepared adding salt to the two PEO-PMMA block copolymers described above. We demonstrate that the magnitude of the concentration fluctuations are larger in the more asymmetric PEO-PMMA polymer electrolyte. This finding, established by using small angle X-ray scattering (SAXS), lends considerable support to ionic SCFT. It is, perhaps, worth noting the difference between PEO-PMMA and the well-studied block copolymer, poly(ethylene oxide)-b-polystyrene (PEO-PS) electrolytes. The phase behavior of PEO-PS in the absence of salt is relatively simple: block copolymers with small chain lengths are disordered while those with large chain lengths are ordered.10 For a symmetric diblock copolymer, the molar mass of PEO-PS that enables access to order-disorder transitions at reasonable temperatures is about 14 kg mol^{-1}.[34] It was relatively straightforward to synthesize polymers in this range of molar masses and study the effect of added salt.[34–36,43] A similar starting point for the study of PEO-PMMA electrolytes did not exist when we began this study. Specifically, there was no rational approach for deciding on the composition and chain length of PEO-PMMA block copolymers to begin investigating the effect of added salt on the thermodynamics of this system.

2.3 Materials and Methods

Macroinitiator Synthesis

PEO (Sigma-Aldrich, molar mass = 10 kg mol^{-1}, 20 g, 2 mmol, 1 equiv., $Đ$ = 1.1) was dissolved in a 250 mL round bottom flask in dichloromethane (200 mL), N-(3-dimethyl aminopropyl)-N$'$-ethylcarbodiimide hydrochloride (EDC.HCL, Carbosynth, 770 mg, 4 mmol, 2 equiv.), 4-(dimethylamino)pyridine (DMAP, Sigma-Aldrich, 26 mg, 0.2 mmol, 10 mol%) and α-bromophenylacetic acid (BPAA, Combi-Blocks, 1.3 g, 6 mmol, 3 equiv.) were added to the solution at room temperature. After 48 hours, the solution was washed three times in a separatory funnel with a saturated solution of sodium bicarbonate and water at room temperature. The solution was dried over magnesium sulfate, concentrated in a rotary evaporator until viscous and then reprecipitated in room temperature diethyl ether.

PEO-PMMA synthesis

PEO-PMMA block copolymer was synthesized via atom transfer radical polymerization (ATRP) using a macroinitiator comprising of a 10 kg mol^{-1} PEO chain with a α-bromophenyl acetate terminus. The PEO-α-bromophenylacetate macroinitiator (1 equiv.) was dissolved in degassed anisole at room temperature in a sealed 10 mL round bottom flask. A copper wire (treated in a solution of HCl in methanol), $CuBr_2$ (0.02 equiv. dissolved in DMSO), *N,N,N$'$,N$''$,N$''$*-pentamethyldiethylenetriamine (PMDETA, 0.18 equiv.) and methyl methacrylate monomer (purified by passing through a column of basic alumina and degassed by nitrogen sparging) were added to the reaction mixture. Two different PEO-PMMA block copolymers were synthesized by allowing the reaction to proceed for 18 and 24 hours at room temperature. The reaction was stopped by dilution with tetrahydrofuran (THF) and subsequent passage through a basic alumina filter to remove the copper ions. The polymers were twice reprecipitated in water. Molar mass was determined with ^{1}H NMR spectroscopy and the dispersity ($Đ$) was determined with GPC. The structure of PEO-PMMA is shown in Scheme 1. The neat copolymers are colorless. Exact quantities of reagents are found in the SI.

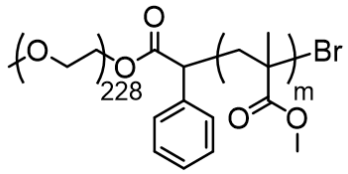

Scheme 2.1: Chemical Structure of PEO_{10K}-PMMA

In this study, polymers are referred to as PEO-PMMA(x-y) where x and y are the molar masses of the respective blocks in kg mol^{-1}. The number of monomers per block was calculated by

$$N_{\mathrm{i}} = \frac{M_{\mathrm{i}}}{\rho_{\mathrm{i}} v_{\mathrm{ref}}} \tag{2.1}$$

where v_{ref} is set to 0.1 nm^3. The total number of monomers for the block copolymer is given as

$$N = N_{\mathrm{PEO}} + N_{\mathrm{PMMA}} \tag{2.2}$$

The list of polymers used in this study is shown in Table 2.1.

PEO-PMMA	M_{PEO} (kg mol^{-1})	M_{PMMA} (kg mol^{-1})	ϕ_{EO} 90°C	N 90°C	$Đ$
10-33	10	33	0.25	624	1.13
10-64	10	64	0.15	1065	1.21

Table 2.1: Polymer Properties

The volume fraction of the neat copolymers is calculated by

$$\phi_{\mathrm{EO}} = \frac{v_{\mathrm{EO}}}{v_{\mathrm{EO}} + \frac{M_{\mathrm{PMMA}} M_{\mathrm{EO}}}{M_{\mathrm{MMA}} M_{\mathrm{PEO}}} v_{\mathrm{MMA}}} \tag{2.3}$$

where v_{EO} and v_{MMA} are the molar volumes of ethylene oxide monomers and methyl methacrylate monomers, respectively, and M_{MMA} and M_{EO} are the molar masses of the respective monomers. Molar volumes are calculated by

$$v_{\mathrm{i}} = \frac{M_{\mathrm{i}}}{\rho_{\mathrm{i}}} \tag{2.4}$$

where i = PEO, PMMA. We use subscripts of EO and MMA for properties of the monomer and subscripts of PEO and PMMA for properties of the polymeric blocks. The following expressions were used to calculate the density of PEO and PMMA as a function of temperature[73]

$$\rho_{\mathrm{PEO}} = 1.139 - 7.31 * 10^{-4} * T \tag{2.5}$$

$$\rho_{\mathrm{PMMA}} = 1.188 - 1.34 * 10^{-4} * T - 9.1 * 10^{-7} * T^2 \tag{2.6}$$

$$\rho_{\mathrm{PMMA}} = 1.223 - 5.29 * 10^{-4} * T - 0.507 * 10^{-6} * T^2 \tag{2.7}$$

^{1}H NMR

The composition of the PEO-PMMA block copolymers was determined using 1H NMR ($CDCl_3$, Brucker AV400). The composition was calculated by integrating the ethylene proton peak at 3.64 ppm against the proton peak for the methyl group on the MMA repeat units at 1.02, 0.85 and 3.60 ppm.[74] The ^{1}H NMR profiles are shown in the supporting information.

Gel Permeation Chromatography

The PEO-PMMA block copolymers were characterized on an Agilent 1260 Infinity Series gel permeation chromatography (GPC) system with Waters Styragel HR3 and HR4 columns with a *N*-methyl-2-pyrrolidone (NMP) mobile phase with 0.05 M LiBr at 70°C. The RI detector was utilized to calculate the polydispersity ($Đ = M_w/M_n$) based upon poly(ethylene oxide) calibration standards. The PEO precursor molar mass was determined to be 9.1 kg/mol ($Đ = 1.2$). NMR was utilized to calculate the molar mass and composition of the PEO-PMMA block copolymers; we used the molar mass of the PEO precursor provided by the manufacturer (10 kg mol^{-1}) in these calculations. GPC traces of the PEO precursor and the block copolymers are shown in the supporting information.

Electrolyte Preparation

Electrolytes were made by mixing LiTFSI with each polymer in the presence of solvent. All electrolytes were prepared in an MBraun argon glovebox to prevent LiTFSI from complexing with water. Water and O_2 levels in the glovebox were kept below 1 and 0.1 ppm respectively during electrolyte preparation. Neat PEO-PMMA was dried under vacuum at 90°C for 72 hours in a glovebox antechamber before electrolyte preparation. Dry polymer and LiTFSI were placed in a scintillation vial and anhydrous THF was added to the mixture. The electrolyte was mixed at 60°C for 2 hours to ensure that both the polymer and salt were completely dissolved. After 2 hours, the caps from the vials were removed, and the solvent was evaporated off at 60°C for 12 hours. The electrolytes were then transferred to a glovebox antechamber and placed under vacuum at 90°C for 72 hours to evaporate off any remaining THF. The dry electrolytes were clear and extremely hard and glassy at room temperature. The salt concentration in the electrolytes was quantified by molality (m), or the ratio of moles of lithium to kilograms of solvent, or polymer in this study.

Small Angle X-Ray Scattering (SAXS) Measurements

SAXS samples were made by melt pressing polymer into 1/16 in thick Viton spacers (McMaster Carr) with an inner diameter of 1/8 in at 140 °C in an MBraun argon glovebox. These spacers were placed in custom airtight aluminum sample holders with Kapton windows and annealed at 140°C under vacuum for 48 hours and then allowed to cool to room temperature for 24 hours. These samples were placed in a custom 8-hole temperature controlled motorized stage and annealed at each target temperature for 30 minutes before taking SAXS measurements. SAXS measurements were taken at beamline 7.3.3 at the Advanced Light Source at Lawrence Berkeley National Lab and Stanford Synchrotron Radiation Light Source beamline 1-5 at the SLAC National Accelerator Laboratory.[75] Silver behenate was used to calculate the beam center and the sample-to-detector distance. The scattering intensity was corrected for air gaps, empty cell scattering and beam transmission. A glassy carbon standard provided by NIST was used to convert the beam intensity into absolute

intensity. The Nika program in Igor Pro was used to azimuthally integrate 2D scattering patterns into one dimensional scattering patterns.[76]

2.4 Results and Discussion

The measured SAXS profiles of PEO-PMMA(10-33) and PEO-PMMA(10-64) electrolytes at a fixed temperature of 90°C are shown in Figure 2.2. Both systems exhibit featureless SAXS profiles in the neat state. For PEO-PMMA(10-33), the addition of salt has no qualitative impact on the SAXS profiles; they are featureless across the salt concentration range $0 \leq m \leq 1.0$ mol Li/kg polymer. In contrast PEO-PMMA(10-64) exhibits a well-defined scattering peak at $q = q^* = 0.16$ nm^{-1} in the salt concentration window $0.22 \leq m \leq 0.44$ mol Li/kg polymer. The peak increases in intensity as m is increased from 0.22 to 0.44. Further increase in salt concentration from $m = 0.44$ mol Li/kg polymer to $m = 0.92$ mol Li/kg polymer results in a featureless SAXS profile. The scattering peaks in Figure 2.2b are due to the emergence of concentration fluctuations that are announcements of a disorder-to-order transition.[27,57] This announcement is only detected in PEO-PMMA(10-64).

If the thermodynamics of PEO-PMMA/LiTFSI mixtures could be explained on the basis of conventional block copolymer SCFT, then PEO-PMMA(10-33) would be closer to the disorder-to-order transition (Figure 2.1b). Instead we see that PEO-PMMA(10-64) is closer to the disorder-to-order transition due to the presence of the SAXS peaks, consistent with the predictions of ionic SCFT (Figure 2.1c).

The scattering profiles in Figure 2.2 were converted to absolute intensity as detailed in the methods section. The total intensity of scattering profiles with a disordered peak are given as

$$I_{\text{tot}}(q) = I_{\text{dis}}(q) + I_{\text{bkgd}}(q), \tag{2.8}$$

where $I_{\text{bkgd}}(q)$ is the background and $I_{\text{dis}}(q)$ is the intensity of the disordered peak. $I_{\text{bkgd}}(q)$ is assumed to be an exponentially decaying function of q, with two adjustable parameters.[34] Figure 2.3 plots the background subtracted scattering profiles of the PEO-PMMA(10-64) $m = 0.22$, 0.28 and 0.44 mol Li/kg polymer electrolytes at 90°C, the only 3 electrolytes that exhibit scattering peaks.

There are no explicit theoretical predictions for the scattering profiles of disordered mixtures of salt and block copolymers that we could use to analyze our data. Lacking a better alternative, we use the random phase approximation (RPA) to interpret the measured scattering profiles; this is similar to the approach used in the study of other disordered block copolymer/salt mixtures.[7,34,36,77,78] The RPA theory predicts the absolute scattering intensity of a monodisperse AB diblock copolymer

$$I_{\text{dis}}(q) = C\left[\frac{S(q)}{W(q)} - 2\chi_{\text{eff}}\right]^{-1} \tag{2.9}$$

where C is the x-ray scattering contrast that is governed by electron density differences.[27] The parameter χ_{eff} is the effective Flory Huggins interaction parameter that describes interactions

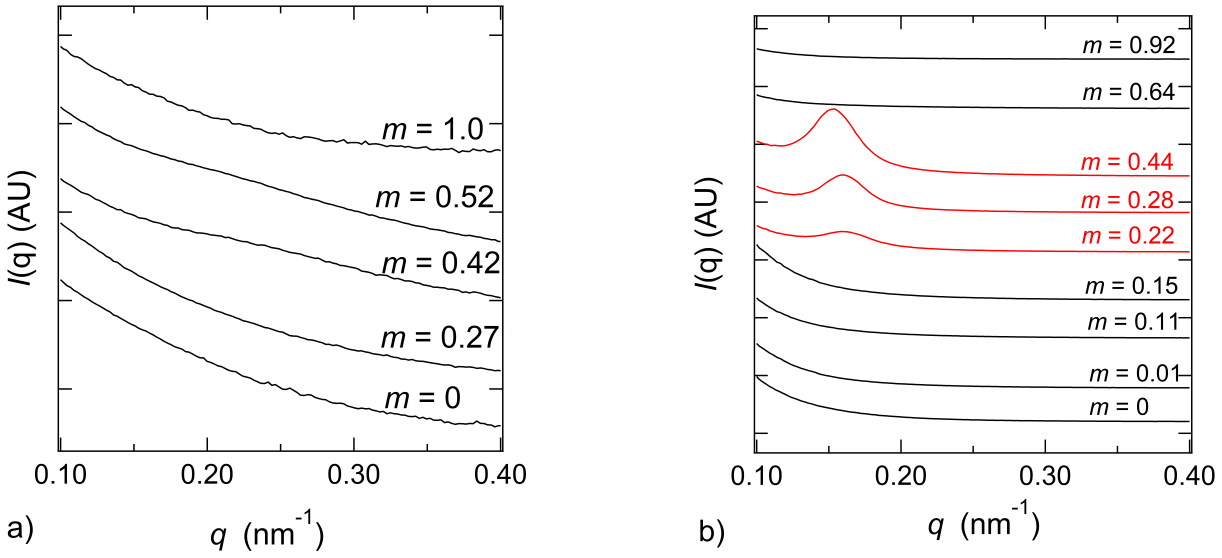

Figure 2.2: SAXS profiles of PEO-PMMA performed at ALS beamline 7.3.3. Scattering intensity is plotted as a function of the scattering vector, q. In (a) profiles are shown of PEO-PMMA(10-33) for a range of salt concentrations at 90°C, offset vertically for clarity. In (b) profiles are shown for PEO-PMMA(10-64) for a range of salt concentrations at 90°C. Salt concentration is given as m = mol Li/ kg polymer. Red curves signify a disordered phase evidenced by a broad primary scattering peak at $q^* = 0.16$ nm^{-1}.

between PEO/LiTFSI and PMMA/LiTFSI units. $W(q)$, and $S(q)$ are the determinant and the sum of the structure factor matrix $\|\mathrm{S_{ij}}\|$. The expressions for $W(q)$ and $S(q)$ are given by

$$W(q) = S_{\mathrm{AA}}{}^{\circ} S_{\mathrm{BB}}{}^{\circ} - (S_{\mathrm{AB}}{}^{\circ})^2 \tag{2.10}$$

$$S(q) = S_{\mathrm{AA}}{}^{\circ} S_{\mathrm{BB}}{}^{\circ} - 2S_{\mathrm{AB}}{}^{\circ} \tag{2.11}$$

where

$$S_{\mathrm{ii}}{}^{\circ} = f_{\mathrm{i}} N_{\mathrm{i}} v_{\mathrm{i}} P_{\mathrm{i}}(q) \quad (\mathrm{i} = \mathrm{A}, \mathrm{B}) \tag{2.12}$$

$$S_{\mathrm{AB}}{}^{\circ} = S_{\mathrm{BA}}{}^{\circ} = (N_{\mathrm{A}} f_{\mathrm{A}} N_{\mathrm{B}} f_{\mathrm{B}})^{\frac{1}{2}} F_{\mathrm{A}}(q) F_{\mathrm{B}}(q) \tag{2.13}$$

and

$$P_{\mathrm{i}}(q) = 2\left[\frac{\exp(-x_{\mathrm{i}}) - 1 + x_i}{x_{\mathrm{i}}^2}\right] \tag{2.14}$$

$$F_{\mathrm{i}} = \frac{1 - \exp(-x_{\mathrm{i}})}{x_{\mathrm{i}}} \tag{2.15}$$

with $x_{\mathrm{i}} = q^2 {R_{\mathrm{g,i}}}^2$. Each block is modeled as a Gaussian chain and

$$R_{\mathrm{g,i}}^2 = \frac{N_{\mathrm{i}}(\alpha\ a_{\mathrm{i}})^2}{6} \ (\mathrm{i} = \mathrm{PMMA}, \mathrm{PEO}) \tag{2.16}$$

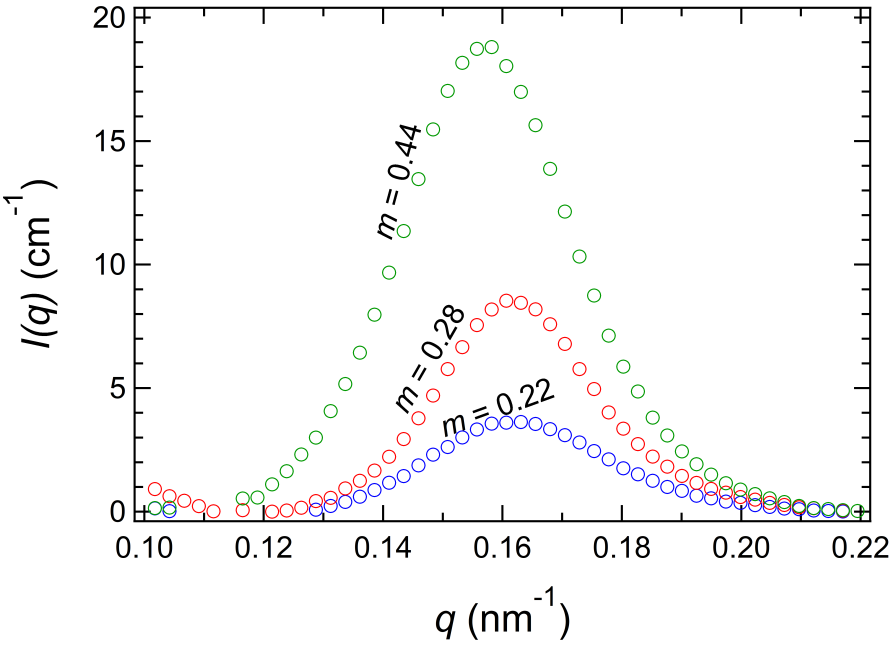

Figure 2.3: Background subtracted absolute intensity SAXS profiles of PEO-PMMA(10-64) $m = 0.22$, 0.28 and 0.44 mol Li/kg polymer plotted as a function of the scattering vector, q. These profiles were taken at 90°C.

where a_{i} is the respective statistical segment length of the block. In this study, we set a_{PEO}= 0.72 and $a_{\mathrm{PMMA}} = 0.54$.[73] In equation 2.16, α represents the chain stretching parameter accounting for the difference between the experimental values of R_{g} and those based on the statistical segment lengths reported in ref. 73. N_{i} in eqs 12, 13 and 16 is the number of repeat units in block i based on a v_{ref} of 0.1 nm^3. Equations 2.9-2.16 are used to calculate the scattering profiles for disordered block copolymer electrolytes.

As described in equation 2.9, the intensity of the disordered peak is both a function of χ_{eff} and contrast. Contrast in neat systems quantifies the difference in electron density in the two blocks of the block copolymer, and is given by

$$C_{\mathrm{neat}} = \left(\frac{b_{\mathrm{EO}}}{v_{\mathrm{EO}}} - \frac{b_{\mathrm{MMA}}}{v_{\mathrm{MMA}}} \right)^2 \tag{2.17}$$

where b_{EO} and b_{MMA} are the respective X-ray scattering lengths of the two components based on pure component densities.

As seen in Figure 2.3, peak intensity increases as salt concentration increases. Increasing peak intensity can correspond to either an increase in χ or an increase in contrast. In block copolymer electrolytes, the contrast depends crucially on salt distribution between the two blocks. If we assume that the salt preferentially segregates in the PEO fluctuations, contrast

is given by

$$C_{\mathrm{PEO-salt}} = v_{\mathrm{ref}} \left(\frac{b_{\mathrm{EO}} + \left(\frac{n_{\mathrm{LiTFSI}}}{n_{\mathrm{EO}}}\right) b_{\mathrm{LiTFSI}}}{v_{\mathrm{EO}} + \left(\frac{n_{\mathrm{LiTFSI}}}{n_{\mathrm{EO}}}\right) v_{\mathrm{LiTFSI}}} - \frac{b_{\mathrm{MMA}}}{v_{\mathrm{MMA}}} \right)^2 \tag{2.18}$$

where n_{EO} is the number of ethylene oxide monomers per chain.[34] At the other extreme, one might assume that salt is uniformly distributed in both kinds of fluctuations and in this case, the contrast is given by

$$C_{\mathrm{uniform\ salt}} = \phi_{\mathrm{polymer}} \left(\frac{b_{\mathrm{EO}}}{v_{\mathrm{EO}}} - \frac{b_{\mathrm{MMA}}}{v_{\mathrm{MMA}}} \right)^2 \tag{2.19}$$

where ϕ_{polymer} is the overall volume fraction of polymer in the polymer-salt mixture.[11] The final option is an adjustable contrast model, first developed by Chintapalli et al., wherein C depends on the partitioning of LiTFSI between the PEO-rich and the PMMA-rich concentration fluctuations.[79] This partitioning is quantified by a salt affinity fit parameter, γ which can vary between 0 and 1. The expression for contrast is

$$C(\gamma) = v_{\mathrm{ref}} \left(\frac{b_{\mathrm{EO}} + p(\gamma) \left(\frac{n_{\mathrm{LiTFSI}}}{n_{\mathrm{EO}}}\right) b_{\mathrm{LiTFSI}}}{v_{\mathrm{EO}} + p(\gamma) \left(\frac{n_{\mathrm{LiTFSI}}}{n_{\mathrm{EO}}}\right) v_{\mathrm{LiTFSI}}} - \frac{b_{\mathrm{MMA}} + (1 - p(\gamma)) \left(\frac{n_{\mathrm{LiTFSI}}}{n_{\mathrm{MMA}}}\right) b_{\mathrm{LiTFSI}}}{v_{\mathrm{MMA}} + (1 - p(\gamma)) \left(\frac{n_{\mathrm{LiTFSI}}}{n_{\mathrm{MMA}}}\right) v_{\mathrm{LiTFSI}}} \right)^2 \tag{2.20}$$

where n_{MMA} is the number of MMA monomers per chain, calculated as $n = M_{\mathrm{Polymer}}/M_{\mathrm{Monomer}}$, and b_{EO}, b_{MMA} and b_{LiTFSI} are the respective X-ray scattering lengths of the three components based on pure component densities.[79] In equation 2.20, p is given by:

$$p(\gamma) = \frac{n_{\mathrm{EO}}\gamma}{n_{\mathrm{EO}}\gamma + n_{\mathrm{MMA}}(1 - \gamma)} \tag{2.21}$$

The parameter γreflects how favorable the LiTFSI-EO interaction is, relative to the LiTFSI-MMA interaction: it is the probability that an LiTFSI molecule will associate with an EO monomer when given the choice between EO or MMA. In the case where $n_{\mathrm{EO}} = n_{\mathrm{MMA}}$, $\mathrm{p}(\gamma) = \gamma$. Thus, $\mathrm{p}(\gamma)$ represents the fraction of LiTFSI in the PEO-rich fluctuations.

An important parameter is the volume fraction of the PMMA-rich fluctuation in the presence of salt. This is given by

$$\phi_{\mathrm{MMA}}(\gamma) = \frac{n_{\mathrm{MMA}} v_{\mathrm{MMA}} + (1 - p(\gamma)) n_{\mathrm{LiTFSI}} v_{\mathrm{LiTFSI}}}{n_{\mathrm{MMA}} v_{\mathrm{MMA}} + n_{\mathrm{LiTFSI}} v_{\mathrm{LiTFSI}} + n_{\mathrm{EO}} v_{\mathrm{EO}}} \tag{2.22}$$

Figure 2.4 plots the best fits of equation 2.9 through the data of PEO-PMMA(10-64)/LiTFSI with $m = 0.44$ mol Li/ kg polymer at 90°C with χ_{eff} and a as adjustable variables. We begin by comparing the predictions using the contrast calculated with the uniform salt assumption (equation 2.19). This fit overestimates the peak intensity and underestimates the intensity in the wings. Next, we compare predictions using the contrast calculated with the PEO-salt assumption (equation 2.18). This fit underestimates the peak intensity and overestimates

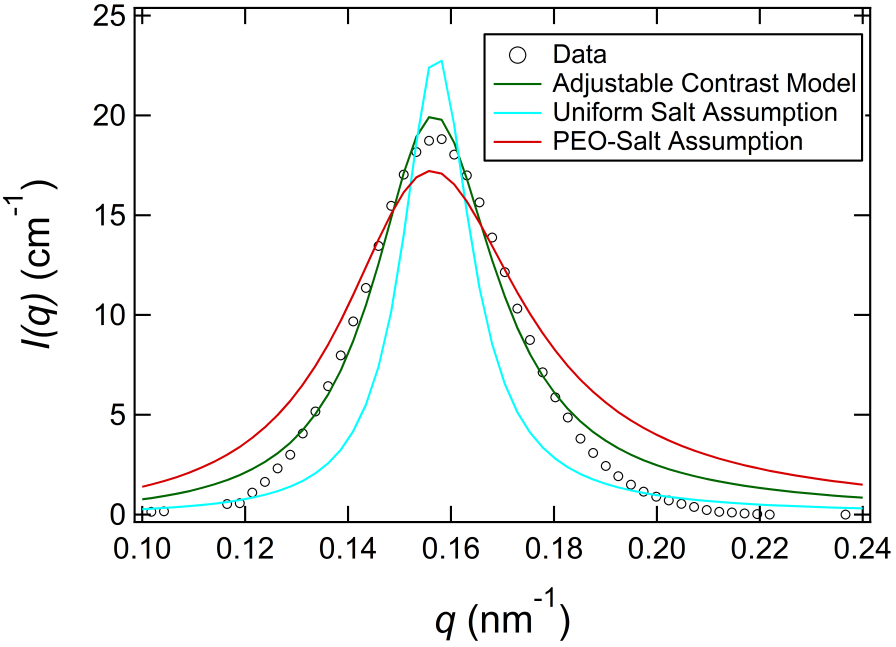

Figure 2.4: The circles represent data of PEO-PMMA(10-64)/LiTFSI with $m = 0.44$ mol Li/ kg polymer at 90°C. The curves represent best fits using three different models with χ_{eff} as the main adjustable parameter.

the intensity in the wings. The lack of agreement between these two fitting procedures indicates that the salt ions are neither completely segregated in the PEO-rich fluctuations, nor uniformly dispersed between the PEO-rich and PMMA-rich fluctuations. We are thus forced to use the adjustable contrast model (equations 20-22) with χ_{eff}, a, and γ as adjustable fit parameters. We find quantitative agreement between the experimental data and this model. The chain stretching parameter, a, ranges between 1.68 and 1.74, as reported in the SI (between 1.68 and 1.74). These values are larger than those for PEO-PS/LiTFSI mixtures which range between 0.8 and 1.4.[7]

Figure 2.5a shows background subtracted scattering profiles of PEO-PMMA(10-64) for the $m = 0.22$ mol Li/ kg polymer electrolyte from 70°C to 150°C. When the temperature is increased from 70°C to 90°C the peak intensity decreases from 6 to 3.5 cm^{-1}: the peak at 90°C is slightly narrower than the peak at 70°C. The peak intensity is insensitive to temperature between 90°C and 130°C but a slight narrowing is evident with increasing temperature. Further increase of temperature from 130°C to 150°C results in a decrease in peak intensity to 3 cm^{-1} and a slight decrease in peak width. In pure copolymer melts, a decrease in peak intensity is a signature of a decrease in χ (C is fixed).[39,80] However, this decrease is generally a smooth function of temperature. Changes in the scattering profiles in Figure 2.5a, which are not smooth, may occur due to changes in C or χ_{eff}. We fitted the data to the adjustable contrast model to distinguish between these two effects. In Figure 2.5b we

compare experimental data with fits. It is evident that the complex trends seen in Figure 2.5a are captured by our model, provided χ_{eff}, a, and γ are used as adjustable parameters. This fitting procedure was applied to scattering curves at $m = 0.22$, 0.28 and 0.44 mol Li/kg polymer for all temperatures. The dependence of χ_{eff} on 1000/T for different salt concentrations is shown in Figure 2.6a. The data obtained at the given salt concentration is consistent with the expression often used to describe the temperature dependence of the Flory Huggins interaction parameter:

$$\chi_{\text{eff}} = \frac{A}{T} + B. \tag{2.23}$$

The solid lines in Figure 2.6a are the fits for each salt concentration based upon equation 2.23 and are used to extract the A and B parameters. The parameters A and B thus obtained are shown in Table 2.2. χ_{eff} decreases with increasing temperature implying that A is positive. The values of A obtained at different salt concentrations are within experimental error; the lines in Figure 2.6a are nearly parallel. The parameter B decreases with salt concentration as shown in Table 2.2.

m (mol Li/ kg polmyer)	Ax10^3	B	R^2
0.22	3.2 ± 0.68	0.025 ± 0.0018	0.89
0.28	3.6 ± 0.46	0.023 ± 0.0012	0.95
0.44	3.0 ± 0.46	0.024 ± 0.0012	0.93

Table 2.2: χ_{eff} fit parameters

It is noteworthy that χ_{eff} is a smooth function of temperature at $m = 0.22$ mol Li/ kg polymer (Figure 2.6a), despite the fact that the peak intensity is not a smooth function of temperature (Figure 2.5a). This conclusion was only reached after the partitioning of LiTFSI was accounted for. At this salt concentration, p lies within a narrow window of 0.90 and 1.0. In other words, most of the LiTFSI is associated with the PEO-rich fluctuations. However, accounting for the small concentration of LiTFSI in the PMMA-rich fluctuations is crucial for quantitative analysis of the SAXS data. The partitioning of salt in the PMMA-rich fluctuations increases with increasing salt concentration as seen in Figure 2.6b. The smallest values of p are obtained at $m = 0.44$ mol Li/ kg polymer: they lie between 0.86 and 0.80. The dependence of p on temperature varies qualitatively with salt concentration. The dependence of a on m and T is given in the SI (Figure 2.12).

Figure 2.7 shows χ_{eff} plotted as a function of salt concentration at 90°C. For the three salt concentrations at which χ_{eff} values were measured explicitly, χ_{eff} decreases more-or-less linearly with increasing m. However, the SAXS data obtained at other salt concentrations indicates a more complex relationship between χ_{eff} and m. In any SAXS experiment on disordered block copolymers, χ_{eff} can only be determined if scattering from the disordered phase rises above the background. Since the scattering intensity increases monotonically

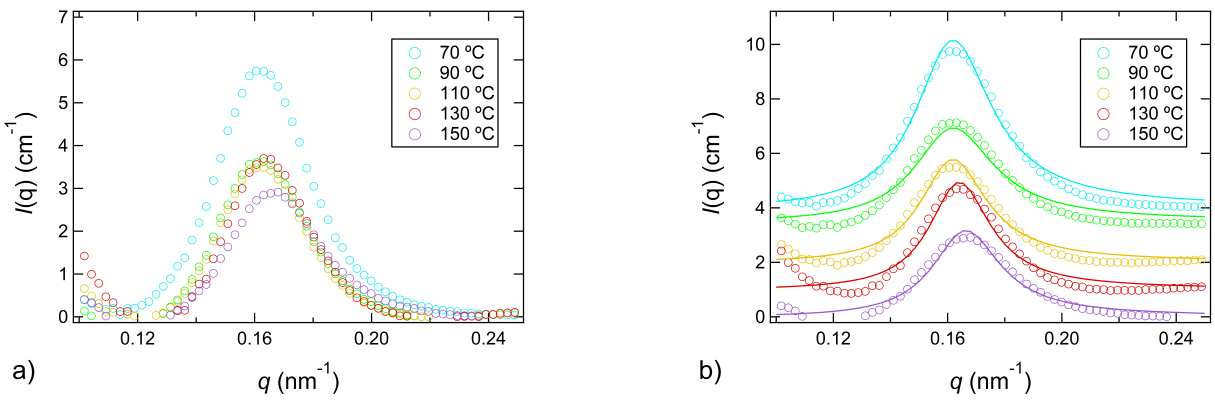

Figure 2.5: In (a) background subtracted scattering profiles of the PEO-PMMA(10-64) m = 0.22 mol Li/kg polymer electrolyte are plotted as a function of the scattering vector, q from 70 to 150°C. In (b) the RPA fits for each scattering profile of the PEO-PMMA(10-64) m = 0.22 mol Li/kg polymer electrolyte are plotted against the background subtracted data as a function of the scattering vector, q from 70 to 150°C. The absolute $I(q)$ for T = 150°C is presented. Data from 130, 110, 90 and 70°C are shifted vertically by 1, 2, 3.5, and 4 cm^{-1} respectively for clarity.

with increasing χ_{eff}, there is an upper limit on the value of χ_{eff} that can be measured. We systematically changed χ_{eff}, calculated $I_{\text{dis}}(q)$ using equations 9 to 16 and found that when $\chi_{\text{eff}} = \chi_{\text{limit}} = 0.029$ the magnitude of $I_{\text{dis}}(q^*)$ is a factor of 1.06 above $I_{\text{bkgd}}(q^*)$. In other words, if χ_{eff} were less than or equal to χ_{limit} then the scattering signature of disordered fluctuations would be undetectable. We know that this is the case for PEO-PMMA/LiTFSI mixtures with $m < 0.22$ mol Li/kg polymer and $m > 0.44$ mol Li/ kg polymer; see scattering profiles in these salt concentration ranges in Figure 2.2. For completeness, we also show χ_{limit} at the salt concentrations where no SAXS peaks were detectable in Figure 2.7. The lines in Figure 2.7 connect adjacent data points. The data in Figure 2.7 reveal that χ_{eff} is a non-monotonic function of m. Below m = 0.22 mol Li/ kg polymer, χ_{eff} increases with added salt. Above m = 0.44 mol Li/ kg polymer χ_{eff} decreases with added salt. It is known that χ between PMMA and PEO in the absence of salt is -7.8E-04.[55,70] Our observation of increasing χ_{eff} with added salt in the low salt concentration regime is consistent with this result, as shown in the inset of Figure 2.7. The non-monotonic relationship between χ_{eff} and salt concentration may be explained by a competition between ion solvation, screening, and entropic effects.[7,37,64,69] At low salt concentrations, ion solvation effects dominate, which drives ordering, while at high salt concentration, entropic effects dominate, which drives disordering. Above m = 0.44 mol Li/ kg polymer, χ_{eff} decreases with added salt. We posit that the lack of scattering peaks in samples with $m > 0.44$ mol Li/ kg polymer in PEO-PMMA(10-64) seen in Figure 2.2b is attributed to the fact that χ_{eff} is below χ_{eff} (0.029). We will return to this point shortly.

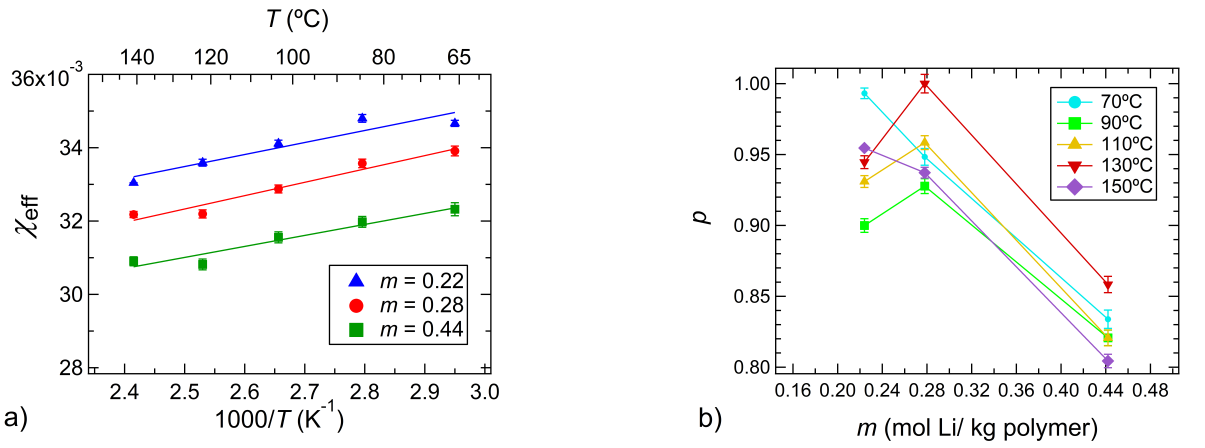

Figure 2.6: In (a) χ_{eff} is plotted against inverse temperature to calculate χ_{eff} as a function of temperature at each salt concentration with a disordered peak. Fit parameters can be seen in Table 2.2. In (b) fraction of lithium salt in PEO fluctuation (p) as derived from RPA fits is plotted as a function of salt concentration. Each trace represents a temperature from SAXS measurements.

Our definition of χ_{limit} is affected by our choice of two parameters: (1) The assumption that a disordered SAXS peak is detectable when $I_{\text{dis}}(q^*)$ is 6% higher than $I_{\text{bkgd}}(q^*)$, and (2) the exact value of m chosen for the calculation. If we assume that disordered SAXS peak is detectable when $I_{\text{dis}}(q^*)$ is 10% higher than $I_{\text{bkgd}}(q^*)$, χ_{limit} would be 0.0315. If we change the value of m to 0.44 mol Li/kg polymer to calculate χ_{limit}, then χ_{limit} is 0.020. Our main conclusions based on the data in Figure 2.7 are unaffected by the particular values we have chosen for these parameters.

In the field of block copolymer electrolytes,[35,36,39,48,49,81,82] it is customary to plot χ_{eff} as a function of salt concentration as we have done in Figure 2.7. For example, in the case of PEO-PS block copolymer systems, it is customary to plot χ_{eff} as a function of r, the molar ratio of lithium ions and ethylene oxide monomers ($r = [\text{Li}]/[\text{EO}]$).[35,39,48] The implicit assumption in such plots is that the salt resides exclusively in the PEO-rich fluctuations. For the case PEO-PMMA/LiTFSI it is important to show χ_{eff} as a function of salt concentration in both PEO-rich and PMMA-rich fluctuations. Using p, we can calculate the amount of lithium in the PEO-rich and PMMA-rich fluctuations as given by

$$r = \frac{p\,[\text{Li}]}{[\text{EO}]} \tag{2.24}$$

and

$$z = \frac{(1-p)\,[\text{Li}]}{[\text{MMA}]} \tag{2.25}$$

In Figure 2.8 we plot χ_{eff} at 90°C as a function of r and z. The thermodynamic properties of PEO-PMMA/LiTFSI mixtures as a function of added salt is described by a trajectory of χ_{eff}

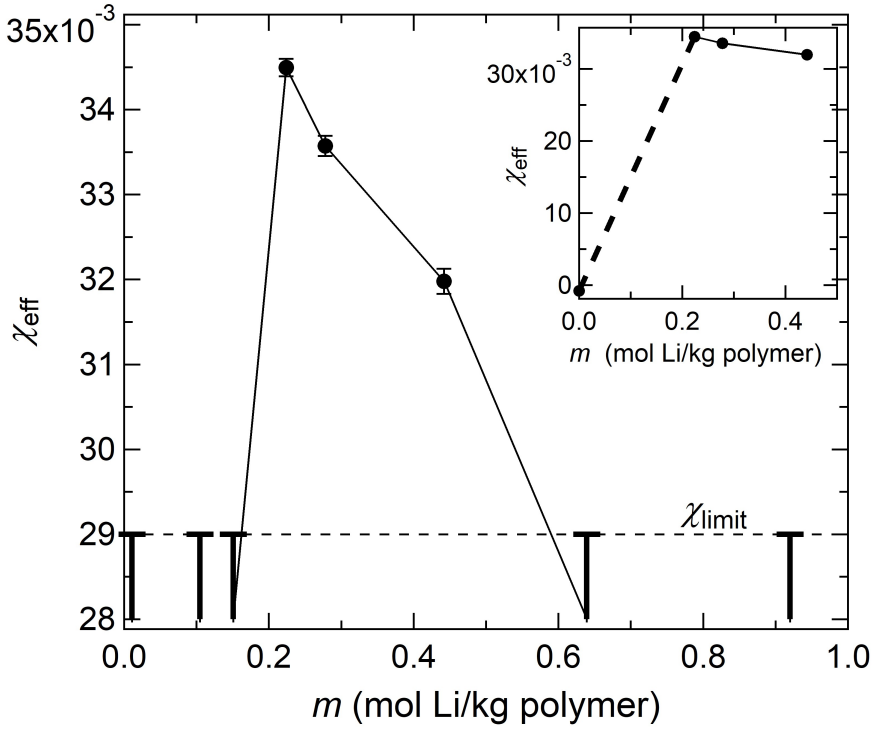

Figure 2.7: χ_{eff} is plotted as a function of salt concentration at 90°C. The error bars represent the minimum χ value required for a disordered peak. The inset plots the three calculated χ_{eff} with the negative χ parameter from Russell and coworkers for a neat PEO-PMMA system.[55] The dotted line represents χ_{limit}, or the minimum χ parameter required to observe a disordered peak.

as a function of r and z. χ_{eff} is a monotonically decreasing function of r but a non-monotonic function of z. At the highest salt concentration studied, the value of r in the PEO-rich fluctuations is 0.15. As this concentration is approached, the value of z increases substantially, suggesting a large driving force for LiTFSI to reside in PMMA-rich fluctuations. It is known that in mixtures of homopolymer PEO and LiTFSI lithium ions are coordinated with 6 ether oxygens, corresponding with $r = 1/6 = 0.16$.[83–85] The data in Figure 2.8 suggests that salt partitioning in to the PMMA-rich fluctuations become significant when this concentration is reached in the PEO-rich fluctuations. Unfortunately, the systems investigated thus far have only revealed a small portion of χ_{eff} as a function of r and z, limiting the conclusions that can be drawn on the mechanisms underlying LiTFSI partition. Despite this limitation, the data shown in Figures 6, 7, and 8 provide a starting point for quantifying the effect of added salt on PEO-PMMA block copolymers.

The most non-intuitive result of our study is contained in Figure 2.2b, where we see that the addition of salt leads to an emergence of a scattering peak that increases in intensity up

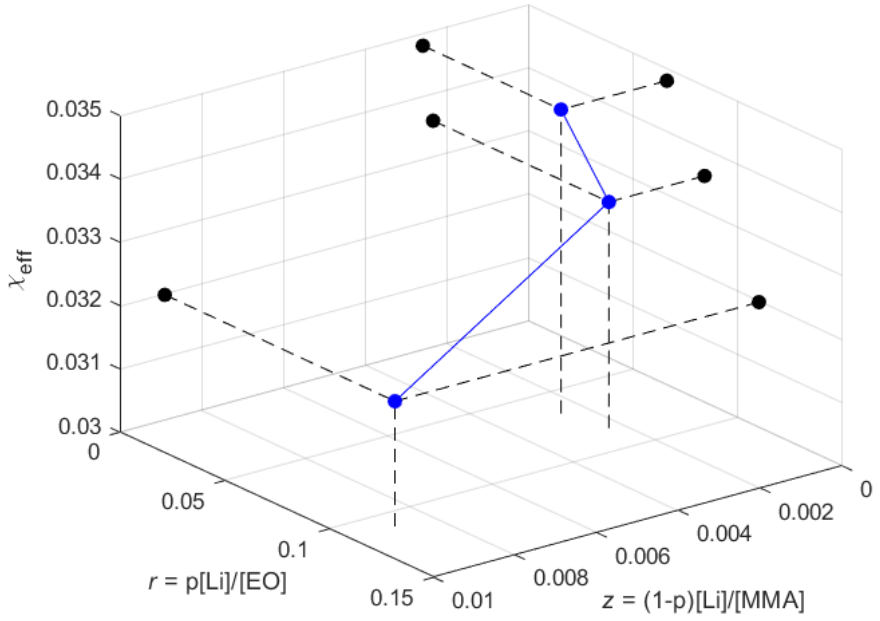

Figure 2.8: χ_{eff} plotted as a function of salt concentrations $r = p$[Li]/[EO] and $z = (1\text{-}p)$[Li]/[MMA]. The blue trace is measured χ_{eff} as a function of both salt concentrations.

to $m = 0.44$ mol Li/ kg polymer: further increase in salt concentration to $m = 0.64$ mol Li/kg polymer results in the disappearance of this peak. To understand this result, we need to quantify the dependence of scattering contrast on m. In Figure 2.9a, we show the scattering length densities of PMMA/LiTFSI and PEO/LiTFSI mixtures as a function of added salt, z and r. The two circles on each curve represent the values of r and z that are covered in this study. The SAXS intensity is affected by the vertical distance between the corresponding points, as shown in Figure 2.9a: C is given by the square of this distance. For completeness, in Figure 2.9b, we plot C as a function of m which is affected by the dependence of p on m, which is also shown in the figure. Here we see that C increases monotonically as a function of m despite the fact that salt partitioning, p, decreases with m. We expect the contrast between PMMA-rich and PEO-rich fluctuations to increase with increasing m. We can thus assert that the lack of a scattering peak at $m = 0.64$ mol Li/ kg polymer is not due to a lack of contrast but a decrease in χ_{eff}. The increase in peak intensity with salt concentration seen in Figure 2.3 is entirely due to an increase in contrast. In fact, χ_{eff} decreases with salt concentration.

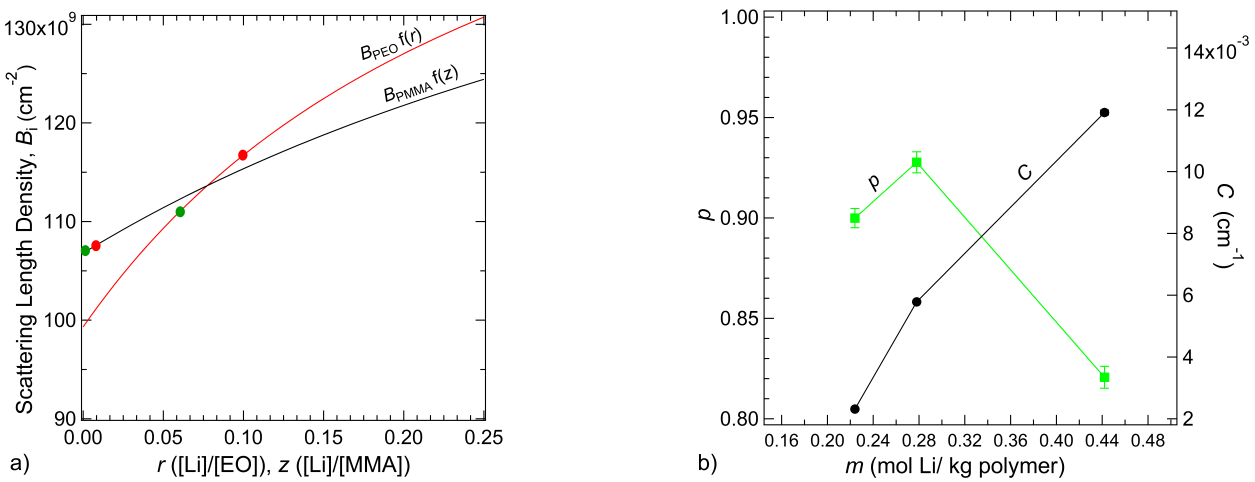

Figure 2.9: In (a) scattering length densities (B_i) for PEO and PMMA are plotted as a function of r and z. The circles on each curve represent the calculated salt concentrations covered within this study. The green circles show the lowest end of the salt concentration and the red circles show the highest end. In (b) p and contrast are plotted as a function of salt concentration (m) at 90°C.

2.5 Conclusions

In this paper, we described the synthesis and characterization of PEO-PMMA block copolymer electrolytes. The polymers were synthesized using a macroinitiator comprising of a 10 kg mol^{-1} PEO chain with a α-bromophenylacetate terminus. The targeted PMMA block was then obtained via ATRP. The thermodynamic interactions between PEO and PMMA were previously characterized by Ito et al. based on SANS experiments on blends containing deuterated PMMA.[55] The Flory Huggins interaction parameter between PEO and PMMA is negative, implying single-phase systems would be obtained regardless of composition, chain length and temperature. Thermodynamic interactions in polymer blends and block copolymers can readily be determined by studying scattering from homogeneous systems that are close to phase boundaries. In these systems the measured scattering profiles contain signatures of concentration fluctuations, that may be considered as announcements of phase transitions. The challenge was to design PEO-PMMA block copolymers that would exhibit these signatures in the presence of added salt. We addressed this challenge by studying two series of mixtures of PEO-PMMA block copolymers and LiTFSI using SAXS.

The SAXS profiles of PEO-PMMA(10-33) were featureless in the neat state and at all salt concentrations. This series of mixtures provided no information on the effect of salt on the thermodynamic interactions between PEO and PMMA. The SAXS profiles of a more asymmetric block copolymer, PEO-PMMA(10-64), exhibited signatures of concentration fluctu-

ations at intermediate salt concentrations. Featureless SAXS profiles were obtained in this series at both low and high salt concentrations. Conventional thermodynamic models of uncharged block copolymer systems lead to the conclusion that signatures of order formation should be suppressed in more asymmetric block copolymers. However, ionic SCFT first developed by de la Cruz and coworkers,[41] indicates that added salt would enhance the signatures of order formation in more asymmetric block copolymers. Our results provide substantial support for the validity of ionic SCFT.

Direct mapping of experimental data on ionic SCFT predictions is non-trivial and has only been done in the case of the well-studied PEO-PS electrolytes.[72] This mapping was possible due to the availability of numerous experimental studies on concentration fluctuations in disordered mixtures of PEO-PS/LiTFSI and determination of phase boundaries in weakly ordered systems. The limited data we currently have on PEO-PMMA/LiTFSI mixtures precludes such mapping. Our analysis is thus based on using the SAXS profiles to estimate χ_{eff} using Leibler's random phase approximation. Our fitting procedure is an extension of previous work on PEO-PS electrolytes,[34] accounting for partitioning of salt between the PEO and PMMA phases. In PEO-PMMA/LiTFSI mixtures we show that χ_{eff} is a complex non-monotonic function of added salt. Such complexities may arise due to the interplay between ion solvation, screening and entropy.[7,37,64,69] The dependence of thermodynamic interactions on added salt is thus presented on a three-dimensional plot that accounts for the partitioning of the salt between the PEO-rich and the PMMA-rich concentration fluctuations (Figure 2.8).

Our work lends considerable support to ionic SCFT and related models that account for polymer-ion interactions for thermodynamic predictions of phase behavior.[41,42,46] It also provides a foundation for designing microphase separated block copolymer electrolytes in systems wherein the blocks exhibit attractive interactions with each other in the absence of salt, a foundation that did not exist when we began this study.

2.6 Acknowledgements

This research was supported by the National Science Foundation grant DMR 1904508 to the University of California, Berkeley, and CHE 2000391 to Carnegie Melon University. This research used resources of the Advanced Light Source, a U.S. DOE Office of Science User Facility under contract no. DE-AC02-05CH11231. Experiments conducted at the Stanford Synchrotron Radiation Lightsource, SLAC National Accelerator Laboratory, is supported by the U.S. Department of Energy, Office of Science, Office of Basic Energy Sciences under Contract No. DE-AC02-76SF00515.

2.7 Nomenclature

a_{i}, statistical segment length of species i (nm)

b_{i}, X-ray scattering length of species i (nm mer^{-1})

C, electron density contrast (cm^{-1})

$Đ$, dispersity

$I(q)$ scattering intensity (cm^{-1})

$I_{\mathrm{dis}}(q)$ disordered scattering intensity (cm^{-1})

$I_{\mathrm{bkgd}}(q)$ background scattering intensity (cm^{-1})

$I_{\mathrm{tot}}(q)$ total scattering intensity (cm^{-1})

M_{i}, molar mass of species i ($g\ mol^{-1}$)

M_{w}, weight-averaged molar mass ($kg\ mol^{-1}$)

M_{n}, number-averaged molar mass ($kg\ mol^{-1}$)

M_{PEO}, molar mass of species poly(ethylene oxide) ($g\ mol^{-1}$)

M_{PMMA}, molar mass of species poly(methyl methacrylate) ($g\ mol^{-1}$)

m, molality (mol Li/ kg polymer)

n_{i}, chemical repeat units for species i

N, degree of polymerization

N_{i}, degree of polymerization for species i

p, fraction of lithium in ethylene oxide fluctuation

q, scattering vector (nm^{-1})

q^*, scattering vector at the primary scattering peak (nm^{-1})

r, salt concentration in PEO ([Li] $[EO]^{-1}$)

R_{g}, radius of gyration (nm)

T, temperature (°C)

z, salt concentration in PMMA ([Li] $[MMA]^{-1}$)

Greeks

γ, affinity parameter between salt and polymer fluctuation

v_{i}, molar volume of species i ($\mathrm{cm^{-3}\ mol^{-1}}$)

v_{ref}, Reference volume of species i ($\mathrm{cm^{3}\ mol^{-1}}$)

ρ_{i}, density of species i ($\mathrm{g\ cm^{-3}}$)

ϕ_{i}, volume fraction of species i

χ, Flory-Huggins interaction parameter

χ_{eff}, Flory-Huggins interaction parameter of PEO-PMMA/LiTFSI

2.8 Supporting Information

NMR Spectra

The composition of the PEO-PMMA block copolymers was determined using ^{1}H NMR ($CDCl_3$, Brucker AV400). The composition was calculated by integrating the ethylene proton peak at 3.64 ppm against the proton peak for the methyl group on the MMA repeat units at 1.02. 0.85 and 3.60 ppm.

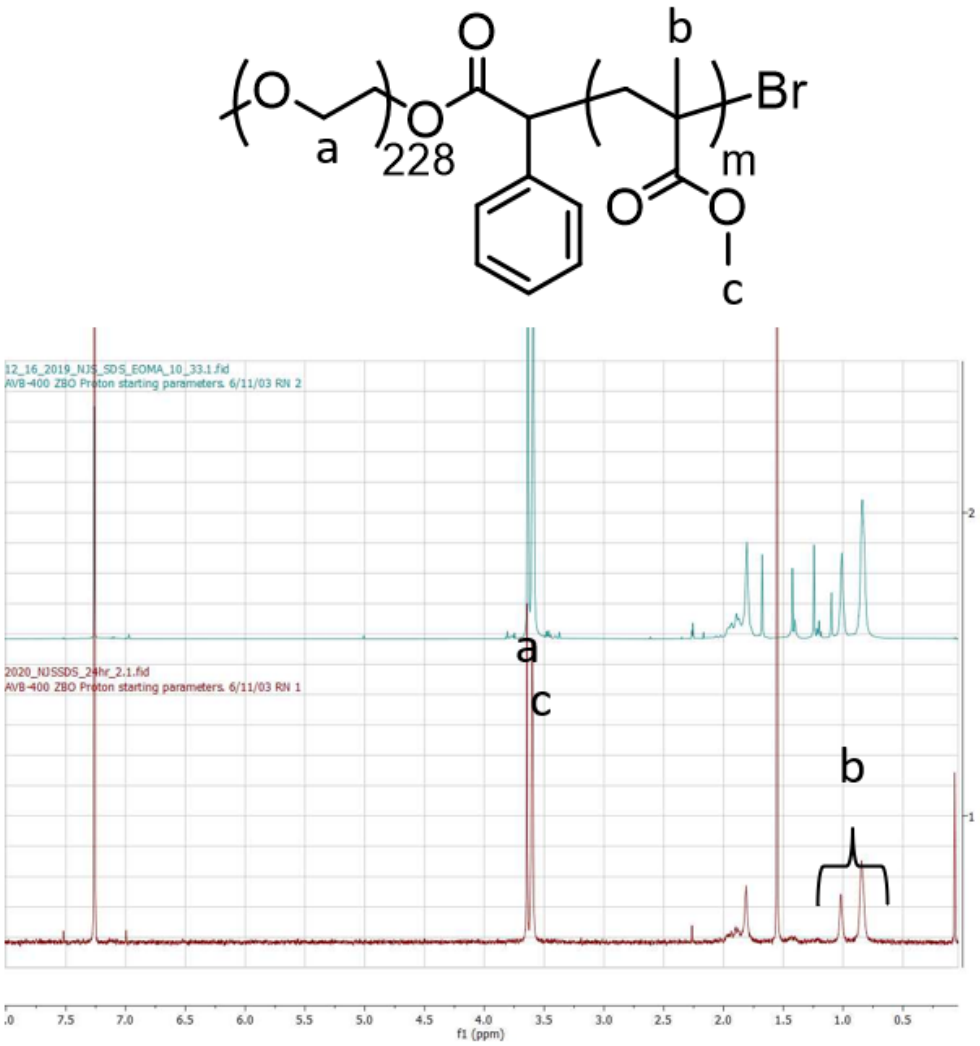

Figure 2.10: ^{1}H NMR of PEO-PMMA. The peak (a) at $\delta = 3.64$ ppm is the hydrogen peak for PEO. Peaks at 0.85 ppm and 1.02 ppm (b) represent the PMMA methyl hydrogens and the peak at 3.60 ppm (c) represents the PMMA carboxyl hydrogen.

Gel Permeation Chromatography

PEO-PMMA was characterized on an Agilent 1260 Infinity Series gel permeation chromatography (GPC) system with Waters Styragel HR3 and HR4 columns with a N-methyl-2-pyrrolidone (NMP) mobile phase. GPC was used to determine molecular weight distribution and was used to verify NMR determined molecular weights.

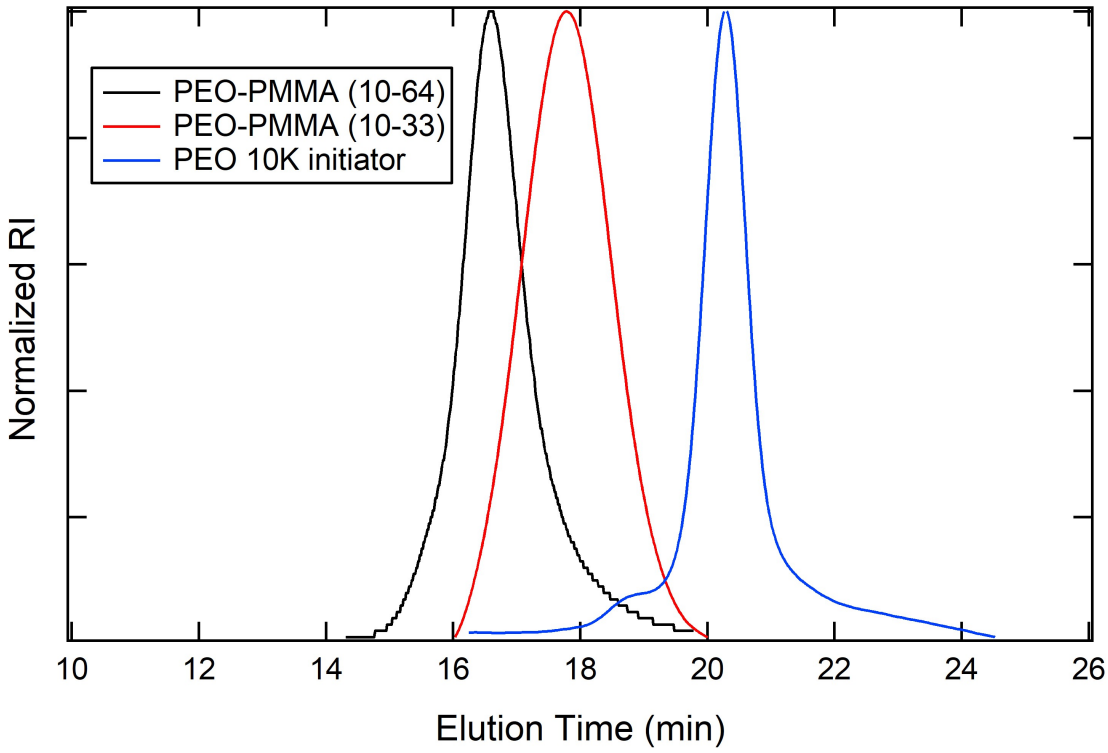

Figure 2.11: Gel permeation chromatography data on PEO-PMMA copolymers and PEO macoinitiator used in this study.

PEO-PMMA Synthesis

PEO-PMMA (10-33)

PEO-PMMA block copolymer was synthesized via atom transfer radical polymerization (ATRP) using a macroinitiator comprising of a 10 kg mol^{-1} PEO chain with a *α*-bromophenylacetate terminus. The PEO-*α*-bromophenylacetate macroinitiator (5 g, 0.5 mmol, 1 equiv.) was dissolved in degassed anisole (20 mL) at room temperature in a sealed 50 mL round bottom flask. A copper wire (treated in a solution of HCl in methanol), $CuBr_2$ (2.1 mg, 9.4 µmol, 0.02 equiv. dissolved in DMSO), *N,N,N',N",N"*-pentamethyldiethylenetriamine (PMDETA, 18 µL, 0.18 equiv.) and methyl methacrylate monomer (20 mL, 188 mmol, 400 equiv.) were added to the reaction mixture. The reaction to proceeded for 18 hours at room temperature. The reaction was stopped by dilution with tetrahydrofuran (THF) and subsequent passage through a basic alumina filter to remove the copper ions. The polymer was twice reprecipitated in water.

PEO-PMMA (10-64)

PEO-PMMA block copolymer was synthesized via atom transfer radical polymerization (ATRP) using a macroinitiator comprising of a 10 kg mol^{-1} PEO chain with a *α*-bromophenylacetate terminus. The PEO-*α*-bromophenylacetate macroinitiator (0.5 g, 0.05 mmol, 1 equiv.) was dissolved in degassed anisole (2 mL) at room temperature in a sealed 10 mL round bottom flask. A copper wire (treated in a solution of HCl in methanol), $CuBr_2$ (0.21 mg, 0.94 µmol, 0.02 equiv. dissolved in DMSO), *N,N,N',N",N"*-pentamethyldiethylenetriamine (PMDETA, 1.8 µL, 0.18 equiv.) and methyl methacrylate monomer (6 mL, 56 mmol, 1130 equiv.) were added to the reaction mixture. The reaction proceeded for 24 hours at room temperature. The reaction was stopped by dilution with tetrahydrofuran (THF) and subsequent passage through a basic alumina filter to remove the copper ions. The polymers were twice reprecipitated in water.

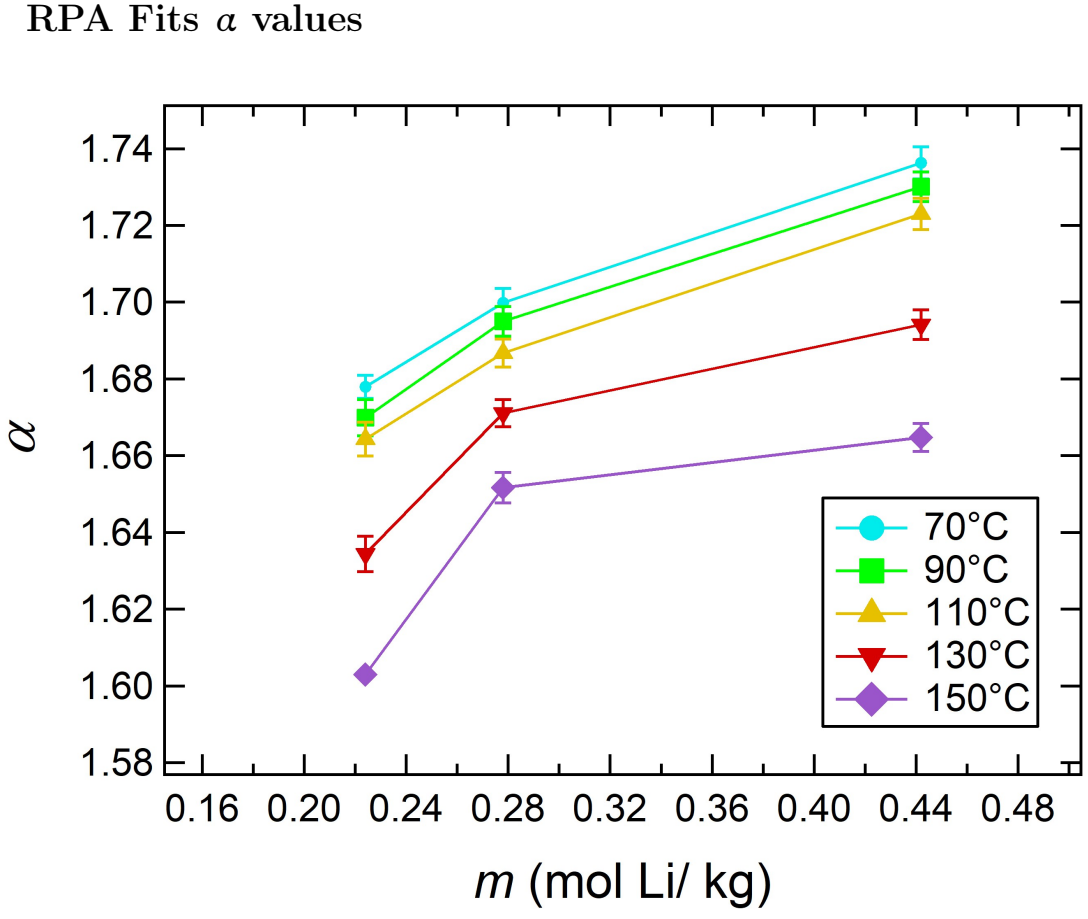

Figure 2.12: Chain stretching (a) of PEO-PMMA copolymers used in this study.

PDI Model Figures

All of the analysis of the SAXS profiles in the main text is based on RPA for monodisperse block copolymers. In this section we quantify the effect of polydispersity on that analysis. The expressions for scattering from a diblock copolymer with finite polydispersity index (PDI) are given below.[33,34] The procedures used to match experiment and theory were identical to those described in the main text and the results are displayed in Figures 2.4 to 2.9. The value of PDI used in the calculation was 1.21. None of the conclusions in the main text are affected by finite polydispersity.

$$S_{\mathrm{ii}}{}^{\circ} = Ng(f_i) \;\; (i = A, B) \tag{2.26}$$

$$S_{\mathrm{AB}}{}^{\circ} = S_{\mathrm{BA}}{}^{\circ} = \left(\frac{N}{2}\right)\left(g\left(1\right) - g\left(f_A\right) - g\left(f_B\right)\right) \tag{2.27}$$

$$k = \frac{1}{PDI - 1} \tag{2.28}$$

$$g\left(f_i\right) = \left(\frac{2}{x^2}\right)\left[f_i x + \left[\frac{k}{(k + f_i x)}\right]^k - 1\right] \;\; (i = A, B) \tag{2.29}$$

$$x = q^2 R_g^2 \tag{2.30}$$

$$R_g^2 = \left(\frac{(N_a b_a^2 + N_b b_b^2)}{6}\right) \tag{2.31}$$

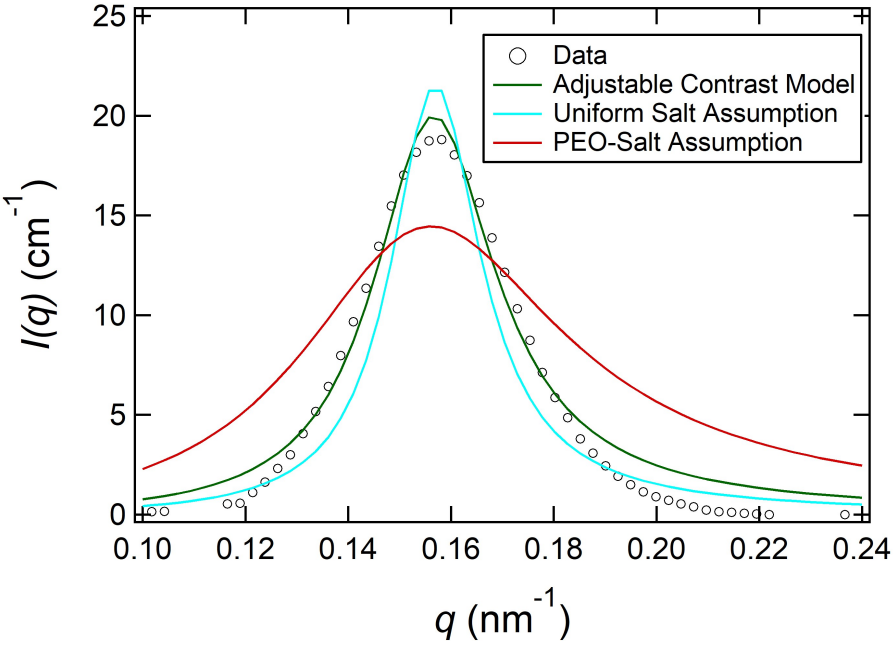

Figure 2.13: The circles represent data of PEO-PMMA(10-64)/LiTFSI with $m = 0.44$ mol Li/ kg polymer at 90 °C. The curves represent best fits using the three different models described in the main text but using equations (2.26-2.31) with PDI equal to 1.21 and χ_{eff} as the main adjustable parameter.

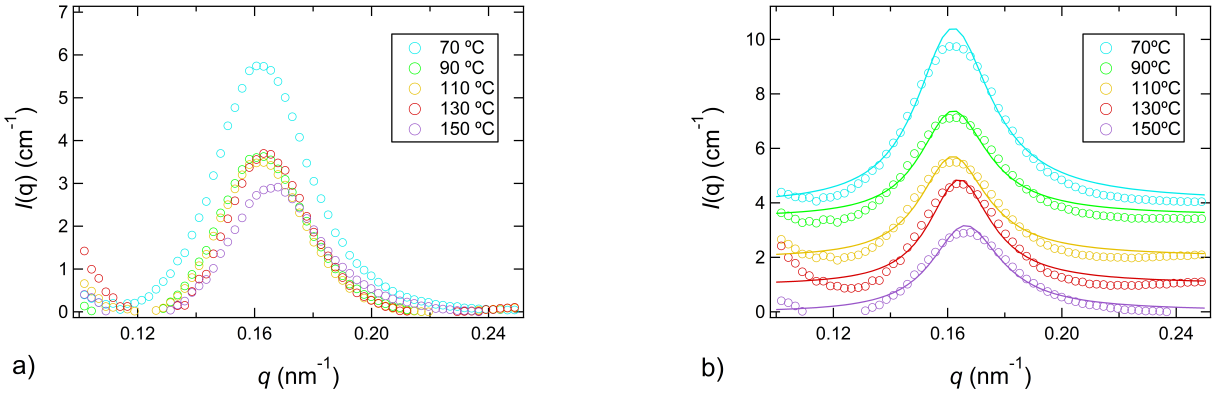

Figure 2.14: In (a) background subtracted scattering profiles of the PEO-PMMA(10-64) m = 0.22 mol Li/kg polymer electrolyte are plotted as a function of the scattering vector, q from 70 to 150°C. In (b) the RPA fits for each scattering profile of the PEO-PMMA(10-64) $m = 0.22$ mol Li/kg polymer electrolyte are plotted against the background subtracted data as a function of the scattering vector, q from 70 to 150°C. The absolute $I(q)$ for $T = 150$°C is presented. Data from 130, 110, 90 and 70°C are shifted vertically by 1, 2, 3.5, and 4 cm^{-1} respectively for clarity.

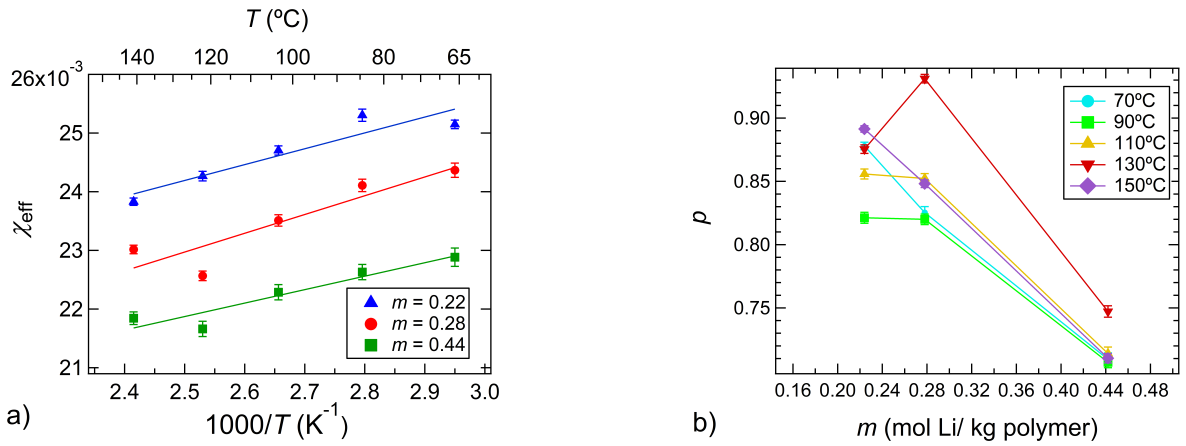

Figure 2.15: In (a) χ_{eff} is plotted against inverse temperature to calculate χ_{eff} as a function of temperature at each salt concentration with a disordered peak. Fit parameters can be seen in Table 2.2. In (b) fraction of lithium salt in PEO fluctuation (p) as derived from RPA fits is plotted as a function of salt concentration. Each trace represents a temperature from SAXS measurements. Both p and χ_{eff} are extracted from RPA fits accounting for a PDI of 1.21.

m (mol Li/ kg polmyer)	Ax10^3	B	R^2
0.22	2.7 ± 0.68	0.017 ± 0.0012	0.87
0.28	3.2 ± 0.85	0.015 ± 0.0023	0.82
0.44	2.3 ± 0.46	0.016 ± 0.0012	0.89

Table 2.3: Alternate χ_{eff} fit parameters from PDI fits

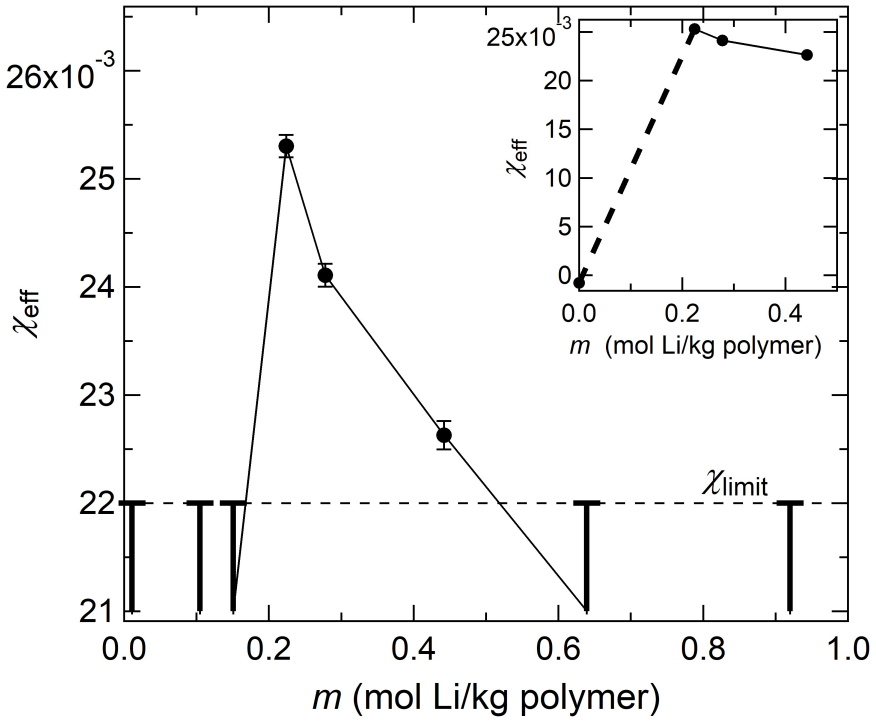

Figure 2.16: χ_{eff} is plotted as a function of salt concentration at 90°C. χ_{eff} was calculated from RPA fits using equations (2.26-2.31) with a PDI equal to 1.21. The error bars represent the minimum χ value required for a disordered peak. The inset plots the three calculated χ_{eff} with the negative χ parameter from Russell and coworkers for a neat PEO-PMMA system.[55] The dotted line represents χ_{limit}, or the minimum χ parameter required to observe a disordered peak.

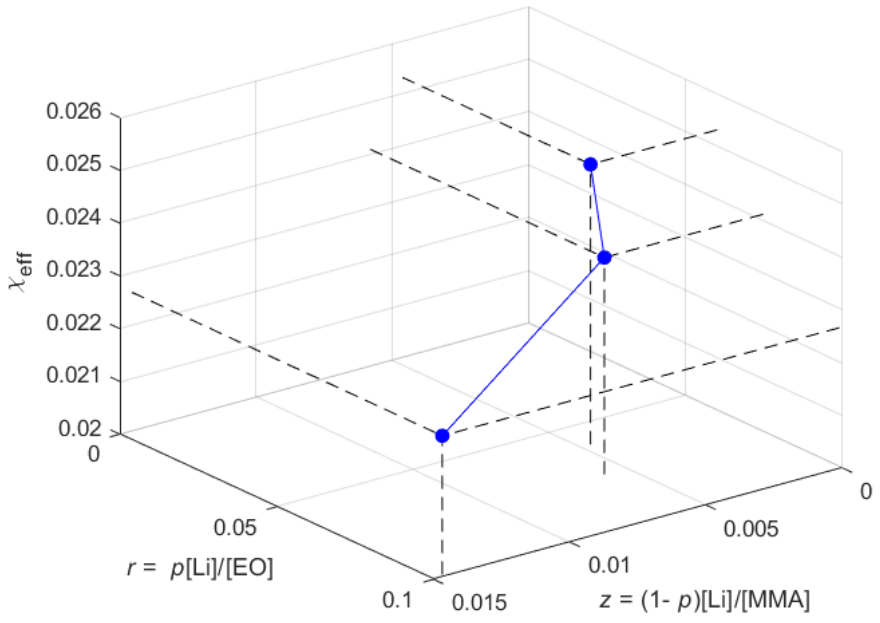

Figure 2.17: χ_{eff} plotted as a function of salt concentrations $r = p$[Li]/[EO] and $z = (1\text{-}p)$[Li]/[MMA]. χ_{eff} was calculated from RPA fits using equations (2.26-2.31) with a PDI equal to 1.21. The blue trace is measured χ_{eff} as a function of both salt concentrations.

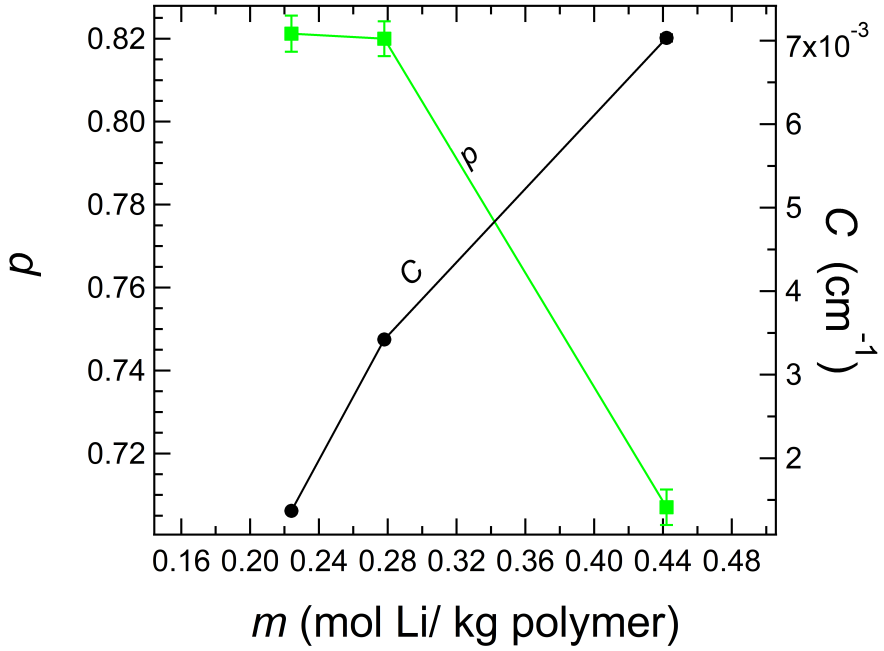

Figure 2.18: p and contrast are plotted as a function of salt concentration (m) at 90°C. p was calculated from RPA fits using equations (2.26-2.31) with a PDI equal to 1.21.

Chapter 3

Thermodynamics and Phase Behavior of Poly(ethylene oxide)/Poly(methyl methacrylate)/Salt Blend Electrolytes Studied by Small Angle Neutron Scattering[2]

3.1 Abstract

We studied the effect of added salt on the thermodynamics of a miscible polymer blend system: poly(ethylene oxide) (PEO) blended with poly(methyl methacrylate) (PMMA). In the absence of salt, PEO/PMMA blends are known to exhibit a negative Flory-Huggins parameter, χ. Not surprisingly, the salt-free PEO/PMMA blends are miscible, regardless of composition. The addition of salt, which in our case was lithium bis(trifluoromethane) sulfonimide (LiTFSI), induced phase separation in majority-PMMA blends while majority-PEO blends remained miscible. The effect of added salt was studied at two salt concentrations, $r = 0.05$ and $r = 0.10$; r is defined as the molar ratio of lithium ions to ether oxygens (r = [Li]/[EO]). The immiscibility window, which was absent at r = 0, grew upon addition of a small amount of salt ($r = 0.05$). Further addition of salt to $r = 0.10$ results in shrinking of the immiscibility window. With small angle neutron scattering (SANS) profiles from homogeneous blends we determined χ in both the presence and absence of salt. We measure the composition dependence of this parameter and use it to predict the phase behavior of PEO/PMMA/LiTFSI blends. We find good agreement between theory and experiment.

[2]Adapted from Shah, N. J., *et al.* Thermodynamics and Phase Behavior of Poly(Ethylene Oxide)/Poly(Methyl Methacrylate)/Salt Blend Electrolytes Studied by Small-Angle Neutron Scattering. ***Macromolecules*** 2023, 56 (7), 2889–2898.

3.2 Introduction

The thermodynamic properties of binary mixtures of two homopolymers have been studied extensively. Numerous papers have been written on the effect of composition, polymer chain length, and temperature on blend miscibility.[16,17,19–26,86,87] The simplest theory that addresses the thermodynamics of binary polymer blends is the Flory-Huggins theory.[14,15] In this theory, the Gibbs free energy of mixing of a homogeneous polymer blend is given by

$$\frac{v\Delta G_{\mathrm{m}}}{k_{\mathrm{B}}T} = \frac{\phi_1 ln\phi_1}{N_1} + \frac{\phi_2 ln\phi_2}{N_2} + \ \chi\phi_1\phi_2 \tag{3.1}$$

where ΔG_{m} is the Gibbs free energy of mixing, k_{B} is the Boltzmann constant, T is the absolute temperature, ϕ_{i} is the volume fraction of component i, N_{i} is the number of repeat units in chain i, v is the reference volume (set to 0.1 nm^3), and χ is the Flory-Huggins interaction parameter, which describes the interactions between monomers of the two polymers labeled 1 and 2.

There is significant interest in studying the effect of added salt on thermodynamic interactions between polymers. Much of this work is motivated by interest in nanostructured electrolytes for lithium batteries which are obtained by mixing salt into a block copolymer wherein the two polymers of interest are covalently linked.[1,39,41,42,62–65,69] In the simplest theories, the thermodynamics of these systems is expressed in terms of an effective Flory-Huggins interaction parameter which captures how the added salt affects the interactions between monomers.[7,35,38,39] The simplest theory that address the thermodynamics of block copolymers is built upon the random phase approximation (RPA), which quantifies the relationship between thermodynamic properties and scattering from neat block copolymers in the absence of salt.[27] The RPA also quantifies the relationship between thermodynamic properties and scattering from binary polymer blends.[12] Small-angle neutron and x-ray scattering profiles obtained from homogenous systems, either neat block copolymers or binary polymer blends, can be fit to expressions based on the RPA to estimate χ. We use the symbol χ to quantify interactions between polymers in the absence of salt. The χ parameter can be used to predict phase behavior: these predictions can then be compared to the experimental data. In principle, χ for block copolymers and polymer blends should be identical and independent of parameters such as chain length and composition. However, the measured χ often depends on these parameters; it is rare to find agreement between χ obtained from block copolymers and polymer blends.[18,88–91] In cases where χ is a function of chain length and composition, the relationship between χ and phase behavior is non-trivial. Additional effects arise when salt is added to polymer mixtures, and it is these effects that are the focus of this paper. In particular, we study the effect of added salt on blends of polyethylene oxide (PEO) and poly (methyl methacrylate) (PMMA).

While numerous papers have been written on the effect of added salt on block copolymers,[35,43,67,92–94] there are only a handful that have been written on the effect of added salt on homopolymer mixtures.[11,40,45] The first study of homopolymer mixtures with added salt was conducted by Xie and coworkers who determined the phase behavior of mixtures of

polystyrene (PS) and PEO with added lithium bis(trifluoromethane) sulfonimide (LiTFSI) salt.[40] In a related study, Wu et al. compared the phase behavior of PEO/PS/LiTFSI with predictions based on an effective χ parameter measured by neutron scattering.[45] In this system, adding salt to a homogeneous blend results in phase separation.[45] Gao et al. studied mixtures of PEO, poly(1,3,6-trioxocane) (P(2EO-MO)) and LiTFSI, and found that the blends phase separated at moderate salt concentrations but homogeneous at high salt concentrations.[11]

While previous studies on salt-containing polymer blends have provided some insight, there are many unknown factors that influence miscibility in these systems. In the absence of salt, PEO/PMMA blends have been thoroughly studied.[50–54] Ito et al. studied a series of PEO/PMMA blends with varying composition and found that all were miscible over the entire temperature window.[55] They used RPA to interpret small angle neutron scattering (SANS) data and found that PEO/PMMA has a negative parameter. Most polymer blends studied in either the absence or presence of salt are characterized[11,17,25,45,70,87] by a positive χ parameter. In Flory-Huggins theory, negative χ parameters occur when the energy of interaction between unlike monomers (1-2 interactions) is less than the average energy of interaction between like monomers (1-1 and 2-2 interactions). In contrast, the well-studied PS/PEO has a positive χ parameter in the salt-free state.[40] The PEO/PMMA/LiTFSI blend electrolyte system provides a unique opportunity to determine the effect of added salt on a system with a negative χ parameter.

In this study, we examine the thermodynamic properties of PEO/PMMA/LiTFSI blend electrolytes. In a related study,[94] SAXS measurements from disordered mixtures of a PEO-PMMA block copolymer and LiTFSI were used to determine the effective χ. We begin our study of blend electrolytes by validating the work of Ito et al., demonstrating that in the absence of LiTFSI, PEO/PMMA blends used in this study are miscible across the entire composition window at the temperature of interest.[55] We then identified the range of salt concentrations and blend compositions over which PEO/PMMA/LiTFSI blends are miscible. We used SANS measurements from homogeneous mixtures to determine the χ parameter and used χ to predict phase boundaries. These predictions are compared to our experiments without resorting to any adjustable parameters.

3.3 Materials and Methods

Polymer Blend Electrolyte Preparation and Composition

The molar masses, M_n, and dispersities, $Đ$, of PEO (Polymer Source), fully deuterated PEO, dPEO (Polymer Source) and PMMA (Polymer Source) used in this study are summarized in Table 3.1. According to Polymer Source the PMMA sample is 57% syndiotactic.

Blends were prepared inside of an Argon glovebox to prevent water exposure to hygroscopic LiTFSI, PEO and dPEO. Oxygen and water levels were kept below 1 ppm for all sample preparation. Electrolytes were made by blending dPEO (M_n = 8 or 8.5 kg mol^{-1}),

PEO (M_n = 8.5 kg mol^{-1}), PMMA (M_n = 47.3 kg mol^{-1}), and LiTFSI. We began this study with dPEO-1 (M_n = 8 kg mol^{-1}). We switched to dPEO-2 (M_n = 8.5 kg mol^{-1}) due to inadequate supplies of the dPEO-1 material. The molar masses of the homopolymers were chosen to match those used in our previous study on PEO-PMMA/LiTFSI block copolymer electrolytes.[94] All polymers were dried in a glovebox antechamber under vacuum at 60°C for 5 days prior to use. LiTFSI was dried at 120°C under vacuum for 4 days prior to use.

Five blend compositions were made in this study: ϕ_1 = 0.15, 0.30, 0.50, 0.70, and 0.85. We denote component 1 as PEO and component 2 as PMMA. In blends with ϕ_1 = 0.70 and 0.85, we used a mixture of dPEO-2 and PEO because of (1) the prohibitive cost associated with making samples with pure dPEO-2, given the mass of each polymer blend sample was roughly 1 g, and (2) the large background scattering that we and others have observed from dPEO.[95,96] The volume fraction of each polymer, on a salt free basis, is given by

$$\phi_1 = \frac{\frac{w_1}{\rho_1}}{\frac{w_1}{\rho_1} + \frac{w_2}{\rho_2}} \tag{3.2}$$

and

$$\phi_2 = 1 - \phi_1 \tag{3.3}$$

where w_i and ρ_i are the mass and density, respectively, of component i in the blend. Most of our analysis is at 110°C, where ρ_1 = 1.16 g cm^{-3} and ρ_i = 1.16 g cm^{-3}.[94] The volume fractions of the blends studied are given in Table 3.2. The volume fraction of the polymer components in the salt-containing blends is given by

$$\phi_{pol} = \frac{\frac{w_1}{\rho_1} + \frac{w_2}{\rho_2}}{\frac{w_1}{\rho_1} + \frac{w_2}{\rho_2} + \frac{w_{salt}}{\rho_{salt}}} \tag{3.4}$$

where w_{salt} is the mass of LiTFSI in the blend and ρ_{salt} = 2.023 g cm^{-3}; we ignore volume changes of mixing. We give salt concentration as r = [Li]/[EO].

Electrolyte r values ranged from 0 to 0.10. Electrolytes were made by first dissolving the polymers and salt in THF (about 10 mL), followed by solvent evaporation. All solutions were completely transparent. The solutions were stirred on a hot plate at 55°C for at least 48 h prior to solvent removal. Most of the solvent was then evaporated off by raising the temperature of the hot plate to 60°C. In the final step, electrolytes were dried in a glovebox antechamber under vacuum at 90°C for 4 days.

Polymer	M_n **(kg mol^{-1})**	$Đ$
PEO	8.5	1.05
dPEO-1	8	1.12
dPEO-2	8.5	1.1
PMMA	47.3	1.05

Table 3.1: Polymer Properties

ϕ_1	**Component 1**	**Component 2**
0.5	dPEO-1	PMMA
0.70	dPEO-2 (ϕ_{dPEO} =0.15) PEO (ϕ_{PEO} =0.55)	PMMA
0.85	dPEO-2 (ϕ_{dPEO} =0.15) PEO (ϕ_{PEO} =0.70)	PMMA
0.15, 0.30	dPEO-2	PMMA

Table 3.2: Polymer Blend Compositions

In blends of dPEO-2/PEO/PMMA, ϕ_1 is the sum of the volume fractions of dPEO-2 and PEO. The numbers in parentheses refer to the volume fractions of the individual polymers.

r	Nominal r	ϕ_1	Nominal ϕ_1	ϕ_{pol}	Miscibility
0	0	0.147	0.15	1	Miscible
0	0	0.301	0.30	1	Miscible
0	0	0.504	0.50	1	Miscible
0	0	0.714	0.70	1	Miscible
0	0	0.855	0.85	1	Miscible
0.056	0.05	0.150	0.15	0.972	Immiscible
0.053	0.05	0.302	0.30	0.948	Immiscible
0.053	0.05	0.499	0.50	0.918	Immiscible
0.050	0.05	0.712	0.70	0.891	Miscible
0.053	0.05	0.857	0.85	0.867	Miscible
0.113	0.10	0.148	0.15	0.946	Immiscible
0.111	0.10	0.299	0.30	0.898	Immiscible
0.095	0.10	0.500	0.50	0.860	Miscible
0.103	0.10	0.712	0.70	0.800	Miscible
0.104	0.10	0.853	0.85	0.768	Miscible

Table 3.3: Polymer Blend Electrolyte Compositions

Blend volume fraction (ϕ_1) and salt concentration (r) can vary from sample to sample. To simplify discussion, we list a nominal polymer volume fraction and salt concentration for each sample, reflecting the planned sample composition and salt concentration. The actual compositions, determined from the final weights of the added components, were slightly different.

SANS Sample Preparation and Experiments

PEO-rich samples ($\phi_1 > 0.50$) samples were prepared by returning the dried electrolytes into the glovebox and scooping them onto a 1.54 mm thick quartz window (Esco Optics) on a hot plate set between 110°C and 120°C. The sample was defined by a 1 mm thick stainless-steel washer with an inner diameter of 12.7 mm and an outer diameter of 25.4 mm placed on the quartz window. The sample with the quartz window and the washer was then transferred to the evacuated antechamber at 110°C for 30 minutes. This resulted in a bubble free polymeric disc. Another quartz window was placed on top, and the quartz-washer-quartz sandwich was then placed in a custom air-free copper holder. PEO-lean samples ($\phi_1 < 0.50$) were scooped into a fluorinated poly(ethylene –propylene) (FEP) bag that contained the stainless-steel washer. This FEP bag with the sample and washer was hot pressed in the glovebox at 110°C until the sample was uniform and bubble free. The stainless-steel washer with the polymer was removed from the FEP bag, sandwiched between two quartz windows, and placed in a custom air-free copper holder.

SANS measurements were conducted at the GP-SANS (CG-2) beamline at Oak Ridge National Lab in Oak Ridge, TN.[97] Measurements were performed with a neutron wavelength of 6 Å, and three sample-to-detector distances of 19.1, 4 and 1 m were used. These configurations give access to a scattering wave-vector magnitude, $q = (4\pi/\lambda)\sin(\Theta)$ ranging from 0.05 nm^{-1} to 6 nm^{-1}. Data were collected between 70 and 130°C in 20°C increments. Samples were equilibrated for at least 10 min at each temperature. A 12-position Peltier cooling/heating sample changer block was used to achieve and maintain a constant sample temperature. Data were reduced using toolkit drtsans developed at ORNL.[98] The total scattering intensity was corrected for background and empty cell contributions as well as sample transmission and thickness.[98] Sample thicknesses were obtained by measuring the thickness of the sample and quartz windows and subtracting the thicknesses of the windows. All sample thicknesses were about 1 mm.

3.4 Results and Discussion

The PEO/PMMA/LiTFSI blends studied in this paper are listed in Table 3.3. The SANS profile of the blends with nominal volume fraction $\phi_1 = 0.70$ and nominal $r = 0.10$ is shown in Figure 3.1a, along with the SANS profile for a dPEO/LiTFSI blend at $r = 0.10$. All the analysis in this paper is restricted to data obtained at 110°C. The exact composition of each blend is given in Table 3.3 and these values are used in all calculations. However, for clarity we label blends using the nominal values of ϕ_1 and r (nominal values are also given in Table 3.3). The dPEO/LiTFSI scattering profiles were collected at fewer salt concentrations relative to the blend electrolytes and thus interpolation was necessary to estimate these profiles at relevant values of r. The coherent, background subtracted scattering profile for the same sample is plotted in Figure 3.1b. We followed the procedures established by Gao et al. and Loo et al.[11,95] to convert absolute SANS profiles into absolute coherent SANS profiles:

$$I_{\text{coh}}(q) = I(q) - \phi_{\text{dPEO}} I_{\text{dPEO-LiTFSI}}(q) - I_{\text{inc}} \tag{3.5}$$

where ϕ_{dPEO} is the calculated volume fraction of dPEO in the blend and $I_{\text{dPEO-LiTFSI}}(q)$ is the scattering intensity from dPEO/LiTFSI blends. Both $I(q)$ and $I_{\text{dPEO-LiTFSI}}$ for the blend with $\phi_1 = 0.70$ and $r = 0.10$ are shown in Figure 3.1a. I_{inc} is the incoherent scattering background intensity calculated by fitting a Debye function plus a constant to the measured $I(q)$ scattering profiles from a q range of 0.2 nm^{-1} to 2 nm^{-1}.[11] The low q upturn seen in both scattering profiles in Figure 3.1a is attributed to either microvoids, solid particles, or deuteration heterogeneity of dPEO in the sample.[20,95,96] Subtracting the scattering intensity of the dPEO/LiTFSI blend eliminates the low q upturn in some cases. However, as shown in Figure 3.1b, this subtraction often has little effect. Establishing proper procedures to account for the low q upturn remains a challenge: equation 3.5 was derived assuming the source of the low q upturn was deuteration heterogeneity.[20]

SANS enables readily qualitative differentiation between miscible and immiscible samples. Figure 3.2 plots $I(q)$ for two PEO/PMMA/LiTFSI blends with volume fraction $\phi_1 = 0.15$, r

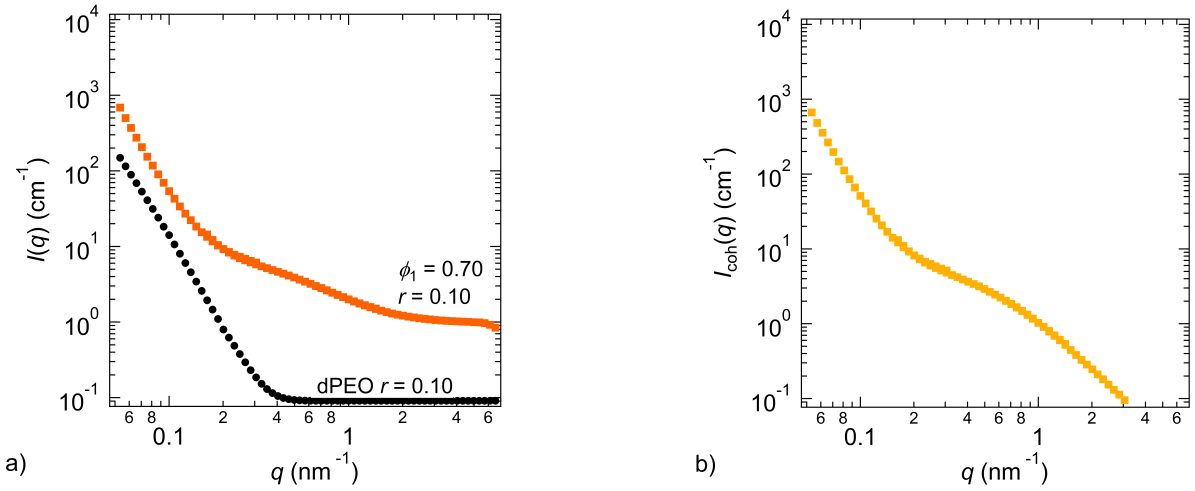

Figure 3.1: SANS profiles of PEO/PMMA/LiTFSI blends at 110°C. (a) Scattering intensity $I(q)(\text{cm}^{-1})$ plotted as a function of scattering vector q (nm^{-1}) for the $\phi_1 = 0.70$, $r = 0.10$ blend electrolyte at 110°C with the scattering data for the dPEO $r = 0.10$ electrolyte at 110°C. In (b) Coherent scattering intensity I_{coh} (cm^{-1}) plotted as a function of scattering vector q (nm^{-1}) calculated from the data in (a) using equation 3.5.

$= 0$ and $r = 0.05$ at 110°C. The $r = 0$ profile, plotted as blue boxes, is an example of a SANS profile for a miscible sample. The $r = 0.05$ profile, plotted as red circles, is an example of a SANS profile for an immiscible sample. Miscible blends exhibit significantly higher values of $I(q)$ in the range $0.2 < q\ (\text{nm}^{-1}) < 1$.[11,16] We utilized these qualitative differences to distinguish between miscible and immiscible systems in all of the blends and the results are listed in Table 3.3. In the discussion that follows, we first focus on miscible systems.

It is customary to extract χ parameters from scattering profiles from miscible binary polymer blends using de Gennes' RPA framework.[31] A simple extension of this framework, assuming that the salt does not partition significantly between concentration fluctuations of dissimilar polymers, was proposed by Gao et al.[11,18,32]

$$I_{\text{coh}}(q) = \phi_{\text{pol}} v_{\text{ref}} \left(B_{\text{dPEO}} - B_{\text{hPMMA}}\right)^2 \left[\frac{1}{S_{11}(q)} + \frac{1}{S_{22}(q)} - 2\chi_{\text{sc}}\right]^{-1} \tag{3.6}$$

where ϕ_{pol} is the total polymer volume fraction in the blend, v_{ref} is the reference volume, B_{i} is the scattering length density of the respective species and S_{ii} is the ideal structure factor for component i. The subscript of the parameter χ_{sc} reflects the fact that it is based on a scattering experiment; it quantifies the effect of added salt on the interactions between PEO and PMMA. The scattering length density is given as

$$B_{\text{i}} = \frac{b_{\text{i}}}{v_{\text{i}}} \tag{3.7}$$

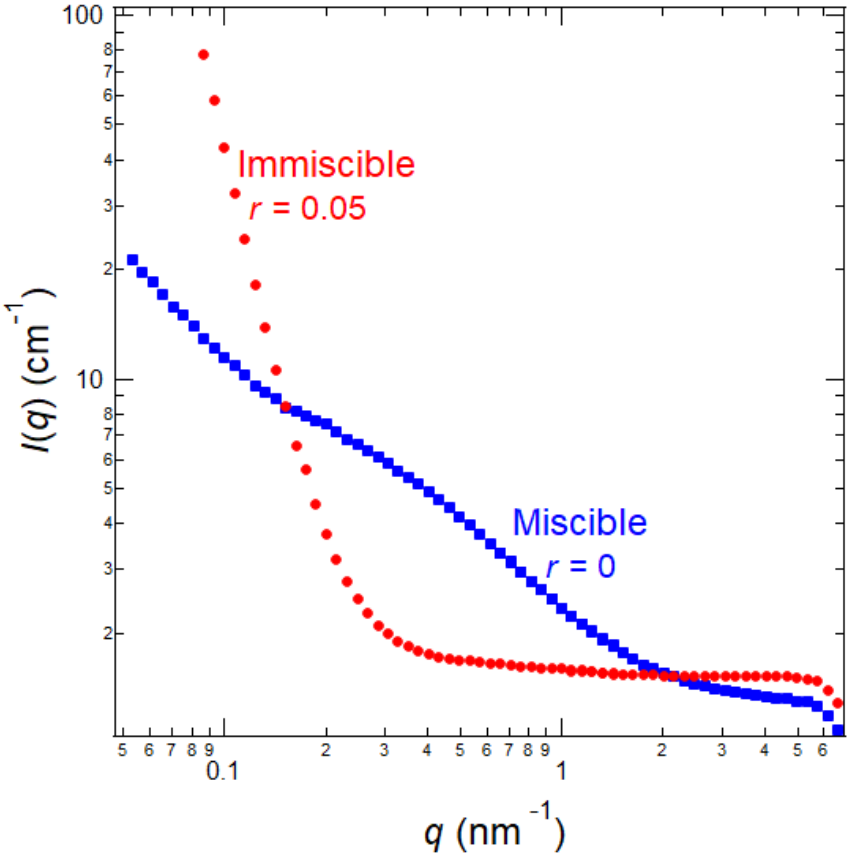

Figure 3.2: SANS profiles for $\phi_1 = 0.15$ PEO/PMMA/LiTFSI blends. Scattering intensity, $I(q)(\text{cm}^{-1})$, plotted as a function of scattering vector q (nm^{-1}) for $r = 0$ and $r = 0.05$ plotted as blue squares and red circles respectively at 110°C.

where b_i is the neutron scattering length and v^i is the molar monomer volume of species i. The neutron scattering lengths for dPEO and PMMA are 4.58 x 10^{-12} cm and 1.49 x 10^{-12} cm, respectively. The molar monomer volumes for dPEO and PMMA are 41.34 cm^3 mol^{-1} and 86.14 cm^3 mol^{-1}, respectively.[73] The ideal structure factors are given by

$$S_\text{ii} = \phi_\text{i} N_\text{i} P_\text{i}(q) \tag{3.8}$$

where ϕ_i is the volume fraction of polymer i on a salt-free basis, and $P_\text{i}(q)$ is the form factor for component i. The form factor $P_\text{i}(q)$ is given by

$$P_\text{i}(q) = 2\left[\frac{\exp(x_\text{i}) - 1 + x_\text{i}}{x_\text{i}^2}\right] \tag{3.9}$$

where $x_\text{i} = q^2 {R_\text{g,i}}^2$. We assume all polymers are flexible Gaussian chains with

$$R_\text{g,i}^2 = \frac{\alpha N_\text{i} l_\text{i}^2}{6} \tag{3.10}$$

where l_i is the statistical segment length for each polymer and a is the chain stretching parameter. The statistical segment length for dPEO was set to 0.72 nm and the segment length for PMMA was set to 0.54 nm.[73] We used these statistical segment lengths in our previous work focusing on scattering from mixtures of LiTFSI and PEO-PMMA block copolymers.[94] The a values in our study ranged from 0.95 to 1.5 and can be found in the supplementary information in Table 3.4.

Our RPA approach (equations 6-10) assumes that the free energy of the polymer electrolyte blends is given by a slightly modified version of equation 3.1, as discussed in ref. 11:

$$\frac{v\Delta G_m}{k_B T} = \phi_{pol}\left(\frac{\phi_1 ln\phi_1}{N_1} + \frac{\phi_2 ln\phi_2}{N_2} + \chi\phi_1\phi_2\right) \tag{3.11}$$

where ΔG_m is the Gibbs free energy of mixing, k_B is the Boltzmann constant, T is the absolute temperature, ϕ_i is the volume fraction of component i, N_i is the number of repeat units in chain i, v is the reference volume (set to 0.1 nm^3), and χ is the Flory-Huggins interaction parameter.

Figures 3.3a, 3.3b and 3.3c plot experimentally determined $I_{coh}(q)$ as a function of q of all miscible samples for $r = 0$, $r = 0.05$ and $r = 0.10$ salt concentrations, respectively. These profiles exhibit q^{-2} power laws in the high q regime ($q > 1$ nm^{-1}), consistent with equation 3.6.[12] These data sets were fit to equations 6-10 with a and χ_{sc} as adjustable parameters. Figure 3.3d shows an example of a fit through the data at $\phi_1 = 0.50$ and $r = 0.10$. There is reasonable agreement between the scattering profile and the RPA fit. SANS profiles from all miscible blends were analyzed using this approach, which enabled estimation of the composition dependence of χ_{sc}.

While this study represents the first attempt to quantify the thermodynamic interactions between PEO/PMMA/LiTFSI blends, numerous studies on the miscibility of PEO/PMMA blends have been conducted.[50–54] In an important study, Ito and coworkers used SANS to estimate the χ_{sc} parameter of PEO/PMMA blends.[55] The results from Ito et al. can be compared to χ_{sc} parameters found in this study for salt-free PEO/PMMA blends to determine experimental repeatability and the effect of chain length on χ_{sc}; different chain lengths were used in the two studies.[55] Figure 3.4 plots χ_{sc} values from Ito et al. and from this study for salt-free PEO/PMMA blends as a function of ϕ_1 . The molar masses of the polymers used by Ito et al. were in the range of 100 kg mol^{-1} while those used in our study were in the range of 10 to 50 kg mol^{-1}. The agreement between the two data sets in Figure 3.4 is reasonable, given the large disparity in molar masses. Some of the observed differences may have arisen due to differences in tacticity of the PMMA samples (the PMMA sample used in ref. 55 was 73% syndiotactic). In principle, if the Flory-Huggins interaction parameter only reflected monomer-monomer interaction energies, then it would be independent of the molar masses of the polymers and blend composition. In practice, the experimentally determined Flory-Huggins interaction parameter is often dependent on these parameters.[26,55,99] In the discussion below, we focus on the dependence of χ_{sc} on composition. In the range between $0.25 < \phi_1 < 0.70$, χ_{sc} obtained both by Ito et al. and by us are approximately linear functions of ϕ_1. The dashed lines in Figure 3.4 are linear fits through this limited data set.

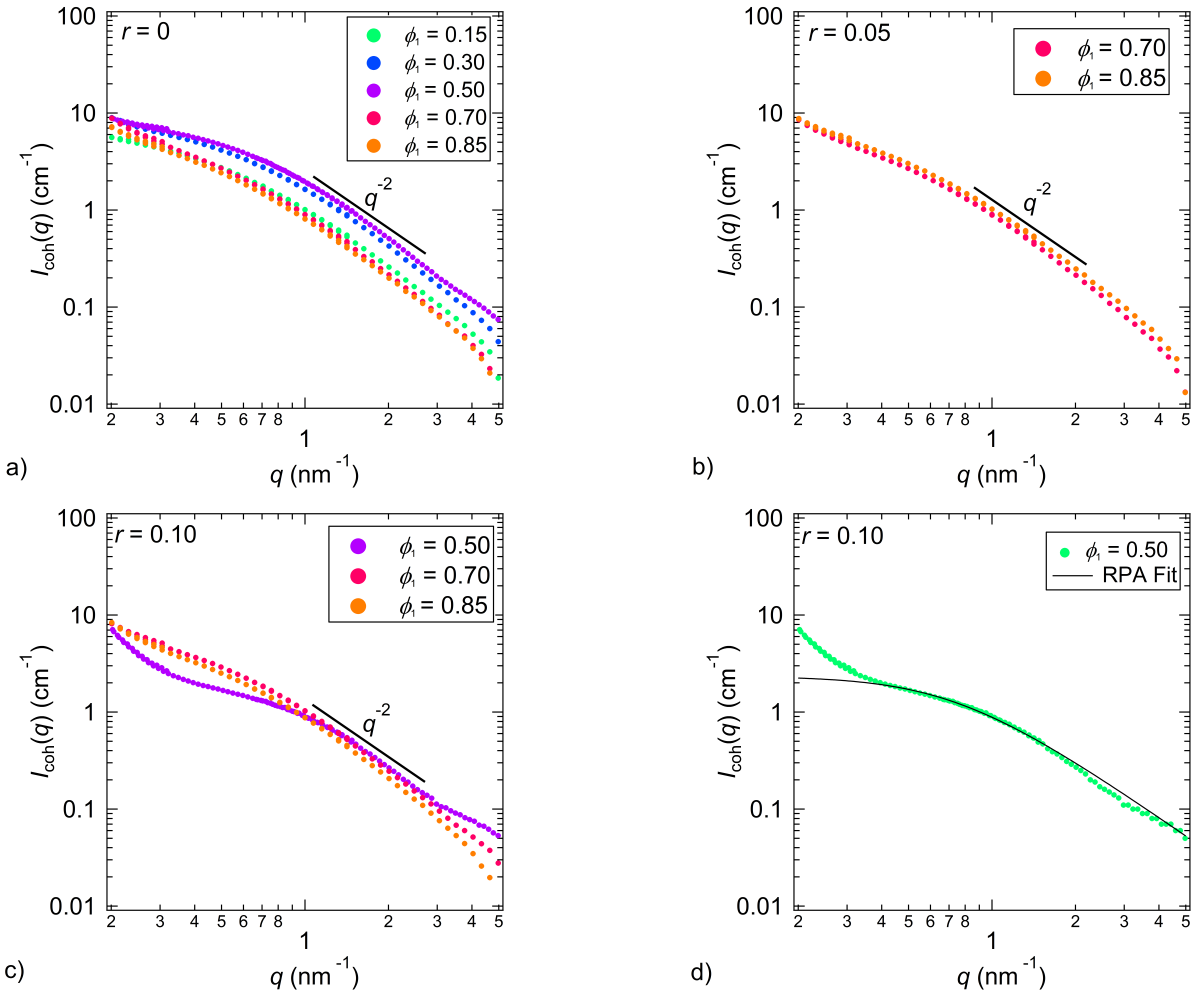

Figure 3.3: The dependence of the coherent SANS intensity, I_{coh} (cm^{-1}), on the magnitude of the scattering vector, q (nm^{-1}), for miscible PEO/PMMA/LiTFSI blends at 110°C. (a) Volume fraction of PEO, $\phi_1 = 0.15$, 0.30, 0.50, 0.70, 0.85 with a salt concentration of $r = 0$ at 110°C. (b) $\phi_1 = 0.70$ and 0.85, $r = 0.05$. (c) $\phi_1 = 0.50$, 0.70 and 0.85, $r = 0.10$ at 110°C. (d) Typical RPA fit through the I_{coh} versus q data.

Sanchez recognized that if χ_{sc} were composition dependent, then this dependence can be used to determine the dependence of χ on composition; χ is the parameter that must be used in equation 3.1.[100] $\chi_{sc} = \chi$ if χ_{sc} is independent of ϕ_1. If χ_{sc} is a linear function of ϕ_1, then it is convenient to express this relationship as,

$$\chi_{sc} = A + B\,(2\phi_1 - 1) \tag{3.12}$$

and χ, based on the Sanchez analysis, is then given by

$$\chi = A + \frac{B}{3}\,(2\phi_1 - 1) \tag{3.13}$$

The dependence of χ_{sc} on ϕ_1 for both sets of data in Figure 3.4 were fit to equation 3.12 to obtain A and B. This enables determination of χ using equation 3.13. The composition dependence of χ for both data sets based on the linear approximation is also shown in Figure 3.4.

The limitation of this approach becomes clear when one examines the full data set in Figure 3.4. The measured χ_{sc} at $\phi_1 = 0.85$ deviates significantly from the linear fit. We will address this limitation shortly.

Figures 3.5a, b and c plot χ_{sc} as a function of ϕ_1 for $r = 0$, $r = 0.05$ and $r = 0.10$ blends, respectively. We have already discussed the $r = 0$ blends. These blends were miscible across the entire composition window. The $r = 0.05$ blends were phase separated for $\phi_1 \leq 0.50$. In addition to the data points, the lower limit of an error bar is shown at $\phi_1 = 0.50$ in Figure 3.5b. This lower limit was calculated assuming the spinodal is an adequate demarcation between miscible and immiscible systems. In the Flory-Huggins theory, the value of χ at the spinodal χ_s is given by:

$$\chi_s = \frac{1}{2}\left(\frac{1}{N_1\phi_1} + \frac{1}{N_2(1-\phi_1)}\right) \tag{3.14}$$

The lower bound in Figure 3.5b represents χ_s for $\phi_1 = 0.50$. The $r = 0.10$ blends were phase separated for $\phi_1 \leq 0.30$. Figure 3.5c shows measured χ_{sc} for these blends along with the lower limit of an error bar that represents χ_s at $\phi_1 = 0.30$.

It is obvious from Figure 3.5 that the composition dependence of χ_{sc} of our blends cannot be described by a linear function. We thus use quadratic fits to describe these composition dependencies.

$$\chi_{sc} = A + B\phi_1 + C\phi_1^2 \tag{3.15}$$

The curves in Figure 3.5 represent quadratic fits through the data sets including χ_s of the phase separated system with the largest value of the plot.

It is important to note that the effect of added salt on PEO/PMMA thermodynamics is non-trivial. In the absence of salt, PEO/PMMA blends are miscible in the range of $0.15 \leq \phi_1 \leq 0.85$. In other words, there is no window of immiscibility at $r = 0$. A wide immiscibility window in the range $0.15 \leq \phi_1 \leq 0.50$ is obtained upon addition of a small amount of salt ($r = 0.05$). This window shrinks to $0.15 \leq \phi_1 \leq 0.30$ upon further addition of salt ($r =$

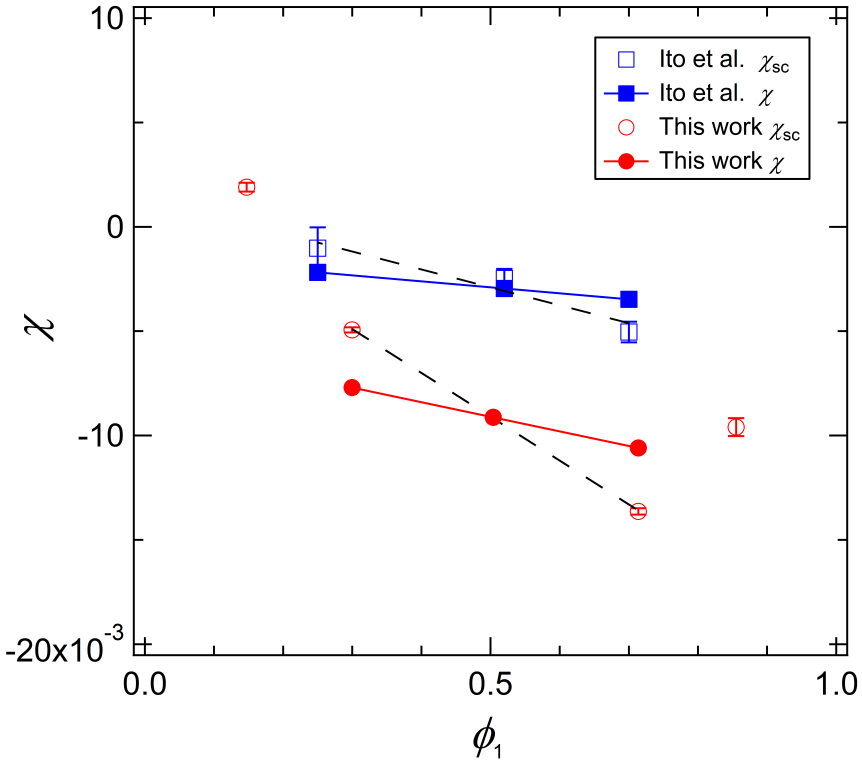

Figure 3.4: Flory-Huggins interaction parameters, χ and χ_{sc} for salt-free PEO/PMMA blends at 110°C as a function of PEO volume fraction, ϕ_1. χ_{sc} values are obtained from SANS data using RPA. The dashed lines are linear fits through the data $0.2 < \phi_1 < 0.8$ data. χ values are obtained from using the Sanchez approach and the linear fits to obtain A and B; see equation 3.13. χ_{sc} labeled Ito et al., are taken from ref. 55. The A and B values for the Ito et al. data set are -0.0029 ± 0.0005 and -0.0043 ± 0.0012. The A and B values for our data set are -0.0091 ± 0.00005 and -0.0105 ± 0.00015. Error bars represent one standard deviation of the χ_{sc} fits.

0.10). The question that we wish to answer is: can a simple expression for χ in equation 3.1 explain the widening and shrinking of the immiscibility window as a function of increasing salt concentration?

The framework of Sanchez[100] can be used even if χ_{sc} is a non-linear function of ϕ_1. For the quadratic function given in equation 3.15, this framework indicates that χ is also a quadratic function as given below. See SI for details.

$$\chi = \left(A + \frac{B}{3} + \frac{C}{6}\right) + \left(\frac{B}{3} + \frac{C}{6}\right)\phi_1 + \frac{C}{6}\phi_1^2 \tag{3.16}$$

In salt containing systems, the Gibbs free energy of mixing is obtained by substituting

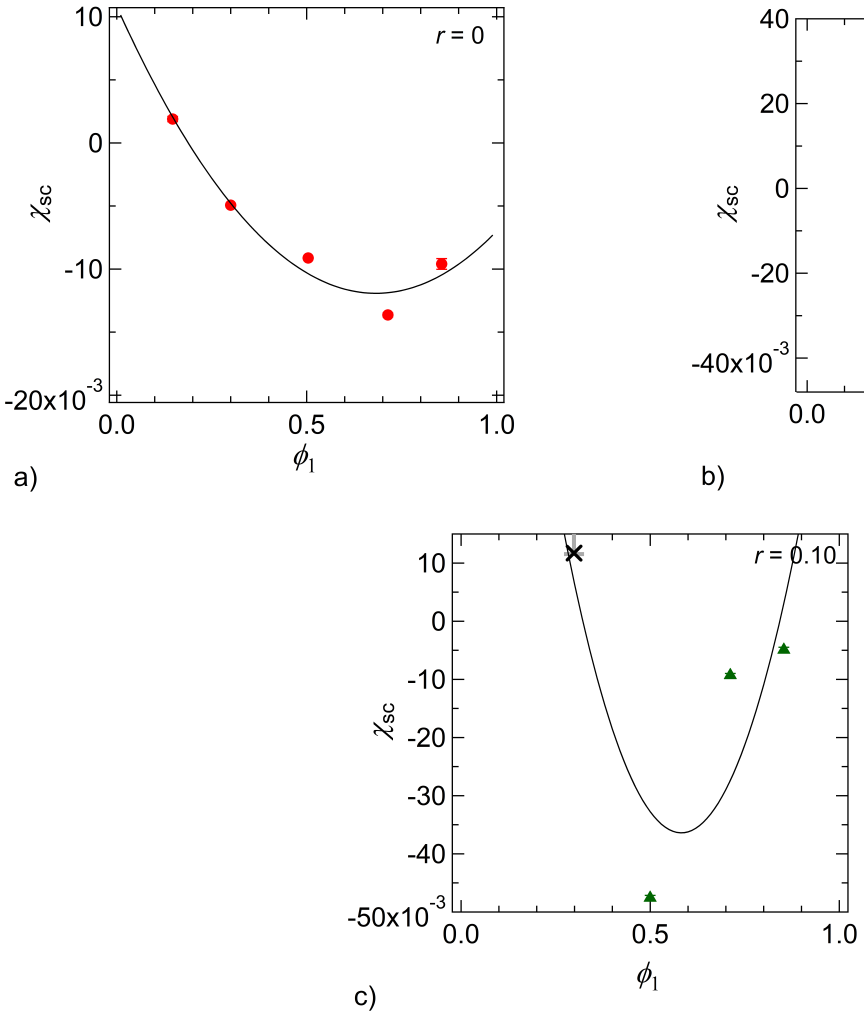

Figure 3.5: χ_{sc} for PEO/PMMA/LiTFSI blends are plotted as a function of salt-free PEO volume fraction ϕ_1 at 110°C. The curves are least-squares quadratic fits. (a) $r = 0$. (b) $r = 0.05$. (c) $r = 0.10$. Blends at the lowest values of ϕ_1 in (b) and (c) were phase separated. The value of χ_s used for the fits was obtained using equation 3.14, representing a lower bound for χ_{sc}.

equation 3.16 into equation 3.11

$$\frac{v\Delta G_{\mathrm{m}}}{k_{\mathrm{B}}T} = \phi_{pol}\left(\frac{\phi_1 \ln \phi_1}{N_1} + \frac{(1-\phi_1)\ln(1-\phi_1)}{N_2} + \left(\left(A + \frac{B}{3} + \frac{C}{6}\right) + \left(\frac{B}{3} + \frac{C}{6}\right)\phi_1 + \frac{C}{6}\phi_1^2\right)\phi_1(1-\phi_1)\right) \tag{3.17}$$

For simplicity, we define phase boundaries using the spinodal,

$$\frac{v_0}{kT\phi_{pol}}\frac{\partial^2 \Delta G_{\mathrm{m}}}{\partial \phi_1^2} = J(\phi_1) = 0 \tag{3.18}$$

The polymer blend electrolytes that we wish to model contain 4 species if we account for the dissociated nature of salt. Our framework is a simple first step toward modeling polymer blend electrolytes wherein we assume that the primary difference between the coexisting phases is the difference in ϕ_1. In addition, we ignore the weak dependence of ϕ_{pol} on ϕ_1. With these simplifications, $J(\phi_1)$ is given by

$$\begin{aligned} J(\phi_1) = \Bigg(&-2A - \frac{2B}{3} - \frac{C}{3} + \frac{1}{N_2(1-\phi_1)} + \frac{1}{N_1\phi_1} \\ &- \frac{2B\phi_1}{3} - \frac{C\phi_1}{3} + \frac{1}{3}C(1-\phi_1)\phi_1 - \frac{C{\phi_1}^2}{3} \\ &+2(1-\phi_1)\left(\frac{B}{3} + \frac{C}{6} + \frac{C\phi_1}{3}\right) - 2\phi_1\left(\frac{B}{3} + \frac{C}{6} + \frac{C\phi_1}{3}\right)\Bigg) \end{aligned} \tag{3.19}$$

Figure 3.6 plots J as a function of ϕ_1 for $r = 0$, 0.05 and 0.10. At $r = 0$, $J(\phi_1) = 0$ has no real roots in the range $0 < \phi_1 < 1$, implying that our model predicts that these blends are all miscible. At $r = 0.05$, $J(\phi_1) = 0$ has 2 real roots at $\phi_1 = 0.02$ and 0.495, implying that our model predicts that these blends are immiscible in the range $0.02 < \phi_1 < 0.495$. At $r = 0.10$, $J(\phi_1) = 0$ has 4 real roots at $\phi_1 = 0.03$, 0.27, 0.88 and 0.98. This implies that our model predicts the presence of two immiscible windows, $0.03 < \phi_1 < 0.27$ and $0.88 < \phi_1 < 0.98$. The possibility of obtaining multiple immiscible windows in salt-containing polymer mixtures was presented in the theoretical work of de la Cruz and coworkers.[46] In reference 46, this effect was due to the presence of ionic correlations. More work is needed to establish the molecular underpinnings of the data in Figure 3.6. In the discussion below, we focus on the low ϕ_1 miscibility window as our experiments are limited to this window.

In Figure 3.7, we show the dependence of the fit parameters A, B and C on r. These parameters change rapidly between $r = 0$ and $r = 0.05$. The dependence of these parameters on salt concentration between $r = 0.05$ and 0.10 is relatively subtle. However, the changes in the thermodynamic behavior predicted by our model are not at all subtle. Increasing concentration in this window results in significant shrinking of the low ϕ_1 immiscibility window and the creation of a new high ϕ_1 immiscibility window.

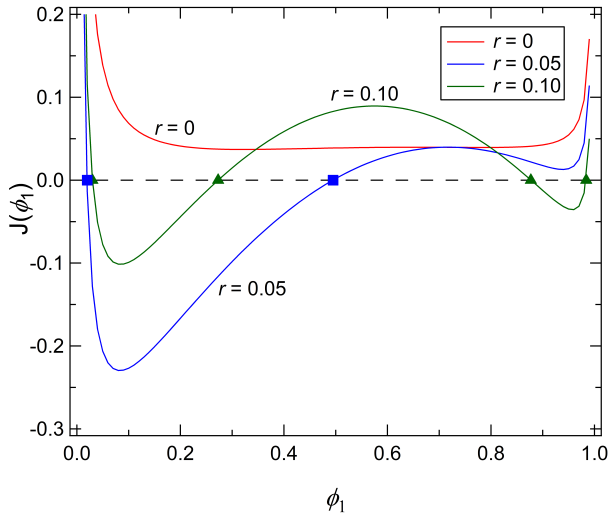

Figure 3.6: The curves represent plots of function $J(\phi_1)$, defined by equation 3.19, which is proportional to the second derivative of the free energy of mixing at $r = 0$, $r = 0.05$ and $r = 0.10$ at 110°C. The locations of the $J(\phi_1) = 0$ points represent the locations of the predicted spinodals. No spinodal is obtained at $r = 0$. Immiscibility is predicted between the spinodal compositions. There is one immiscible region at $r = 0.05$ and two at $r = 0.10$.

In Figure 3.8, we compare the observed phase behavior of our polymer blend electrolytes with theoretical predictions based on equation 3.19. The theory predicts the appearance of a wide immiscibility window at $r = 0.05$ which shrinks upon further addition of salt to $r = 0.10$. This is in good agreement with the experimental observations. The answer to the question posed above, "can a simple expression for χ in equation 3.1 explain the widening and shrinking of the immiscibility window as a function of increasing salt concentration?", is yes.

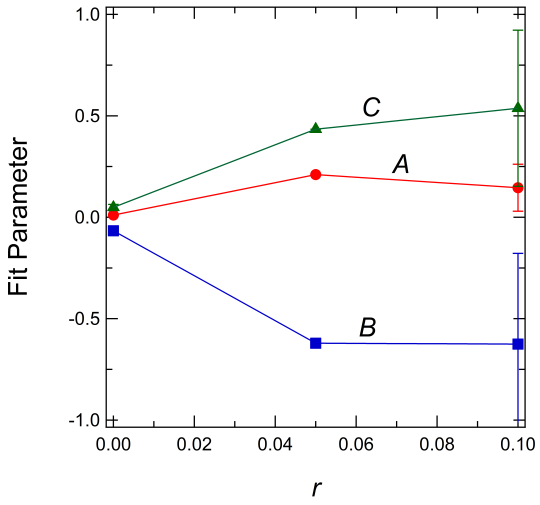

Figure 3.7: Fit parameters A, B, and C, plotted as a function of salt concentration r from the quadratic Sanchez framework, using χ_{sc} data collected at 110°C. Error bars represent the standard deviation of each parameter.

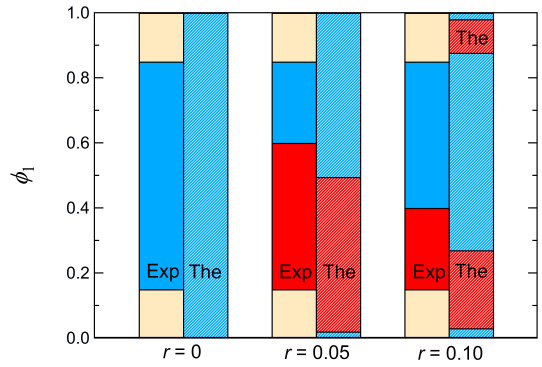

Figure 3.8: Phase transition comparison between experimental data and spinodal analysis based on the proposed modification of the Flory-Huggins theory. Red regions denote immiscibility and blue regions denote miscibility. The tan regions represent compositions with no experimental data. Experimental data are shown as solid colors and the results of the Flory-Huggins analysis are shown as hashed colors.

3.5 Conclusions

We have completed a comprehensive study of the thermodynamics of a miscible polymer blend system with added salt. We conducted SANS experiments on a series of PEO/PMMA /LiTFSI blends with compositions ranging from $\phi_1 = 0.15$ to $\phi_1 = 0.85$, and salt concentrations ranging from $r = 0$ to $r = 0.10$ (PEO is component 1). The model we used for quantifying the free energy of mixing of the ternary system was based on the Flory-Huggins theory. All the salt-free samples in this study were miscible, and the χ parameters determined by SANS were negative. SANS measurements of our salt containing polymer blends revealed an unusual relationship between miscibility, salt concentration and blend composition. The PEO-rich blends were miscible at all salt concentrations, while all salt containing PEO-lean blends were immiscible at all salt concentrations. The immiscibility window, which is nonexistent in salt-free blends ($r = 0$), is wider at low salt concentration ($r = 0.05$) than at high salt concentration ($r = 0.10$). We used the de Gennes' RPA framework to determine interaction parameters χ for our blends from SANS scattering profiles of miscible blends. The experimentally derived interaction parameters χ_{sc} are a strong nonlinear function of ϕ_1 at all salt concentrations. Given this complexity, it would be desirable to collect data at additional values of ϕ_1 to improve upon the uncertainty in our model. However, the calculated spinodal curves from our current model were in remarkable agreement with the experimental observations. The theory suggests the presence of two immiscibility windows. Further experimental work is needed to establish the presence or absence of the high ϕ_1 window. We hope to establish the molecular underpinnings of our free energy model in future studies.

3.6 Acknowledgements

This work was supported by the Joint Center for Energy Storage Research (JCESR), an Energy Innovation Hub funded by the U.S. Department of Energy, Office of Science, Office of Basic Energy Science, under Contract No. DE-AC02-06CH11357. Partial support for N.J.S. was provided by National Science Foundation grant DMR 1904508 to the University of California, Berkeley. K. W. G. acknowledges funding from a National Defense and Science Engineering Graduate Fellowship. This research used resources at the High Flux Isotope Reactor, a DOE Office of Science User Facility operated by the Oak Ridge National Laboratory.

3.7 Nomenclature

A, B, C, empirical fitting constants for χ_{sc}

b_{i}, neutron scattering length of species i (nm mer^{-1})

$Đ$, dispersity

ΔG_{m}, Gibbs free energy of mixing per unit volume (J m^{-3})

$I(q)$, scattering intensity (cm^{-1})

$I_{\mathrm{coh}}(q)$, coherent scattering intensity (cm^{-1})

k_{B}, Boltzmann constant (m^2 kg s^{-2} K^{-1})

l_{i}, statistical segment length of species i (nm)

M_{i}, molar mass of species i (g mol^{-1})

M_{w}, weight-averaged molar mass (kg mol^{-1})

M_{n}, number-averaged molar mass (kg mol^{-1})

M_{PEO}, molar mass of species poly(ethylene oxide) (g mol^{-1})

M_{PMMA}, molar mass of species poly(methyl methacrylate) (g mol^{-1})

n_{i}, chemical repeat units for species i

N, degree of polymerization

N_{i}, degree of polymerization for species i

q, scattering vector (nm^{-1})

r, salt concentration in PEO ([Li] $[\mathrm{EO}]^{-1}$)

R_{g}, radius of gyration (nm)

S_{ii}, structure factor

T, absolute temperature (K)

Greeks

a, chain stretching parameter

v_{i}, molar volume of species i (cm^3 mol^{-1})

v_{ref}, reference volume of species i (cm^3 mol^{-1})

ρ_{i}, density of species i (g cm^{-1})

ϕ_1, volume fraction of species i on a salt-free basis

Θ, scattering angle

λ, wavelength (nm)

χ, Flory-Huggins interaction parameter

χ_{sc}, Flory-Huggins interaction parameter determined from SANS data

χ_{s}, Spinodal Flory-Huggins interaction parameter

3.8 Supporting Information

Sanchez Quadratic Function Derivation

$$\chi_{\mathrm{sc}} = A + B\phi_1 + C\phi_1^2 \tag{3.20}$$

$$\chi = \ \phi_2\chi_{\mu 1} + \ \phi_1\chi_{\mu 2} \tag{3.21}$$

$$\chi_{\mu 1} = \ \frac{2}{(1-\phi_1)^2}\int_0^{\varphi_2}(1-\phi_1')\chi_{\mathrm{sc}}d(1-\phi_1') \tag{3.22}$$

$$\chi_{\mu 2} = \ \frac{2}{{\phi_1}^2}\int_0^{\varphi_1}\phi_1'\chi_{sc}d\phi_1' \tag{3.23}$$

$$\chi_{\mu 1} = \ \frac{2}{(1-\phi_1)^2}\int_0^{\phi_2}(1-\phi_1')\left(A + B\phi_1 + C\phi_1^2\right)\ d(1-\phi_1') \tag{3.24}$$

$$\chi_{\mu 1} = A + B + C - \frac{2B\,(1-\phi_1)}{3}\ - \frac{4C\,(1-\phi_1)}{3} + \ \frac{C(1-\phi_1)^2}{2} \tag{3.25}$$

$$\chi_{\mu 2} = \ \frac{2}{{\phi_1}^2}\int_0^{\phi_1}\phi_1'\left(A + B\phi_1 + C\phi_1^2\right)d\phi_1' \tag{3.26}$$

$$\chi_{\mu 2} = A + \frac{2B\phi_1}{3} + \ \frac{C\phi_1^2}{2} \tag{3.27}$$

$$\begin{aligned}\chi = \ (1-\phi_1)\,(A + B + C \\ - \frac{2B\,(1-\phi_1)}{3}\ - \frac{4C\,(1-\phi_1)}{3} + \ \frac{C\,(1-\phi_1)^2}{2}) \\ + (\phi_1)(A + \frac{2B\phi_1}{3} + \ \frac{C\phi_1^2}{2})\end{aligned} \tag{3.28}$$

$$\chi = \left(A + \frac{B}{3} + \ \frac{C}{6}\right) + \left(\frac{B}{3} + \frac{C}{6}\right)\phi_1 + \frac{C}{6}\phi_1^2 \tag{3.29}$$

Spinodal Derivation

$$\frac{v\Delta G_{\mathrm{m}}}{k_{\mathrm{B}}T} = \phi_{\mathrm{pol}}\left(\frac{\phi_1 ln\phi_1}{N_1} + \frac{\phi_2 ln\phi_2}{N_2} + \ \chi\phi_1\phi_2\right) \tag{3.30}$$

We assume $\boldsymbol{\phi_{\mathrm{pol}}}$ is a constant

$$\begin{aligned}\frac{v\Delta G_{\mathrm{m}}}{k_{\mathrm{B}}T} = \phi_{pol}\Bigg(&\frac{\phi_1 \ln\phi_1}{N_1} + \ \frac{(1-\phi_1)\ln(1-\phi_1)}{N_2} \\ &+ \ \left(\left(A + \frac{B}{3} + \ \frac{C}{6}\right) + \left(\frac{B}{3} + \frac{C}{6}\right)\phi_1 + \frac{C}{6}\phi_1^2\ \right)\phi_1(1-\phi_1)\Bigg)\end{aligned} \tag{3.31}$$

Definition of the spinodal

$$\frac{\partial^2 \Delta G_{\mathrm{m}}}{\partial \phi_1^2} = 0 \tag{3.32}$$

$$\begin{aligned}\frac{v}{k_{\mathrm{B}}T}\frac{\partial \Delta G_{\mathrm{m}}}{\partial \phi_1} \ &= \phi_{pol}\left(\frac{-1}{N_2} + \ \frac{1}{N_1} + (\phi_1(1-\phi_1))\left(\frac{B}{3} + \frac{C}{6} + \frac{C\phi_1}{3}\right)\right. \\ &+ (1-\phi_1)\left(\left(A + \frac{B}{3} + \ \frac{C}{6}\right) + \left(\frac{B}{3} + \frac{C}{6}\right)\phi_1 + \frac{C}{6}\phi_1^2\ \right) \\ &- \phi_1\left(\left(A + \frac{B}{3} + \ \frac{C}{6}\right) + \left(\frac{B}{3} + \frac{C}{6}\right)\phi_1 + \frac{C}{6}\phi_1^2\right) - \frac{(1-\phi_1)\ln(1-\phi_1)}{N_2} \\ &\left. + \ \frac{\phi_1 \ln\phi_1}{N_1}\right)\end{aligned} \tag{3.33}$$

$$\begin{aligned}\frac{v}{kT\phi_{pol}}\frac{\partial^2 \Delta G_{\mathrm{m}}}{\partial \phi_1^2} = \Bigg(&-2A - \frac{2B}{3} - \frac{C}{3} + \ \frac{1}{N_2(1-\phi_1)} + \frac{1}{N_1\phi_1} \\ &- \frac{2B\phi_1}{3} - \frac{C\phi_1}{3} + \frac{1}{3}C(1-\phi_1)\phi_1 - \frac{C{\phi_1}^2}{3} \\ &+2(1-\phi_1)\left(\frac{B}{3} + \frac{C}{6} + \frac{C\phi_1}{3}\right) - 2\phi_1\left(\frac{B}{3} + \frac{C}{6} + \frac{C\phi_1}{3}\right)\Bigg)\end{aligned} \tag{3.34}$$

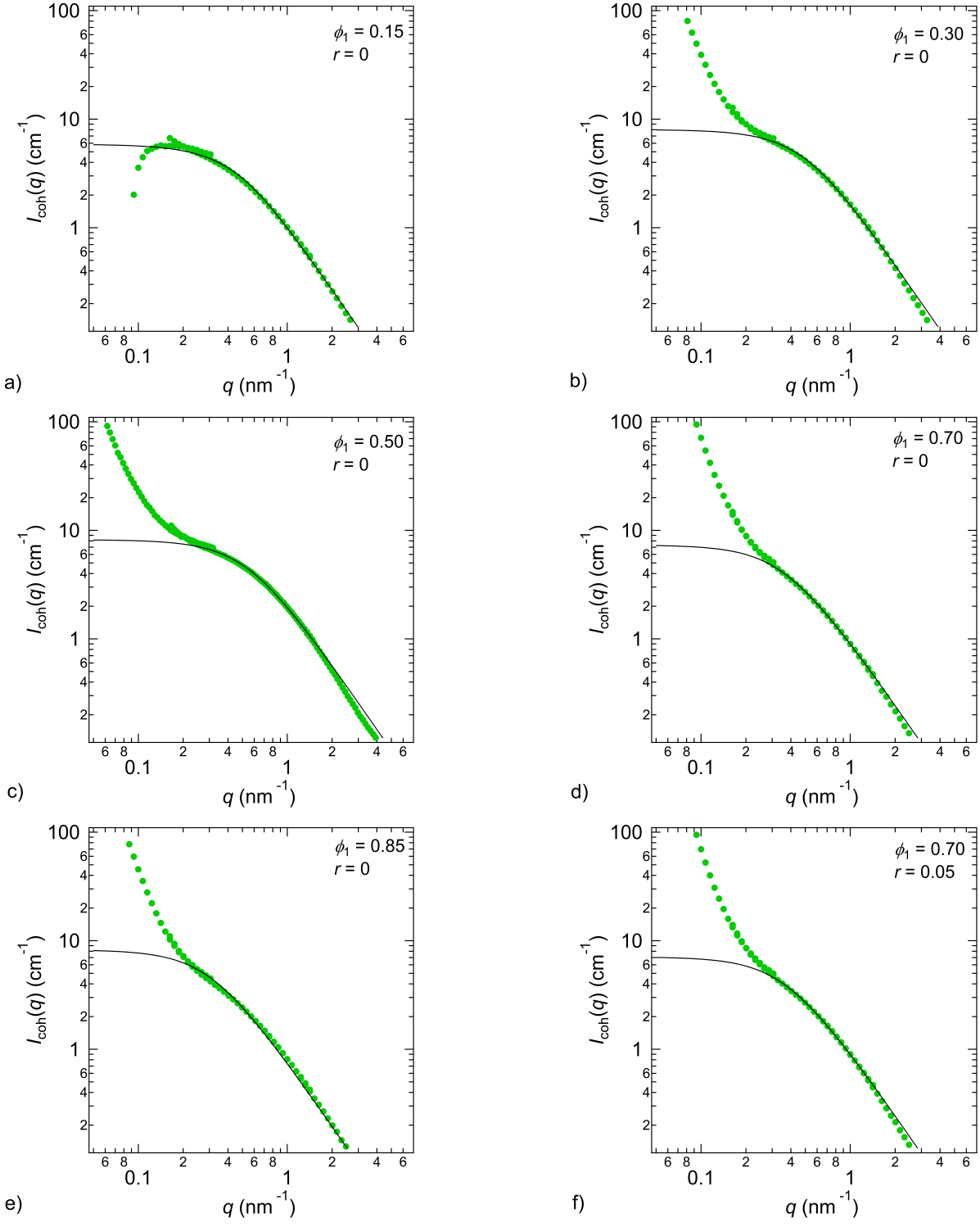
a)
ϕ_1 = 0.15
r = 0
b)
ϕ_1 = 0.30
r = 0
c)
ϕ_1 = 0.50
r = 0
d)
ϕ_1 = 0.70
r = 0
e)
ϕ_1 = 0.85
r = 0
f)
ϕ_1 = 0.70
r = 0.05
$I_{coh}(q)$ (cm^{-1})
q (nm^{-1})
0.1
1
10
100

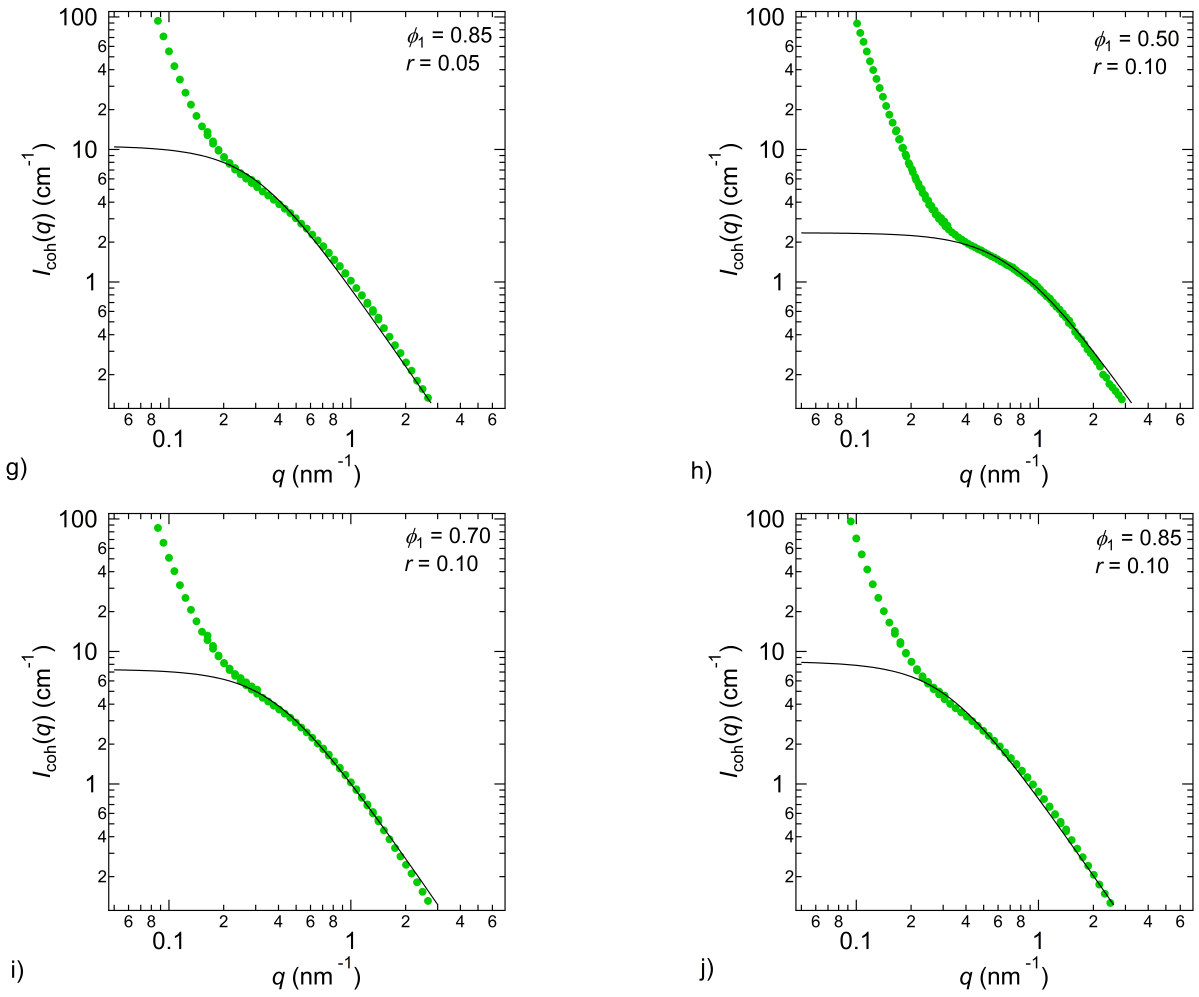

Figure 3.10: In Figure 3.10(a-i) $I_{\mathrm{coh}}(q)$ is plotted as a function of q as filled green circles at 110°C. RPA fits for these scattering profiles are plotted as a black trace on each plot.

Chain Stretching Parameters (a)

r	Nominal r	ϕ_1	Nominal ϕ_1	ϕ_{pol}	Miscibility	a
0	0	0.147	0.15	1	Miscible	0.95
0	0	0.301	0.30	1	Miscible	0.98
0	0	0.504	0.50	1	Miscible	1.0
0	0	0.714	0.70	1	Miscible	1.5
0	0	0.855	0.85	1	Miscible	1.4
0.056	0.05	0.150	0.15	0.972	Immiscible	-
0.053	0.05	0.302	0.30	0.948	Immiscible	-
0.053	0.05	0.499	0.50	0.918	Immiscible	-
0.050	0.05	0.712	0.70	0.891	Miscible	1.4
0.053	0.05	0.857	0.85	0.867	Miscible	1.2
0.113	0.10	0.148	0.15	0.946	Immiscible	-
0.111	0.10	0.299	0.30	0.898	Immiscible	-
0.095	0.10	0.500	0.50	0.860	Miscible	1.2
0.103	0.10	0.712	0.70	0.800	Miscible	1.2
0.104	0.10	0.853	0.85	0.768	Miscible	1.2

Table 3.4: Polymer Blend Electrolyte Chain Stretching Parameters

Chapter 4

Chimney-Shaped Phase Diagram in a Polymer Blend Electrolyte[3]

4.1 Abstract

The phase behavior of polymer blend electrolytes comprising poly(ethylene oxide) (PEO)/ poly(methyl methacrylate) (PMMA)/ lithium bis(trifluoromethanesulfonyl)imide (LiTFSI) was determined using a combination light and small angle neutron scattering (SANS) experiments. The results at a fixed temperature (110°C) are presented on a PEO concentration versus salt (LiTFSI) concentration plot. The blends are miscible at all PEO concentrations in the absence of salt. With added salt, a region of immiscibility is obtained in PEO-lean polymer blend electrolytes; blends rich in PEO remain miscible at most salt concentrations. A narrow region of immiscibility juts into the miscible region, giving the phase diagram a chimney-like appearance. The data are qualitatively consistent with a simple extension of Flory-Huggins theory with a composition-dependent Flory-Huggins interaction parameter, χ, that was determined independently from SANS data from homogeneous blend electrolytes. Phase diagrams like the one we have obtained were anticipated by self-consistent field theory calculations that account for correlations between ions. The relationship between these theories and measured χ remains to be established.

4.2 Introduction

The effect of added salt on the phase behavior of polymers is a subject of continuing interest.[35,39,40,43] These materials may provide an avenue for enabling the next generation of rechargeable lithium batteries. In particular, mechanically robust electrolytes have the potential to enable electrodes such as lithium metal and silicon, which can lead to batteries with increased energy density.[66] In mixtures of one homopolymer and salt, there is an inverse

[3]Adapted from **Shah, N. J.**, **Shalaby, M.**, *et al.* Chimney-Shaped Phase Diagram in a Polymer Blend Electrolyte. ***Macro Letters*** 2023, 12 (7), 874-879.

relationship between ion transport rates and mechanical robustness;[101] strategies to improve ion transport rates generally result in a decrease in the shear (or tensile) modulus of the electrolytes. Microphase separated block copolymer electrolytes with an ionically conductive microphase and a rigid non-conducting microphase provide one avenue for decoupling electrical and mechanical properties of polymer electrolytes.[102,103] Rational design of such systems requires an understanding of the effect of added salt on the thermodynamic interactions between chemically distinct polymers.[35,39,43] Polymer blend electrolytes wherein salt is added to a mixture of two polymers are the simplest platform for determining this effect. While numerous theoretical papers have been written on this subject,[3,37,46,104–106] there are relatively few experimental datasets[9,40,45,107] that can be used to test the predictions of the theories.

In neat polymer blends without added salt, phase diagrams are generally presented on plots of temperature versus blend composition.[16,21,26,108] In polymer blend electrolytes, salt concentration is the new variable that affects phase diagrams in addition to temperature. Diagrams wherein the boundary between miscible and immiscible blends (at fixed temperature) are presented on plots of salt concentration versus blend composition provide one avenue for testing theoretical predictions. It may seem surprising that there are only two such experimental phase diagrams in the current literature. In pioneering work, Xie and Lodge studied the phase behavior of a polyolefin oligomer (squalane, SQ), poly(ethylene oxide) (PEO), and lithium bis(trifluoromethane) sulfonimide (LiTFSI).[40] In the absence of salt, the interactions between SQ and PEO are characterized by a positive Flory-Huggins interaction parameter, which may be interpreted as "repulsive" interactions between the polymers. As is often the case in such systems, the two homopolymers are only miscible in the low molecular weight limit (less than 1 kg/mol for the SQ/PEO case). The phase boundary reported in ref. 40, when plotted with salt concentration as the x-axis and the volume fraction of PEO as the y-axis, is shaped like a dome. In the absence of salt, SQ/LiTFSI mixtures are immiscible. The addition of PEO leads to a miscible system, and the boundary between miscible and immiscible depends on salt concentration; the immiscibility window increases in magnitude with increasing salt concentration. This phase behavior was shown to be quantitatively consistent with the Born-solvation-theory-based predictions of Wang[38] which accounts for the "self-energy" of the ions. The ions have a propensity to partition into the PEO-rich phase which is the high dielectric constant polymer and this induces phase separation. In other words, the addition of salt leads to an increase in the effective Flory-Huggins interaction parameter between the polymers. The same qualitative phase behavior is expected based on measurements of the effective Flory-Huggins interaction parameter based on small angle neutron scattering experiments in polystyrene/PEO/LiTFSI mixtures.[45] The phase diagram for mixtures of two polymers and salt, where one of the components is PEO and the other polymer has a positive Flory-Huggins interaction parameter with PEO in the absence of salt, is shown qualitatively in Figure 4.1. It may be considered as the classical phase diagram of polymer blend electrolytes.

In addition to self-energy, the locations of ions are correlated due to coulombic interactions that are mediated by two polymers with different dielectric constants. A theory that accounts

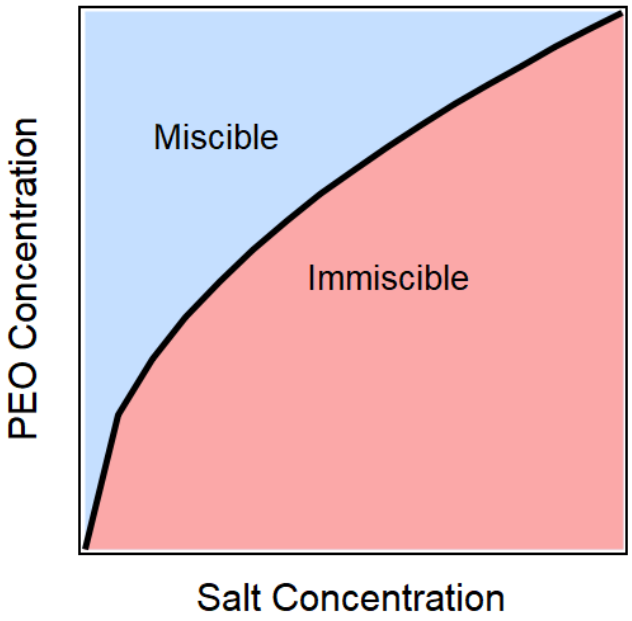

Figure 4.1: Classical phase diagram of a polymer blend electrolyte, a mixture of two polymers and lithium salt, mapped on a PEO concentration versus salt concentration plot. This diagram is anticipated in the case the two polymers exhibit repulsive interactions and salt partitions selectively into the PEO-rich phase.

for this was first presented by de la Cruz and coworkers.[46,47,109] In this case, phase boundaries that take on the shape of chimneys and closed loops appear when the polymer blend is characterized by a negative Flory-Huggins interaction parameter, i.e., the polymer blend is miscible in the absence of salt. The purpose of this paper is to present experimental evidence for the phase behavior of polymer blend electrolytes comprising of poly(methyl methacrylate) (PMMA), PEO, and LiTFSI. Unlike binary SQ/PEO and PS/PEO blends, which are only miscible when the molecular weights of the polymers are in the vicinity of 1.5 kg/mol,[110] PEO/PMMA blends are miscible at all molecular weights and compositions studied thus far.[50,51,53–55] The experimental phase diagram of PEO/PMMA/LiTFSI blends at a fixed temperature is presented on a PEO concentration versus salt concentration plot. In a previous study, we have reported on the phase behavior of these blends over a limited composition window based on small angle neutron scattering.[111] We augment that study with additional compositions wherein the phase behavior was determined by light scattering. We present the first direct evidence of a chimney-shaped phase boundary in polymer blend electrolytes. Experimental data are compared with predictions based on a model presented in ref. 111.

4.3 Materials and Methods

In this study we utilized PMMA with number averaged molar mass, M_{n}, of 47.3 kg mol^{-1} in all blends. The other polymeric component was a combination of hPEO and dPEO polymers with M_{n} ranging from 8 kg mol^{-1} to 8.5 kg mol^{-1}. We chose these molar masses to match those used in our previous PEO-PMMA/LiTFSI block copolymer study.[94] dPEO was used in blends characterized by SANS in ref. 111 to obtain neutron scattering contrast. In ref. 111, we presented the data on a number of blends and classified them into "miscible" and "immiscible" categories. We ran light scattering experiments on a subset of these blends to ensure that our classification based on this optics-based approach was robust. Blends characterized solely via light scattering contained only hPEO (to conserve expensive dPEO) while those characterized by both SANS and light scattering contained combinations of dPEO and hPEO. Both polymers and LiTFSI salt were dried thoroughly in an argon glovebox. Blends of PEO, PMMA and LiTFSI were made by solution blending followed by drying. All of the steps were conducted in an argon glovebox (see ref. 111 for details). The compositions of the blends studied by light scattering are given in Table 4.1. The entire set of samples used to determine phase behavior are given in Table 4.3 of SI.

Blend compositions are defined by two parameters, ϕ_1, the volume fraction of PEO (defined as component 1) on a salt-free basis and r, the molar ratio of LiTFSI to ether oxygens in PEO. For simplicity, we use ϕ_1 to represent the PEO volume fraction (including both hPEO and dPEO in the case of blends studied by SANS and light scattering). The volume fractions of hPEO and dPEO in each blend are given in Table 4.3 of SI. We calculate ϕ_1 as

$$\phi_1 = \frac{\frac{w_1}{\rho_1}}{\frac{w_1}{\rho_1} + \frac{w_2}{\rho_2}} \tag{4.1}$$

and

$$\phi_2 = 1 - \phi_1 \tag{4.2}$$

where w_{i} and ρ_{i} are the mass and density, respectively of component i in the blend. All of our analysis is at 110°C where $\rho_{\mathrm{i}} = 1.16$ g cm^{-3} (dPEO) and $\rho_2 = 1.16$ g cm^{-3} (PMMA).[73] For blends comprising of mixtures of hPEO and dPEO appropriate corrections were made to account for deuteration ($\rho_1 = 1.06$ g cm^{-3} for hPEO). The total polymer volume fraction of our blend electrolyte is given by

$$\phi_{\mathrm{pol}} = \frac{\frac{w_1}{\rho_1} + \frac{w_2}{\rho_2}}{\frac{w_1}{\rho_1} + \frac{w_2}{\rho_2} + \frac{w_{\mathrm{salt}}}{\rho_{\mathrm{salt}}}} \tag{4.3}$$

where w_{salt} is the mass of LiTFSI in our blend and $\rho_{\mathrm{salt}} = 2.023$ g cm^{-3}. We define salt concentration, r, as

$$r = \frac{[\mathrm{Li}]}{[\mathrm{EO}]} = \frac{\frac{w_{salt}}{M_{LiTFSI}}}{\frac{w_1}{M_{EO}}} \tag{4.4}$$

where $M_{\mathrm{LiTFSI}} = 287.09$ g/mol and $M_{\mathrm{EO}} = 44.05$ g/mol. For blends comprising of mixtures of hPEO and dPEO appropriate corrections were made to account for deuteration ($M_{\mathrm{dEO}} = 48.08$ g/mol).

Sample Number	$\boldsymbol{\phi_1}$	$\boldsymbol{r}$	$\boldsymbol{P_t}$%	$\boldsymbol{P_s}$%	**Miscibility**	**Characterization Method**
1	0.16	0.22	0.21	7.93	Immiscible	LS
2	0.30	0	71.4	1.26	Miscible	LS + SANS
3	0.30	0.053	0.051	1.08	Immiscible	LS + SANS
4	0.30	0.11	0.74	2.49	Immiscible	LS + SANS
5	0.30	0.14	0.037	2.23	Immiscible	LS
6	0.31	0.20	0.33	12.8	Immiscible	LS
7	0.42	0	64.9	2.63	Miscible	LS
8	0.42	0.048	0.050	2.19	Immiscible	LS
9	0.42	0.098	0.016	1.09	Immiscible	LS
10	0.50	0	19.6	19.0	Miscible	LS + SANS
11	0.50	0.053	0.072	2.26	Immiscible	LS + SANS
12	0.63	0	71.4	0.68	Miscible	LS
13	0.62	0.049	20.9	9.05	Miscible	LS
14	0.62	0.092	0.085	1.58	Immiscible	LS
15	0.71	0	71.2	1.90	Miscible	LS + SANS
16	0.71	0.050	32.5	15.8	Miscible	LS + SANS
17	0.71	0.10	41.0	5.92	Miscible	LS + SANS

Table 4.1: Compositions of blends studied, light scattering results, and conclusions regarding miscibility

In Table 4.1, P_{t} is the percent of power transmitted through the sample, and P_{s} is the percent of power scattered by the sample in the forward direction.

4.4 Results and Discussion

We begin by describing the model developed in ref. 111 to predict the phase behavior of polymer blend electrolytes. The free energy of mixing, ΔG_{m} is given by a simple extension of the Flory-Huggins theory that accounts for the presence of salt:

$$\frac{v\Delta G_{\mathrm{m}}}{k_{\mathrm{B}}T} = \frac{\phi_1 ln\phi_1}{N_1} + \frac{\phi_2 ln\phi_2}{N_2} + \chi\left(\phi_1, \phi_{\mathrm{s}}, T\right)\phi_1\phi_2 \tag{4.5}$$

where ΔG_{m} is the Gibbs free energy of mixing, k_{B} is the Boltzmann constant, T is the absolute temperature, N_{i} is the number of repeat units in chain i, ϕ_{i} is the volume fraction

of component i, v is the reference volume (set to 0.1 nm^3), the volume fraction of added salt is ϕ_s, and ϕ_{pol} = 1 - ϕ_s, and the interactions between the salt and the polymers is captured by an effective χ parameter that depends not only on temperature but also on salt concentration.[35,39,43] Both ϕ_1 and ϕ_2 represent the volume fractions of polymer 1 and 2 respectively, on a salt free basis. χ for PEO/PMMA /LiTFSI blends at 110°C is given by:

$$\chi(\phi_1, r) = \left(A(r) + \frac{B(r)}{3} + \frac{C(r)}{6}\right) + \left(\frac{B(r)}{3} + \frac{C(r)}{6}\right)\phi_1 + \frac{C(r)}{6}\phi_1^2 \tag{4.6}$$

where A, B and C were obtained by fitting SANS data from the blends at 3 different r values. In Figure 4.2, we plot these fitting parameters as a function of r. Their values at intermediate values of r are given by linear interpolation:

$$A(r) = \zeta_A r + \tau_A \tag{4.7}$$

$$B(r) = \zeta_B r + \tau_B \tag{4.8}$$

$$C(r) = \zeta_C r + \tau_C \tag{4.9}$$

The values of ζ_i and τ_i (i = A, B, or C) for the two regimes, $0 \leq r < 0.05$ and $0.05 \leq r < 0.10$ are given in the caption of Figure 4.2. The phase boundary between miscible and immiscible systems is assumed to be given by the spinodal curve (details are provided in ref. 111).

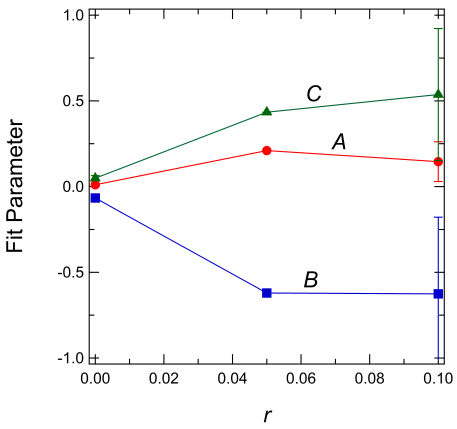

Figure 4.2: Fit parameters A, B and C from ref. 111 are plotted as a function of salt concentration, r. These are the parameters used in equation 4.6 to determine χ. The solid lines from $0 \leq r < 0.05$ and $0.05 \leq r < 0.10$ are used to interpolate the data; see equations 7, 8, and 9. For the interpolation lines in the $0 \leq r \leq 0.05$ range, ζ_A= 3.99 and τ_A = 0.0108; ζ_B= -11.1 and τ_B = -0.0666; ζ_C= 7.70 and τ_C = 0.0488. For the interpolation lines in the $0.05 \leq r \leq 0.10$ range, ζ_A= -1.29 and τ_A = 0.275; ζ_B= -0.09 and τ_B = -0.615; ζ_C= 2.06 and τ_C = 0.331.

Next, we discuss light scattering (LS) data. While light scattering has often been used to determine blend miscibility,[18,112–115] its efficacy can vary based upon the relative refractive indices of the system components.[114,116] In some cases, it is sufficient to measure the intensity of the forward-scattered light,[18] while in samples exhibiting such strong multiple scattering that they are nearly opaque, it is more informative to measure the fraction of the incident beam power that is transmitted through the sample.[40,117,118] The addition of salt to a binary polymer blend system poses further complications due to the large difference between the refractive index of salt and polymers, and the partitioning of salt in the phase separated systems. In Figure 4.3, we plot the % of transmitted power against the % of scattered power in the forward direction (between scattering angles of 1.3 and 13 degrees). The % scattered power varied from 1 to 19%. There was no correlation between this parameter and miscibility determined by SANS. In contrast, the measured % of transmitted power values fell clearly into two groups; the blends that were determined to be immiscible by SANS exhibited % of transmitted power values less than 1%, while blends that were determined to be miscible by SANS exhibited % of transmitted power values greater than 20% (in some cases, as high as 80%). We thus used the % of transmitted power to distinguish between miscible and immiscible samples in cases where we only had access to light scattering data. All samples that fell within the dashed box in Figure 4.3 were labeled immiscible while those outside the box were labeled miscible.

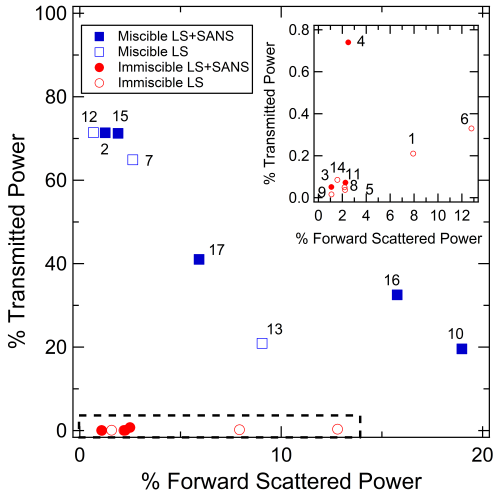

Figure 4.3: A plot of % transmitted power versus % forward-scattered power obtained by light scattering on PEO/PMMA/LiTFSI blends at 110°C. Inset shows an enlargement of the dashed box at the bottom of the main plot. Data from miscible samples are indicated by squares and data from immiscible samples are indicated by circles. Filled squares and circles represent samples characterized by both light scattering and SANS while empty squares and circles represent samples characterized by light scattering alone. The numbers correspond to the sample numbers indicated in Table 4.1.

The compositions of the miscible and immiscible PEO/PMMA/LiTFSI blend electrolytes are depicted in Figure 4.4a on a ϕ_1 versus r plot. The phase boundary is determined by bisecting lines drawn between two adjacent data points at the miscible/immiscible boundary. The vertical line at $r = 0.045$ is a parsimonious extrapolation of the phase boundary determined at $\phi_1 = 0.5$. All salt-free PEO/PMMA blends are miscible. A region of immiscibility develops upon the addition of salt. Particularly striking is the appearance of an immiscible "chimney" in Figure 4.4a. This chimney is defined by two immiscible samples: $\phi_1 = 0.50$, $r = 0.053$ and $\phi_1 = 0.62$, $r = 0.092$. Several samples with compositions close to these two samples were miscible. In Figure 4.4b, we show the phase boundary for our PEO/PMMA/LiTFSI blends at 110°C based on the model described above. The model-based boundary contains two separate immiscible regions. The lower region at $\phi_1 = 0.50$ is in quantitative agreement with the experimental phase diagram. The upper region, which is narrow along ϕ_1 and broad along r is in qualitative agreement with the experimental chimney (Figure 4.4a). The main discrepancies between the experiments and the model are: (1) The experimentally determined upper immiscible window occurs at lower values of ϕ_1, and (2) the experimentally determined upper immiscible window is connected to the large lower immiscibility window.

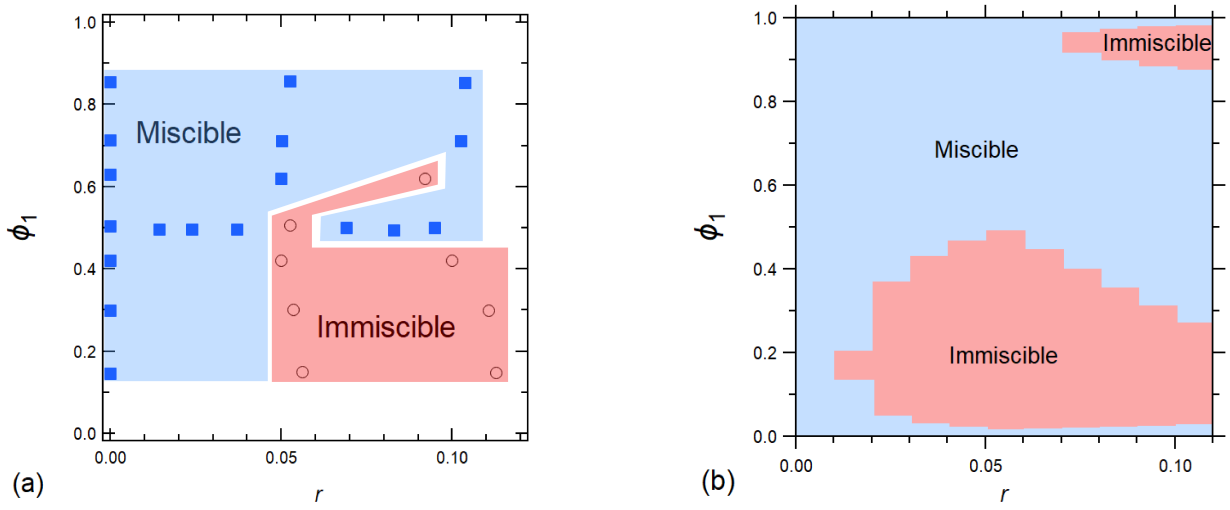

Figure 4.4: Phase behavior of PEO/PMMA/LiTFSI blends showing miscible and immiscible blends on a plot of salt-free volume fraction of PEO, ϕ_1, versus salt concentration, r at 110°C. Component 1 is PEO. (a) Experiments. Filled blue squares indicate a miscible blend, and empty circles indicate an immiscible blend. The white regions surrounding the phase diagram were not explored, (b) Model predictions.

4.5 Conclusions

In this study we developed a comprehensive map of PEO/PMMA/LiTFSI phase behavior, combining data from both SANS and light scattering. The results are presented on a PEO composition (ϕ_1) versus salt concentrations (r) phase diagram. The immiscible window has a broad base at low values of ϕ_1 ($\phi_1 < 0.4$), and it narrows at higher compositions ($\phi_1 > 0.4$) resulting in a crooked chimney that is broad along the r–axis. A simple Flory-Huggins type model with χ parameters determined fitting SANS data from homogeneous systems provides a basis for predicting the complex phase behavior that we have observed. The SANS data indicate a quadratic dependence of χ on ϕ_1 with coefficients that depend on r. It is likely that these dependencies arise from ionic correlations,[105,106] but the connection between them and our model remains to be established. A more detailed experimental study of the dependence of the thermodynamics of PEO/PMMA/LiTFSI blends as a function of composition and chain length seems warranted.

4.6 Acknowledgements

This work was supported by the National Science Foundation grant DMR 1904508 to the University of California, Berkeley and grant DMR 1904537 to New York University. Any opinions, findings, and conclusions or recommendations expressed in this paper are those of the authors and do not necessarily reflect the views of the National Science Foundation. We thank Dr. David Halat for insightful discussions. This research used resources at the High Flux Isotope Reactor, a DOE Office of Science User Facility operated by the Oak Ridge National Laboratory.

4.7 Nomenclature

A, B, C, empirical fitting constants for χ

$Đ$, dispersity

ΔG_{m}, Gibbs free energy of mixing per unit volume (J m^{-3})

k_{b}, Boltzmann constant (m^2 kg s^{-2} K^{-1})

M_{i}, molar mass of species i (g mol^{-1})

M_{w}, weight-averaged molar mass (kg mol^{-1})

M_{n}, number-averaged molar mass (kg mol^{-1})

q, scattering vector (nm^{-1})

r, salt concentration in PEO ([Li] [EO]$^{-1}$)

T, absolute temperature (K)

Greeks

ζ_i, slope of linear fits of fitting constants A, B, and C

τ_i, intercept of linear fits of fitting constants A, B, and C

v_{ref}, reference volume of species i (cm^3 mol^{-1})

ρ_i, density of species i (g cm^{-1})

ϕ_i, volume fraction of species i on a salt-free basis

Θ, scattering angle

λ, wavelength (nm)

χ, Flory-Huggins interaction parameter

4.8 Supporting Information

Materials and Methods

Polymer Blend Electrolyte Preparation and Composition

The polymer blend electrolytes used in this study were prepared in a glovebox, following methods detailed by Shah et al.[111] The molar masses, Mn, dispersities, $Đ$, of PEO (Polymer Source), fully deuterated PEO, dPEO (Polymer Source), and PMMA (Polymer Source) used in this study are summarized in Table 4.2. Blends that were characterized using SANS contained dPEO, while blends characterized using only LS contained PEO. The exact composition of each blend electrolyte, as well as polymer volume fraction and characterization method are shown Table 4.2.

Polymer	M_n **(kg mol^{-1})**	$Đ$
PEO	8.5	1.05
dPEO-1	8	1.12
dPEO-2	8.5	1.1
PMMA	47.3	1.05

Table 4.2: Polymer Properties

LS Sample Preparation

LS samples were made by melt pressing the polymer into 1/32 in thick Viton Spacers (McMaster Carr) with an inner diameter of 1/8 in an argon glovebox at 110°C. These spacers were placed in custom airtight aluminum sample holders with fused silica windows (Esco Optics). LS measurements were conducted at NYU in the Garetz lab.

LS Experiments

The LS setup is shown in Figure S1. The laser source for the LS experiments was a Coherent OBIS 640 nm LX 40 mW cw diode laser, which emits up to 40 mW of power at a wavelength of 640 nm. The polymer sample was inserted into a heating block and was heated to 110°C by two stainless steel cartridge heating rods (Omega Engineering, Inc). The temperature was controlled with an Omega Engineering controller. The temperature was measured with a thermocouple mounted in the heating block, and a second temperature sensor was attached to the sample to help calibrate the temperature of the sample.

The laser beam entered the sample through a fused silica window, and the transmitted beam and forward-scattered light exited through a second fused silica window. The forward scattered light was collected by a large biconvex lens (diameter 6 cm and focal length 5 cm) and was measured by a photodetector positioned near the lens focal point. In an

older setup, the transmitted laser beam was blocked by mounting a small black disk to the center of the input side of the collection lens.[18] For this study, this beam block was replaced with a small 45° mirror with a 6 mm diameter, which redirects the transmitted beam to a second photodetector. Both photodetectors were Coherent PowerMax USB UV/VIS Quantum Power Sensors. The two detectors could simultaneously measure the total forward-scattered power and the transmitted laser-beam power. The incident laser beam power was extremely stable, and was typically set to 12 mW during LS experiments.

In order to account for any spatial anisotropies of a given polymer blend sample, the sample was positioned so that the incident laser entered the sample a little bit off center. The sample could then be rotated by 60-70° to irradiate different portions of the sample. This was repeated at least 3 times for each sample.

Depending on the transparency/opacity of the sample, different magnitude signals were recorded by the two photodetectors. For nearly transparent samples (miscible blends), the transmitted power was high and the forward-scattered power was low. For nearly opaque samples (immiscible blends), the transmitted power was low and the forward-scattered power was also low. For translucent samples (also miscible blends), the transmitted power was intermediate, and the forward scattered power was intermediate.

SANS Sample Preparation and Experiments

SANS sample preparation for this study was previously described in ref 1. SANS measurements were conducted at the GP-SANS beamline at Oak Ridge National Lab in Oak Ridge, TN. SANS measurements were conducted at a neutron wavelength of 6 Å at sample to detector distances of 19.1, 4 and 1 m. This configuration allowed access to a scattering wave-vector magnitude, $q = (4\pi/\lambda)\sin(\Theta)$ ranging from 0.05 nm^{-1} to 6 nm^{-1} from 0.05 nm^{-1} to 6 nm^{-1}. Data were collected at temperatures ranging from 70°C to 130°C in 20°C steps. Sample temperature was controlled by a 12-position Peltier cooling/heating sample changer block. SANS data were reduced using a custom Python script in Jupyter written by ORNL beamline scientists.[98] The total scattering intensity was corrected for sample thickness variations, empty cell and background contributions.[98]

LS Setup

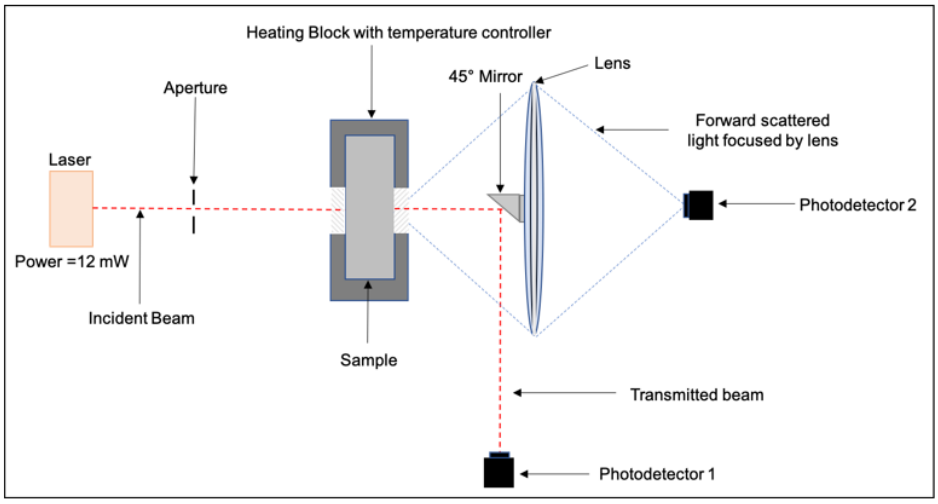

Figure 4.5: A schematic diagram of the setup used for light scattering experiments. A 640 nm-wavelength laser was used as a light source, emitting a beam with a power of 12 mW. Photodetector 1 detects the transmitted beam, and photodetector 2 measures the forward-scattered power.

ϕ_1	r	**Component 1**	**Component 2**	**Characterization Method**
0.15	0	dPEO-2	PMMA	SANS
0.15	0.056	dPEO-2	PMMA	SANS
0.15	0.11	dPEO-2	PMMA	SANS
0.16	0.22	PEO	PMMA	LS
0.30	0	dPEO-2	PMMA	LS + SANS
0.30	0.053	dPEO-2	PMMA	LS + SANS
0.30	0.11	dPEO-2	PMMA	LS + SANS
0.30	0.14	PEO	PMMA	LS
0.31	0.20	PEO	PMMA	LS
0.42	0	PEO	PMMA	LS
0.42	0.048	PEO	PMMA	LS
0.42	0.098	PEO	PMMA	LS
0.50	0	dPEO-1	PMMA	LS + SANS
0.50	0.014	dPEO-1	PMMA	SANS
0.50	0.024	dPEO-1	PMMA	SANS
0.50	0.037	dPEO-1	PMMA	SANS
0.50	0.053	dPEO-1	PMMA	LS + SANS
0.51	0.069	dPEO-1	PMMA	SANS
0.50	0.083	dPEO-1	PMMA	SANS
0.50	0.095	dPEO-1	PMMA	SANS
0.63	0	PEO	PMMA	LS
0.62	0.049	PEO	PMMA	LS
0.62	0.092	PEO	PMMA	LS
0.71	0	dPEO-2 ($\phi_{\mathrm{dPEO}} = 0.15$) ($\phi_{\mathrm{PEO}} = 0.55$)	PMMA	LS + SANS
0.71	0.050	dPEO-2 ($\phi_{\mathrm{dPEO}} = 0.15$) ($\phi_{\mathrm{PEO}} = 0.55$)	PMMA	LS + SANS
0.71	0.10	dPEO-2 ($\phi_{\mathrm{dPEO}} = 0.15$) ($\phi_{\mathrm{PEO}} = 0.55$)	PMMA	LS + SANS
0.86	0	dPEO-2 ($\phi_{\mathrm{dPEO}} = 0.15$) ($\phi_{\mathrm{PEO}} = 0.70$)	PMMA	SANS
0.86	0.053	dPEO-2 ($\phi_{\mathrm{dPEO}} = 0.15$) ($\phi_{\mathrm{PEO}} = 0.70$)	PMMA	SANS
0.85	0.10	dPEO-2 ($\phi_{\mathrm{dPEO}} = 0.15$) ($\phi_{\mathrm{PEO}} = 0.70$)	PMMA	SANS

Table 4.3: Polymer Blend Electrolyte Samples

Error Analysis

To test the robustness of our model, we varied the coefficients A, B and C by $\pm 20\%$ and calculated phase diagrams. The results are shown in Figure S2.

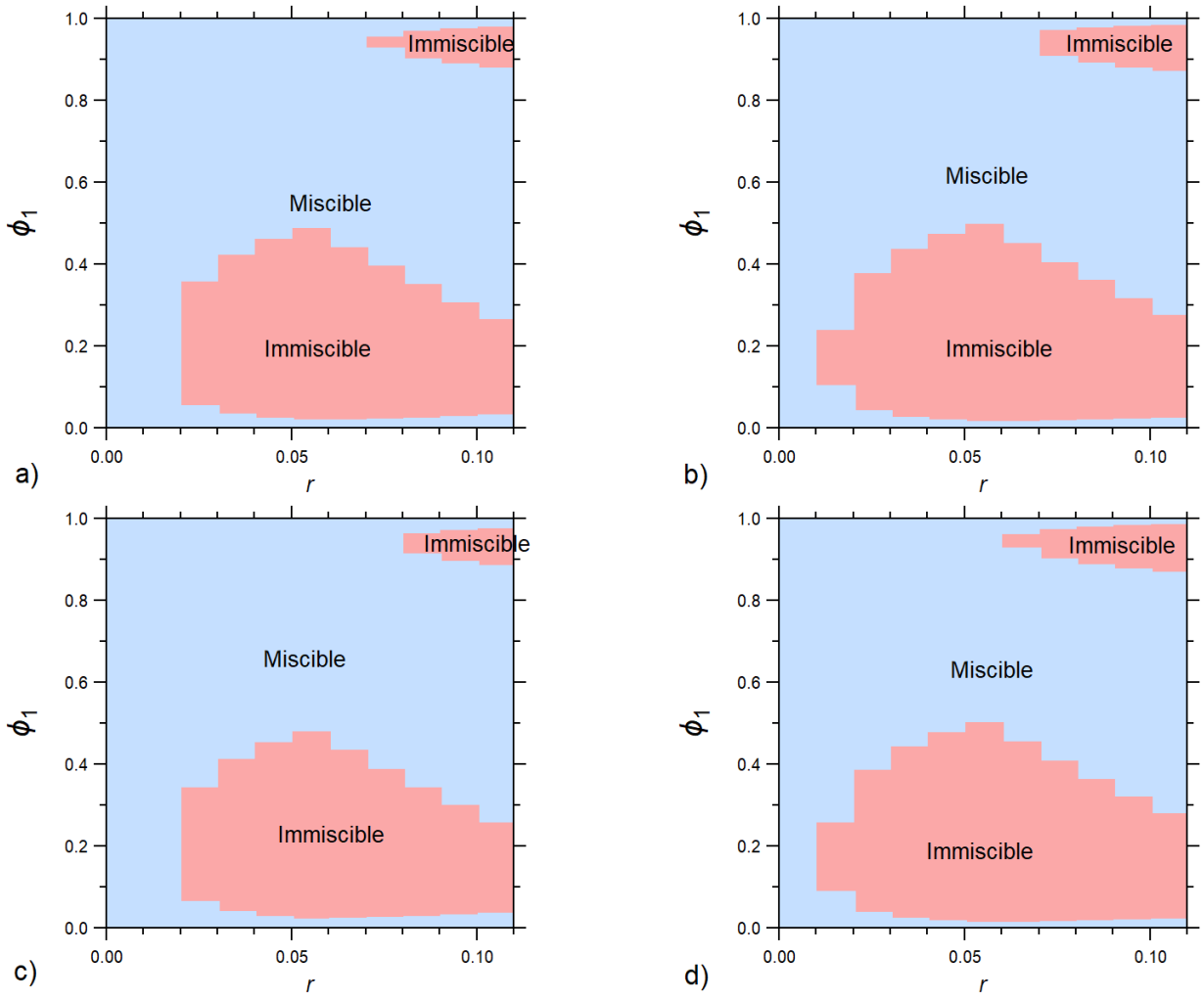

Figure 4.6: Theoretical phase diagrams wherein (a), A, B and C are reduced by 10%. In (b) A, B and C are increased by 10%. In (c) A, B and C are reduced by 20%. In (d) A, B and C are increased by 20%. All increases and reductions are relative to values of parameters provided in the main text.

Chapter 5

Conclusion

The development of solid polymer electrolytes is critical to enabling functional lithium metal anode batteries. Careful analysis of the thermodynamics and phase behavior of polymer electrolytes is essential for the design of next generation polymer electrolytes. In this work, we analyzed the effect of added salt on a miscible polymer electrolyte system, calculated thermodynamic interaction parameters, characterized the phase behavior, and created a preliminary thermodynamic model for polymer electrolyte phase behavior.

In Chapter 2, we synthesized two PEO-PMMA block copolymers: PEO-PMMA(10-33) and PEO-PMMA(10-64). We created a series of electrolytes by adding LiTFSI salt and characterized the phase behavior via small angle X-ray scattering (SAXS). Based on the predictions of Fredrickson and Cochran,[28] we expected to see phase separation in PEO-PMMA(10-33), not PEO-PMMA(10-64). However, all scattering profiles of PEO-PMMA(10-33) were featureless whereas scattering profiles of PEO-PMMA(10-64) samples with moderate amounts of added salt featured a single broad peak. This single broad peak may be interpreted as a hallmark of phase separation.[27,57] The preliminary evidence of phase separation in the PEO-PMMA(10-64) electrolytes supported the predictions of ionic self consistent field theory, developed by Sing and coworkers.[41] We utilized an extension of Leibler's random phase approximation to calculate salt distribution between the PEO and PMMA blocks and determine χ_{eff} as a function of salt concentration in both blocks.[27,79] We found that χ_{eff} is a non-monotonic function of salt concentration in our system.

In Chapter 3, we created a series of PEO/PMMA blend electrolytes, based upon our previously studied PEO-PMMA block copolymer electrolytes. We characterized the phase behavior of these blends via small angle neutron scattering (SANS). We created blends with compositions ranging from $\phi_1 = 0.15$ to $\phi_1 = 0.85$ with salt concentrations ranging from $r = 0$ to $r = 0.10$ (component 1 is PEO). We found that the addition of salt in PEO-lean blends induced phase separation, while PEO-rich blends remained miscible upon the addition of salt. The symmetric blends ($\phi_1 = 0.50$) only phase separated at $r = 0.05$. All salt free ($r = 0$) blends were miscible. Intriguingly, the window of phase separation in $r = 0.05$ blends was larger than the window of phase separation in $r = 0.10$ blends. In this blend system, blend composition has a stronger influence on miscibility than salt concentration. We

utilized de Gennes random phase approximation to calculate experimental thermodynamic interaction parameters. We used our calculated χ parameters, in conjunction with theoretical work by Sanchez, and the Flory-Huggins framework to calculate a spinodal curve.[14,15,100] We utilized our spinodal curve to predict the phase behavior of our blends, and found exceptional agreement between theory and experiment.

In Chapter 4, we expanded on the work in Chapter 3, by creating additional blends at intermediate volume fractions and characterizing the phase behavior of these blends using light scattering to create a comprehensive phase diagram for PEO/PMMA/LiTFSI blends. We plotted the phase behavior on a composition versus salt concentration diagram. The window of immiscibility covers PEO-lean blends ($\phi_1 < 0.40$) where $r \geq 0.05$. This window narrows at higher compositions ($\phi_1 > 0.40$) resulting in the formation of a chimney along the r axis. We utilized our Flory-Huggins model to create a simulated phase diagram, which was in excellent agreement with our experimental phase diagram. The presence of a chimney provided experimental evidence for theoretical work by de la Cruz and coworkers which predicted the presence of multiple immiscible windows in salt containing polymer blends.[46]

From the comprehensive study of miscible block copolymer electrolytes and polymer blend electrolytes we found that the underlying thermodynamics of polymer-salt interactions are incredibly complex. While early theories had suggested that thermodynamic interaction parameters would increase linearly with respect to salt concentration, our work demonstrates that in PEO/PMMA/LiTFSI systems, interaction parameters depend non-linearly on salt concentration. The results from this study suggest that this non-linearity could be driven by electrostatic cohesion, ionic correlations and other effects previously theorized by Sing, de la Cruz and others.[41,42,46] More research is required to clearly define the molecular underpinnings of the data collected in this work. Future studies should comprise measurements of χ, by synthesizing a larger variety of PEO-PMMA block copolymers and PEO/PMMA blends with a wider range of salt compositions and chain lengths. Techniques like Fourier-transform infrared spectroscopy can shed further light into salt distribution in these systems, further enhancing the models developed in this work. This work provides a starting point for the analysis of complex thermodynamics in polymer electrolytes.

References

(1) Young, W. S.; Kuan, W. F.; Epps, T. H. *Journal of Polymer Science, Part B: Polymer Physics* **2014**, *52*, 1–16.

(2) Lin, D.; Liu, Y.; Cui, Y. *Nature Nanotechnology* **2017**, *12*, 194–206.

(3) Blatt, M. P.; Hallinan, D. T. *Industrial and Engineering Chemistry Research* **2021**, *60*, 17303–17327.

(4) Panday, A.; Mullin, S.; Gomez, E. D.; Wanakule, N.; Chen, V. L.; Hexemer, A.; Pople, J.; Balsara, N. P. *Macromolecules* **2009**, *42*, 4632–4637.

(5) Xu, K. *Chemical Reviews* **2004**, *104*, 4303–4417.

(6) Hallinan, D. T.; Balsara, N. P. *Annual Review of Materials Research* **2013**, *43*, 503–525.

(7) Loo, W. S.; Sethi, G. K.; Teran, A. A.; Galluzzo, M. D.; Maslyn, J. A.; Oh, H. J.; Mongcopa, K. I.; Balsara, N. P. *Macromolecules* **2019**, *52*, 5590–5601.

(8) Fenton, D. E.; Parker, J. M.; Wright, P. V. *Polymer* **1973**, *14*, 589.

(9) Nguyen, N.; Blatt, M. P.; Kim, K.; Hallinan, D. T.; Kennemur, J. G. *Polymer Chemistry* **2022**, *13*, 4309–4323.

(10) Glynos, E.; Petropoulou, P.; Mygiakis, E.; Nega, A. D.; Pan, W.; Papoutsakis, L.; Giannelis, E. P.; Sakellariou, G.; Anastasiadis, S. H. *Macromolecules* **2018**, *51*, 2542–2550.

(11) Gao, K. W.; Loo, W. S.; Snyder, R. L.; Abel, B. A.; Choo, Y.; Lee, A.; Teixeira, S. C.; Garetz, B. A.; Coates, G. W.; Balsara, N. P. *Macromolecules* **2020**, *53*, 5728–5739.

(12) De Gennes, P. G., *Scaling Concepts in Polymer Chemistry*; Cornell University Press: Ithaca, NY, 1979, p 109.

(13) Bates, F. S.; Fredrickson, G. H. *Physics Today* **1999**, *52*, 32–38.

(14) Flory, P. J. *Journal of Chemical Physics* **1942**, *10*, 51–61.

(15) Huggins, M. L. *The Journal of Chemical Physics* **1941**, *9*, 440.

(16) Schwahn, D.; Mortensen, K.; Springer, T.; Yee-Madeira, H.; Thomas, R. *The Journal of Chemical Physics* **1987**, *87*, 6078–6087.

(17) Reichart, G. C.; Register, R. A.; Graessley, W. W.; Lohse, D. J. *Macromolecules* **1995**, *04*, 8862–8864.

(18) Balsara, N. P.; Fetters, L. J.; Hadjichristidis, N.; Lohse, D. J.; Han, C. C.; Graessley, W. W.; Krishnamoorti, R. *Macromolecules* **1992**, *25*, 6137–6147.

(19) Schwahn, D.; Hahn, K.; Streib, J.; Springer, T. *The Journal of Chemical Physics* **1990**, *93*, 8383–8391.

(20) Balsara, N. P.; Lohse, D. J.; Graessley, W. W.; Krishnamoorti, R. *The Journal of Chemical Physics* **1994**, *100*, 3905–3910.

(21) Londono, J. D.; Narten, A. H.; Wignall, G. D.; Honnell, K. G.; Hsieh, E. T.; Johnson, T. W.; Bates, F. S. *Macromolecules* **1994**, *27*, 2864–2871.

(22) Cabral, J. T.; Higgins, J. S. *Macromolecules* **2009**, *42*, 9528–9536.

(23) Beaucage, G.; Sukumaran, S.; Clarson, S. J.; Kent, M. S.; Schaefer, D. W. *Macromolecules* **1996**, *29*, 8349–8356.

(24) Thudium, R. N.; Han, C. C. *Macromolecules* **1996**, *29*, 2143–2149.

(25) Bates, F. S.; Muthukumar, M.; Wignall, G. D.; Fetters, L. J. *The Journal of Chemical Physics* **1988**, *89*, 535–544.

(26) Han, C. C.; Bauer, B. J.; Clark, J. C.; Muroga, Y.; Matsushita, Y.; Okada, M.; Tran-cong, Q.; Chang, T.; Sanchez, I. C. *Polymer* **1988**, *29*, 2002–2014.

(27) Leibler, L. *Macromolecules* **1980**, *13*, 1602–1617.

(28) Cochran, E. W.; Garcia-Cervera, C. J.; Fredrickson, G. H. *Macromolecules* **2006**, *39*, 2449–2451.

(29) Bates, F. *Annual Review of Physical Chemistry* **1990**, *41*, 525–557.

(30) Floudas, G.; Vazaiou, B.; Schipper, F.; Ulrich, R.; Wiesner, U.; Iatrou, H.; Hadjichristidis, N. *Macromolecules* **2001**, *34*, 2947–2957.

(31) De Gennes, P. *Journal de Physique* **1970**, *31*, 235–238.

(32) Hammouda, B. *Journal of Non-Crystalline Solids* **1994**, *172-174*, 927–931.

(33) Mori, K.; Tanaka, H.; Hasegawa, H.; Hashimoto, T. *Polymer* **1989**, *30*, 1389–1398.

(34) Teran, A. A.; Balsara, N. P. *Journal of Physical Chemistry B* **2014**, *118*, 4–17.

(35) Young, W. S.; Epps, T. H. *Macromolecules* **2009**, *42*, 2672–2678.

(36) Wanakule, N. S.; Virgili, J. M.; Teran, A. A.; Wang, Z. G.; Balsara, N. P. *Macromolecules* **2010**, *43*, 8282–8289.

(37) Nakamura, I.; Balsara, N. P.; Wang, Z. G. *Physical Review Letters* **2011**, *107*, 1–5.

(38) Nakamura, I.; Wang, Z. G. *Soft Matter* **2012**, *8*, 9356–9367.

(39) Ruzette, A. V. G.; Soo, P. P.; Sadoway, D. R.; Mayes, A. M. *Journal of the Electrochemical Society* **2001**, *148*, 537–543.

(40) Xie, S.; Lodge, T. P. *Macromolecules* **2018**, *51*, 266–274.

(41) Sing, C. E.; Zwanikken, J. W.; Olvera De La Cruz, M. *Nature Materials* **2014**, *13*, 694–698.

(42) Hou, K. J.; Qin, J. *Macromolecules* **2018**, *51*, 7463–7475.

(43) Loo, W. S.; Galluzzo, M. D.; Li, X.; Maslyn, J. A.; Oh, H. J.; Mongcopa, K. I.; Zhu, C.; Wang, A. A.; Wang, X.; Garetz, B. A.; Balsara, N. P. *Journal of Physical Chemistry B* **2018**, *122*, 8065–8074.

(44) Loo, W. S.; Balsara, N. P. *Journal of Polymer Science, Part B: Polymer Physics* **2019**, *57*, 1177–1187.

(45) Wu, X.; Song, T.; Wei, Z.; Shen, L.; Jiang, H.; Ke, Y.; He, C.; Yang, H.; Shi, W. *Polymer* **2022**, *260*, 125307.

(46) Kwon, H. K.; Ma, B.; Olvera De La Cruz, M. *Macromolecules* **2019**, *52*, 535–546.

(47) Sing, C. E.; Olvera De La Cruz, M. *ACS Macro Letters* **2014**, *3*, 698–702.

(48) Gartner, T. E.; Morris, M. A.; Shelton, C. K.; Dura, J. A.; Epps, T. H. *Macromolecules* **2018**, *51*, 1917–1926.

(49) Sethi, G. K.; Jung, H. Y.; Loo, W. S.; Sawhney, S.; Park, M. J.; Balsara, N. P.; Villaluenga, I. *Macromolecules* **2019**, *52*, 3165–3175.

(50) Chow, T. *Macromolecules* **1990**, *23*, 333–337.

(51) Colby, R. H. *Polymer* **1989**, *30*, 1275–1278.

(52) Schmidt, M.; Maurer, F. H. J. *Journal of Polymer Science, Part B: Polymer Physics* **1997**, *36*, 1061–1080.

(53) Lodge, T. P.; Wood, E. R.; Haley, J. C. *Journal of Polymer Science, Part B: Polymer Physics* **2006**, *44*, 756–763.

(54) Silvestre, C.; Cimmino, S.; Martuscelli, E.; Karasz, F. E.; MacKnight, W. J. *Polymer* **1987**, *28*, 1190–1199.

(55) Ito, H.; Russell, T. P.; Wignall, G. D. *Macromolecules* **1987**, *20*, 2213–2220.

(56) Gunkel, I.; Stepanow, S.; Thurn-Albrecht, T.; Trimper, S. *Macromolecules* **2007**, *40*, 2186–2191.

(57) Fredrickson, G. H.; Helfand, E. *The Journal of Chemical Physics* **1987**, *87*, 697–705.

(58) Chanpuriya, S.; Kim, K.; Zhang, J.; Lee, S.; Arora, A.; Dorfman, K. D.; Delaney, K. T.; Fredrickson, G. H.; Bates, F. S. *ACS Nano* **2016**, *10*, 4961–4972.

(59) Lee, S.; Leighton, C.; Bates, F. S. *Proceedings of the National Academy of Sciences of the United States of America* **2014**, *111*, 17723–17731.

(60) Liu, M.; Qiang, Y.; Li, W.; Qiu, F.; Shi, A. C. *ACS Macro Letters* **2016**, *5*, 1167–1171.

(61) Matsen, M. W.; Schick, M. *Physical Review Letters* **1994**, *72*, 2660–2663.

(62) Ganesan, V.; Jayaraman, A. *Soft Matter* **2014**, *10*, 13–38.

(63) Martin, J. M.; Li, W.; Delaney, K. T.; Fredrickson, G. H. *Journal of Chemical Physics* **2016**, *145*, DOI: 10.1063/1.4964680.

(64) Grzetic, D. J.; Delaney, K. T.; Fredrickson, G. H. *ACS Macro Letters* **2019**, *8*, 962–967.

(65) Soo, P. P.; Huang, B.; Jang, Y.-I.; Chiang, Y.-M.; Sadoway, D. R.; Mayes, A. M. *Journal of The Electrochemical Society* **1999**, *146*, 32–37.

(66) Morris, M. A.; An, H.; Lutkenhaus, J. L.; Epps, T. H. *ACS Energy Letters* **2017**, *2*, 1919–1936.

(67) Gopinadhan, M.; Majewski, P. W.; Osuji, C. O. *Macromolecules* **2010**, *43*, 3286–3293.

(68) Nakamura, I.; Wang, Z. G. *ACS Macro Letters* **2014**, *3*, 708–711.

(69) Marko, J. F.; Rabin, Y. *Macromolecules* **1992**, *25*, 1503–1509.

(70) Eitouni, H. B.; Balsara, N. P. In *Physical Properties of Polymers Handbook*, 2nd; Springer: New York, 2006; Chapter 19, pp 339–356.

(71) Matyjaszewski, K. *Advanced Materials* **2018**, *30*, 1–22.

(72) Hou, K. J.; Loo, W. S.; Balsara, N. P.; Qin, J. *Macromolecules* **2020**, *53*, 3956–3966.

(73) Mark, J. E., *Physical Properties of Polymers Handbook*, Second; Springer: Philadelphia, PA, 2007.

(74) Sun, X.; Zhang, H.; Zhang, L.; Wang, X.; Zhou, Q. F. *Polymer Journal* **2005**, *37*, 102–108.

(75) Hexemer, A.; Bras, W.; Glossinger, J.; Schaible, E.; Gann, E.; Kirian, R.; MacDowell, A.; Church, M.; Rude, B.; Padmore, H. *Journal of Physics: Conference Series* **2010**, *247*, 1–11.

(76) Ilavsky, J. *Journal of Applied Crystallography* **2012**, *45*, 324–328.

(77) Gunkel, I.; Thurn-Albrecht, T. *Macromolecules* **2012**, *45*, 283–291.

(78) Naidu, S.; Ahn, H.; Gong, J.; Kim, B.; Ryu, D. Y. *Macromolecules* **2011**, *44*, 6085–6093.

(79) Chintapalli, M.; Timachova, K.; Olson, K. R.; Mecham, S. J.; Desimone, J. M.; Balsara, N. P. *Macromolecules* **2020**, *53*, 1142–1153.

(80) Lin, C. C.; Jonnalagadda, S. V.; Kesani, P. K.; Dai, H. J.; Balsara, N. P. *Macromolecules* **1994**, *27*, 7769–7780.

(81) Chintapalli, M.; Chen, X. C.; Thelen, J. L.; Teran, A. A.; Wang, X.; Garetz, B. A.; Balsara, N. P. *Macromolecules* **2014**, *47*, 5424–5431.

(82) Huang, J.; Tong, Z. Z.; Zhou, B.; Xu, J. T.; Fan, Z. Q. *Polymer* **2013**, *54*, 3098–3106.

(83) Borodin, O.; Smith, G. D. *Macromolecules* **2006**, *39*, 1620–1629.

(84) Edman, L. *Journal of Physical Chemistry B* **2000**, *104*, 7254–7258.

(85) Diddens, D.; Heuer, A.; Borodin, O. *Macromolecules* **2010**, *43*, 2028–2036.

(86) Balsara, N. P.; Fetters, L. J.; Hadjichristidis, N.; Lohse, D. J.; Han, C. C.; Graessley, W. W.; Krishnamoorti, R. *Macromolecules* **1992**, *25*, 6137–6147.

(87) Krishnamoorti, R.; Graessley, W. W.; Balsara, N. P.; Lohse, D. J. *The Journal of Chemical Physics* **1994**, *100*, 3894–3904.

(88) Maurer, W. W.; Bates, F. S.; Lodge, T. P.; Almdal, K.; Mortensen, K.; Fredrickson, G. H. *Journal of Chemical Physics* **1998**, *108*, 2989–3000.

(89) Jangareddy, S.; Sun, T.; Burns, A. B.; Register, R. A. *Macromolecules* **2021**, *54*, 3999–4009.

(90) Hillmyer, M. A.; Maurer, W. W.; Lodge, T. P.; Bates, F. S.; Almdal, K. *Journal of Physical Chemistry B* **1999**, *103*, 4814–4824.

(91) Ryu, D. Y.; Park, M. S.; Chae, S. H.; Jang, J.; Kim, J. K.; Russell, T. P. *Macromolecules* **2002**, *35*, 8676–8680.

(92) Irwin, M. T.; Hickey, R. J.; Xie, S.; Bates, F. S.; Lodge, T. P. *Macromolecules* **2016**, *49*, 4839–4849.

(93) Jo, G.; Kim, O.; Kim, H.; Hyeok Choi, U.; Lee, S. B.; Jeong Park, M. *Polymer Journal* **2016**, *48*, 465–472.

(94) Shah, N. J.; Dadashi-Silab, S.; Galluzzo, M. D.; Chakraborty, S.; Loo, W. S.; Matyjaszewski, K.; Balsara, N. P. *Macromolecules* **2021**, *54*, 1414–1424.

(95) Loo, W. S.; Mongcopa, K. I.; Gribble, D. A.; Faraone, A. A.; Balsara, N. P. *Macromolecules* **2019**, *52*, 8724–8732.

(96) Xie, S.; Zhang, B.; Mao, Y.; He, L.; Hong, K.; Bates, F. S.; Lodge, T. P. *Macromolecules* **2020**, *53*, 7141–7149.

(97) Heller, W. T.; Cuneo, M.; Debeer-Schmitt, L.; Do, C.; He, L.; Heroux, L.; Littrell, K.; Pingali, S. V.; Qian, S.; Stanley, C.; Urban, V. S.; Wu, B.; Bras, W. *Journal of Applied Crystallography* **2018**, *51*, 242–248.

(98) Heller, W. T. et al. *SoftwareX* **2022**, *19*, 101101.

(99) Nedoma, A. J.; Robertson, M. L.; Wanakule, N. S.; Balsara, N. P. *Macromolecules* **2008**, *41*, 5773–5779.

(100) Sanchez, I. C. *Polymer* **1989**, *30*, 471–475.

(101) Lascaud, S.; Perrier, M.; Vallée, A.; Besner, S.; Prudhomme, J.; Armand, M. *Macromolecules* **1994**, *27*, 7469–7477.

(102) Yan, L.; Rank, C.; Mecking, S.; Winey, K. I. *Journal of the American Chemical Society* **2020**, *142*, 857–866.

(103) Kambe, Y.; Arges, C. G.; Czaplewski, D. A.; Dolejsi, M.; Krishnan, S.; Stoykovich, M. P.; De Pablo, J. J.; Nealey, P. F. *Nano Letters* **2019**, *19*, 4684–4691.

(104) Sing, C. E.; Zwanikken, J. W.; De La Cruz, M. O. *Journal of Chemical Physics* **2015**, *142*, 1–18.

(105) Kwon, H. K.; Zwanikken, J. W.; Shull, K. R.; Olvera De La Cruz, M. *Macromolecules* **2015**, *48*, 6008–6015.

(106) Sing, C. E.; Zwanikken, J. W.; Olvera De La Cruz, M. *ACS Macro Letters* **2013**, *2*, 1042–1046.

(107) Kim, K.; Nguyen, N.; Marxsen, S. F.; Smith, S.; Alamo, R. G.; Kennemur, J. G.; Hallinan, D. T. *Macromolecular Chemistry and Physics* **2021**, *222*, 1–9.

(108) Nedoma, A. J.; Lai, P.; Jackson, A.; Robertson, M. L.; Wanakule, N. S.; Balsara, N. P. *Macromolecules* **2011**, *44*, 3077–3084.

(109) Sing, C. E.; Olvera De La Cruz, M. *ACS Macro Letters* **2014**, *3*, 698–702.

(110) Frielinghaus, H.; Pedersen, W. B.; Larsen, P. S.; Almdal, K.; Mortensen, K. *Macromolecules* **2001**, *34*, 1096–1104.

(111) Shah, N. J.; He, L.; Gao, K. W.; Balsara, N. P. *Macromolecules* **2023**, *56*, 2889–2898.

(112) Lee, J. H.; Ruegg, M. L.; Balsara, N. P.; Zhu, Y.; Gido, S. P.; Krishnamoorti, R.; Kim, M. H. *Macromolecules* **2003**, *36*, 6537–6548.

(113) Graessley, W. W.; Krishnamoorti, R.; Balsara, N. P.; Fetters, L. J.; Lohse, D. J.; Schulz, D. N.; Sissano, J. A. *Macromolecules* **1993**, *26*, 1137–1143.

(114) Snyder, H. L.; Meakin, P.; Reich, S. *Macromolecules* **1983**, *16*, 757–762.

(115) Meier, G.; Momper, B.; Fischer, E. W. *The Journal of Chemical Physics* **1992**, *97*, 5884–5897.

(116) Fukuda, T.; Nagata, M.; Inagaki, H. *Macromolecules* **1986**, *19*, 1291–1494.

(117) Weitz, D. A.; Pine, D. J. *MRS Bulletin* **1994**, *19*, 39–44.

(118) Ishimaru, A., *Wave Propagation and Scattering in Random Media*; Academic Press: New York, 1978.

Appendices

Appendix A

Beamtime Advice

This appendix section is intended to be a basic "how-to" guide to approaching beamtime.

A.1 Proposal Writing

Writing a proposal for a new scattering technique can be very intimidating. The best way to prepare is to do some background research. Most beamline scientists write review articles on their beamline, or technique. These articles are often a good starting point to learning the basic physics of the beamline. Keep in mind that even these articles can be very technically dense. The goal of this literature review is to gain familiarity with the technique you want to learn. You do not need to become an expert overnight. Try to find papers in your field using this technique (i.e. a paper on SANS for polymer blends). If you are writing a proposal for the first time, make sure to start writing at least 2 months in advance of the due date.

The key to proposal success is organization. Find the website of the beamline facility you wish to use and take careful note of the proposal due dates and proposal length and content requirements. The page limit, formatting and reference requirements vary widely from national lab to national lab. If you have not performed this technique before, it can be very useful to reach out to the beamline scientist at the facility you want to work at to get their input on your proposal. Beamline scientists love to help users design experiments. However, beamline scientists do not like being contacted for proposal help a week before the deadline. Try to reach out at least 1 to 2 months before the deadline to start the conversation. Before you meet with the beamline scientist try organizing your goals for the experiment. You should be able to clearly explain why you want to use this particular beamline technique, why you think you could learn something interesting from the experiment, and why you think your experiment is viable at this facility. Take careful notes on all the feedback the beamline scientist gives you and pay special attention to technical details about instrument operating conditions, limitations, and estimated amount of beamtime you need for your experiment.

Once you have done some background research it's time to write your proposal. Try to clearly lay out why your research project is interesting, what you hope to learn at the

beamline and why you think this technique is important. Outline exactly what samples you are planning on running, and how much beamtime you will need for your experiment. This is where input from the beamline scientist is essential. You want to request a reasonable amount of beamtime for your experiment. Make sure your proposal adheres to all formatting guidelines from the national lab and is below the page limit. Make sure all graph labels and captions are legible. Have a friend proofread your proposal. Make sure you submit your proposal on time.

A.2 Beamtime Sample Preparation

Good sample preparation is essential for a successful beamtime. As with everything the key is planning. Once you are given a date for your beamtime, mark it on the calendar, and start working out how much time you need to prepare your samples. If the beamline facility is not local (such as ORNL) remember that you will have to ship your samples. Even with overnight shipping, account for 1.5 weeks for transportation since shipping facilities at national labs can be slow. Try to estimate how many samples you can make per day and calculate how much time it would take to prepare all your samples. Once you have this estimate, double it. For example, if you think you need 1 week to prep samples, plan on sample preparation taking at least 2 weeks. Shipping delays, equipment malfunctions, injuries and other unforeseen events can drastically slow down sample preparation. Take good notes on sample preparation methods; this will be useful when you are writing up your work. Overestimate the amount of time you need so you don't need to scramble at the last minute. Also consider sample stability if you are shipping your samples to outside facilities. If your samples are hygroscopic, it is often best practice to seal your sample holders in pouches. If you using an unfamiliar type of sample holder, make sure you understand how to assemble the sample holder properly, and confirm with your beamline scientist. Once you ship your samples, confirm with the beamline scientist that they have arrived at the destination facility. If you are extremely concerned about sample stability, many facilities have gloveboxes and are happy to temporarily store your samples under argon. Label your samples clearly so both you and the beamline scientist easily understand what they are.

A.3 Day of the Experiment

Try to get a good night's sleep before your experiment starts. If you are planning on a long day, pack some snacks and a meal if necessary. Once you arrive at the beamline facility, confirm where your samples are. During safety training at the beamline, take extremely careful notes and pay attention. Many of these facilities utilize high energy radiation, so attention to detail is essential. Take extremely careful notes on how to operate the beamline equipment and computers. Beamtime experiments often go late into the night, and you need to be able to handle problems by yourself. A step-by-step operating procedure of the

beamline will be essential. If a problem happens or if the beamline goes down, take a deep breath, and assess the situation. Above all else, prioritize the safety of yourself and those around you, and follow all safety training given to you by the beamline scientist. If the problem is simple, like the computer freezing, you may be able to resolve it by yourself. If the problem is more significant, contact the beamline scientist. It is useful to ask the beamline scientist during training what problems are common at the beamline, and which merit calling the beamline scientist. Take extremely careful notes on the order of samples you run, operating conditions such as temperature and exposure time and any issues that crop up during the experiment.

A.4 Data Analysis

When analyzing data from a beamtime, keep your files organized, and make sure your file names make sense to you, and anyone else who might work on the project. Most beamline facilities use some kind of specialty software to convert the raw data from the equipment into .txt files. Familiarize yourself with this software, and don't hesitate to ask the beamline scientists questions. As you analyze your data, keep the beamline scientist in the loop. They are an excellent source of knowledge and great resources. It is generally good practice to include the beamline scientist as an author in a resulting publication, but it can vary on a case-by-case basis. Make sure to include the proper acknowledgement for the user facility in your paper acknowledgements.